University of Texas at El Paso
DigitalCommons@UTEP

Open Access Theses & Dissertations

2016-01-01

Microstructural Investigation Of Vintage Pipeline Steels Highly Susceptible To Stress Corrosion Cracking

Monica Adriana Torres
University of Texas at El Paso, matorres9@miners.utep.edu

Follow this and additional works at: https://digitalcommons.utep.edu/open_etd

 Part of the Materials Science and Engineering Commons, and the Mechanics of Materials Commons

Recommended Citation
Torres, Monica Adriana, "Microstructural Investigation Of Vintage Pipeline Steels Highly Susceptible To Stress Corrosion Cracking" (2016). *Open Access Theses & Dissertations*. 972.
https://digitalcommons.utep.edu/open_etd/972

This is brought to you for free and open access by DigitalCommons@UTEP. It has been accepted for inclusion in Open Access Theses & Dissertations by an authorized administrator of DigitalCommons@UTEP. For more information, please contact lweber@utep.edu.

MICROSTRUCTURAL INVESTIGATION OF VINTAGE PIPELINE STEELS HIGHLY SUSCEPTIBLE TO STRESS CORROSION CRACKING

MONICA TORRES

Doctoral Program in Materials Science and Engineering

APPROVED

Stephen, W. Stafford, Ph.D., Chair

Felicia, S. Manciu, Ph.D.

Russell, R. Chianelli, Ph.D.

Roy, Arrowood, Ph.D.

Charles H. Ambler, Ph.D.
Dean of the Graduate School

Copyright ©

by

Monica Torres

2016

MICROSTRUCTURAL INVESTIGATION OF VINTAGE PIPELINE STEELS HIGHLY SUSCEPTIBLE TO STRESS CORROSION CRACKING

By

MONICA TORRES, MS

DISSERTATION

Presented to the Faculty of the Graduate School of

The University of Texas at El Paso

in Partial Fulfillment

of the Requirements

for the Degree of

Doctor of Philosophy

Metallurgical and Materials Engineering

THE UNIVERSITY OF TEXAS AT EL PASO

May 2016

Abstract

The use of pipelines for the transmission of gas offers not only efficiency, but a number of economic advantages. Nevertheless, pipelines are subject to aggressive operating conditions and environments which can lead to in-service degradation [1] and thus to failures. These failures can have catastrophic consequences, such as environmental damage and loss of life [2]. One of the most dangerous threats to pipeline integrity is stress corrosion cracking (SCC). Despite the substantial progress that has been achieved in the field, due to the complex nature of this phenomenon there is still not a complete understanding of this form of external corrosion. This makes its detection and prevention a challenge and therefore a risk to pipeline integrity, and most importantly, to the safety of the population.

SCC cracks are the result of the interaction between a corrosive environment, applied stresses, and a susceptible microstructure. To date, what defines a susceptible microstructure remains ambiguous, as SCC has been observed in a range of steel grades, microstructures, chemical composition, and grain sizes. Therefore, in order to be able to accurately predict and prevent this hazardous form of corrosion, it is imperative to advance our knowledge on the subject and gain a better understanding on the microstructural features of highly susceptible pipeline materials, especially in the subsurface zone where crack nucleation must take place. Therefore, a microstructural characterization of the region near the surface layer was carried-out utilizing TEM. TEM analysis revealed the dislocation character, ferrite morphology, and apparent carbide precipitation in some grain boundaries. Furthermore, light microscopy, SEM, and hardness testing were performed to expand our knowledge on the microscopical features of highly SCC susceptible service components. This investigation presents a new approach to SCC characterization, which exposed the sub-surface region microscopical characteristics of service components with confirmed SCC.

Table of Contents

List of Tables

List of Figures

Introduction

Natural gas is one of the most energy efficient fossil fuels, [3] providing sustainable energy capable of satisfying the future energy demand without an adverse impact to the environment [3]. Therefore, its popularity is expected to markedly increase in the near future [4-5]. The emergence of natural gas as a global commodity underlies the importance of its processing, transmission, and distribution [1,3] as an increasing demand will require higher operating pressures and the expansion of current pipeline networks to increment the capacity of the existing systems [4,6]. Furthermore, with an aging gas transmission infrastructure and the depletion of onshore gas reserves located in less hostile environments and conditions it would be required to go farther and deeper which means many more challenges to ensure the structural integrity of the gas infrastructure in order to deliver in a safely manner [3-4,7].

The efficiency and economic advantages that gas transmission pipelines offer as compared to other means of transportation such as train, truck, and others are certainly significant [3-4]. However, buried pipelines are exposed to aggressive service environments and therefore subject to in-service degradation [1] that can have catastrophic consequences, leading not only to environmental damage, but to the loss of life [2]. Figure 1 illustrates the catastrophic impact that a pipeline accident can have [8-11]. Among the different potential threats to gas pipeline integrity, stress corrosion cracking (SCC) continues to be one of the most complex and least understood failure mechanisms. SCC is a time-dependent [2], environmentally induced crack propagation mechanism [4,12] in which the interaction between a corrosive environment, applied stresses, and a susceptible microstructure lead to the initiation and propagation of cracks on the surface of the pipeline that can result in pipeline failure [13]. In the event of a pipeline rupture, the escaping gas can flow at the speed of sound [2,14] and form a combustible atmosphere when mixed with air or with certain oxidizing agents, and thus feed a fire that can ignite in about 1-2 minutes after the failure [2,14]. Consequently, one of the main pipeline rupture hazards is the thermal radiation from a sustained fire [14]. Given that during a pipeline failure, the full bore of the pipeline will be open to the environment, the pipe diameter plays a key role in determining the consequences of the failure [2,14]. Hence, transmission pipelines pose a larger threat as compared to distribution lines, as they are larger diameter steel pipelines

designed to move large volumes of gas [15] and thus operate at higher pressures (over 20% of yield pressure) [2].

Figure 1. Pipeline failure consequences (A) Carlsbad New Mexico, 2000 stress corrosion cracking failure, 12 casualties; (B) Milford Texas, 2013 third party damaged, burned for 36 hours; (C) New York, 2014 leaky cast iron pipeline, 8 casualties; and (D) Taiwan, 2014 leaky propane pipeline, 27 causalities [8-11].

To date, a number of disastrous pipeline failures that have led to death and/or injury have been the result of SCC—a particularly tragic incident caused by SCC, occurred in Nashitoses, Lousiana, where 17 people died—and despite the fact that there have been many advances in the field no particular manufacturer, manufacturing technique, or steel grade has been linked to SCC occurrence [4,16]. Therefore, its detection remains a challenge to the industry as it is virtually impossible to inspect 100% of the buried piping [17]. In order to develop proper prevention methods to guarantee the integrity of the pipeline system, it is important to expand our understanding of the mechanism behind this form of corrosion [18], particularly on what constitutes susceptible materials. The aim of this investigation is to

characterize and compare the general microstructure and the microstructure of the sub-surface region of different transmission linepipe steels with confirmed SCC susceptibility, in order to gain insight into what makes these API5L pipe steels more vulnerable to SCC and thus help develop better materials and detection techniques to prevent future failures [4].

Statement of the Problem and Justification

The recent deadly explosion in New York City (2014) that lead to the collapse of two buildings and cost the lives of at least 8 people, has highlighted not only the unpredictable and destructive nature of a gas blast, [19] but also the fact that many mayor cities lie on extensive networks of outdated, fragile, and vulnerable gas pipelines [20]. For example, it has been reported that in the area of Manhattan, Bronx, and Queens, about 60% of the gas systems are made of unprotected steel or cast iron; additionally, in Washington DC about 5900 gas leaks were detected [19,21]. Gas leaks from an aging and/or damaged infrastructure can have catastrophic consequences, not only for human safety, [22-25] but also for the environment, as escaping gas contributes to air pollution and greenhouse gases [19].

Among the different threats to the gas transmission infrastructure, stress corrosion cracking (SCC) is one of the most complex forms of external corrosion that contributes to pipeline failure. To date, many countries such as USA, Iran, Brazil, Canada, Russia, Iraq, Italy, Pakistan, Australia, and others have experienced SCC, prompting a growing interest in the subject [26]. Furthermore, the multivariate nature of this form of corrosion makes the prediction and location of SCC cracks on operational pipelines difficult, expensive, and inconvenient [27-28]. One of the required factors for SCC to develop is a susceptible microstructure. However, despite the extensive efforts and substantial progress made after many years of research, there remains gaps in the understanding of SCC, particularly on what characterizes a susceptible microstructure. To date, no particular metallurgical features have been associated with SCC, [4] as it has been observed in a range of steel grades, dimensions, grain sizes, and microstructures [2,4]. Therefore, the effect of microstructure and chemistry of various pipeline steels in SCC occurrence remains unclear [29]. Consequently, it is important to expand our knowledge of this subject and build upon past experiences [17]. Previous SCC failures can help gain insight into the relationship between material properties and SCC occurrence and therefore delimit the boundaries of this ubiquitous form of corrosion [17]. In this manner, we can develop better materials and procedures to prevent, predict and eliminate SCC failures [22,30-31].

This study will perform an extensive microstructural investigation on the state of the region near the outside diameter (O.D.) of vintage pipelines removed from service due to the detection of SCC. The

analysis will be done to a depth of approximately 200μm from the surface layer where crack nucleation must take place. The region to be characterized will be referred as the sub-surface zone. In conducting the microstructural sub-surface region characterization this investigation aims to determine the conditional state of this region and therefore establish a relationship with the factors involved in sub-critical crack formation. Microstructural characterization will be performed through optical and transmission electron microscopy (TEM). Optical microscopy will be used to observe the materials general microstructure—microconstituents, inclusions, grain size—and crack morphology. On the other hand, TEM will be used to observe the dislocation structure, phase constituents, the distribution of alloying elements, and inclusions in these sub-surface zone. Optical emission spectrometry (OES) and scanning electron microscopy (SEM) will be used to determine the chemical composition of the pipeline. Microhardness testing will be used to examine hardness gradients and to determine the general mechanical properties of the pipeline material.

In this manner, this investigation will further our knowledge of the microscopical conditions typifying the sub-surface zone and general metallurgical characteristics of actual service components and how they relate to the macroscopic mechanical behavior of the material. This can help advance our understanding of the actual material deterioration process, and therefore accurately predict the remaining service life of the pipeline. Additionally, by furthering our understanding of the mechanistic connections between stress corrosion cracking and the surface layer microstructure, we can gain insight on what makes the material so susceptible and develop robust processes and steels resistant to SCC to the benefit of future pipelines [32].

Background Information

SCC is an undesirable type of external corrosion that has caused significant impact to the oil and gas industry. The formation of stress corrosion cracks occurs below the yield strength of the material [18] as result of the interaction between a corrosive medium and tensile stress. A schematic of the SCC process is shown in Figure 2. Hence, buried pipelines transporting pressurized product appear to provide the optimal conditions for SCC to develop. With more than two million pipeline miles just in the USA, SCC continues to be a challenge and a threat which keeps growing as the pipeline infrastructure continues to age. Therefore, we must further our knowledge about this critical subject [22].

Figure 2. SCC phenomena conceptual schematic.

2.1 Gas Transmission Industry

The Natural Gas business is a key sector in the energy industry and therefore to the economies of a number of countries [33]. Currently, about 25% of the total energy consumed in the United States comes from natural gas [34]. In fact, natural gas consumption and trade have been growing progressively over the past two decades [3] and it is expected that oil and gas will remain the primary energy supply for the foreseeable future [31]. In order to satisfy the ever increasing demand for this clean-burning fuel [4] a complex and extensive transmission and distribution pipeline network [15,33] has been constructed over the last 70+ years in the United States [35]. The construction of the North America pipeline

infrastructure—one of the largest and oldest in the world [36]—initiated with the use of wooden pipes that were first replaced by lead pipes [3] and subsequently by modern seamless steel pipes (1920), allowing the use of higher operating pressures [2-3].

According to the US Department of Transportation, over 50% of the installed pipeline system was constructed between 1950-1969 which is approximately 142,000 miles of the current 306,000 miles of the gas transmission system [34-35], about 5% was built before 1940, and the remaining since 1970 [2]. Table 1 presents the decade of installation for transmission and distribution pipelines [35] and Figure 3 shows the transmission pipe mileage per decade [2].

Table 1. Gas Pipelines Installation Period

Installation Period	*Transmission Pipelines*	*Distribution Pipelines*
Pre-1940	4%	5%
1940-1949	8%	2%
1950-1959	23%	9%
1960-1969	24%	15%
1970-1979	11%	13%
1980-1989	10%	16%
1990-1999	11%	21%
2000-present	9%	19%

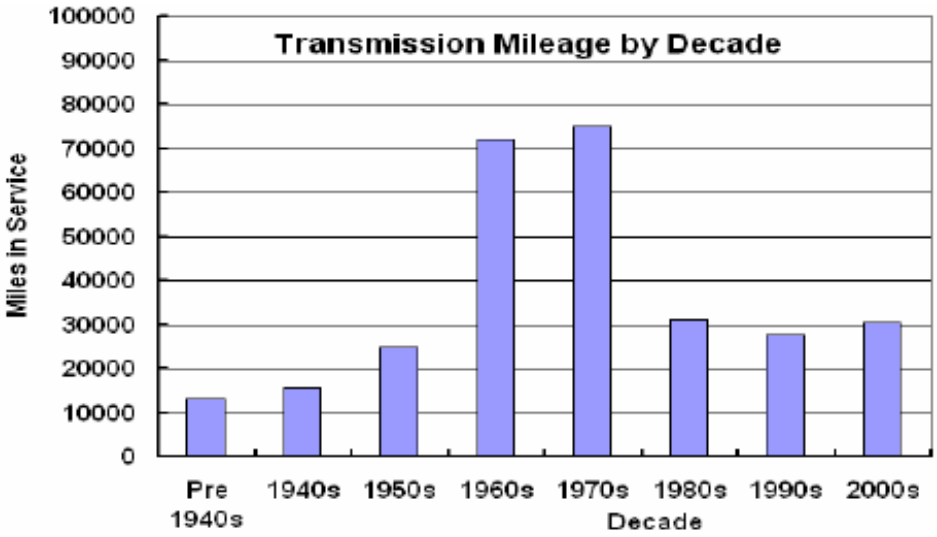

Figure 3. Transmission pipes mileage per decade[2].

The development of new technologies, the increasing demand, the economic changes, and the need for safer systems led to the introduction of new processes and therefore to the abandonment of old pipe manufacturing practices now referred as historic [2]. The pipes constructed with historic practices (steel, pipe, and pipeline construction) are now considered vintage pipelines, while those built with newer techniques are referred to as modern piping [2].The different pipe and pipeline construction practices and the periods of usage are shown in Figure 4 [2].

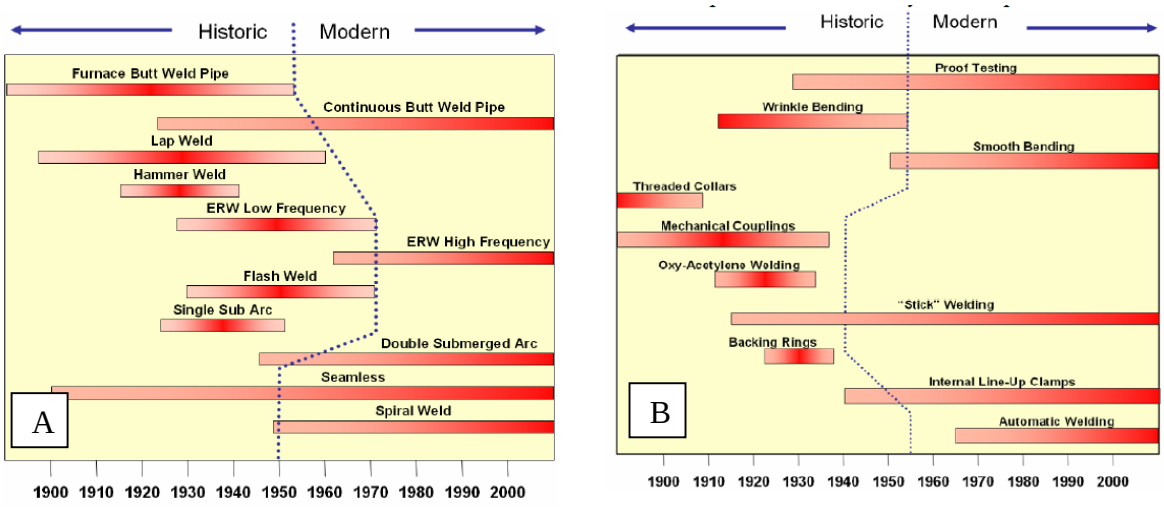

Figure 4. Pipe (a) and (b) pipeline construction methods and usage period [2].

Among the advances in pipeline technology was the introduction of pressure testing (1960). This technique allowed for the detection of critical defects [1-2]. However, it has been reported that hydrotesting does not necessarily detect SCC, such as in the Williams Lake case—this demonstrates the complexity of the SCC phenomenon [4]. Moreover, during 1970 another milestone in the development of pipeline steels was achieved with the application of thermo-mechanical processing (TMCP) to substitute the traditional heat treatment techniques [1-2]. Thermomechanical controlled processes led to the development of X70 steel grade pipes which are characterized by an acicular ferrite and bainite microstructure instead of the mix ferrite/pearlite structure [4]. Subsequently, accelerated cooling after controlled rolling was introduced, whereby higher strength levels were reached (X80 steel) [1-2]. Currently, advanced high-strength steels like APIX80, X100, and X120 are being evaluated for potential application for high-pressure and long distance gas transmission pipelines such as the 2140 mile-Alaska pipeline (operating pressure of 2500 psi) [4]. Nevertheless, not enough evidence is available to conclude whether high strength steels such as X80 and X100 are more or less susceptible to SCC [4]. The evolution of various pipeline steel grades and the time period (worldwide) in which they have been mostly used is shown in Table 2 [4,37]. It may be added that the "X" indicates the yield strength (psi) of the steel [38].

Table 2. Pipeline Steel Evolution

Time Period	*Steel Grade*	*Microstructure*
1950	APIX52 and lower steel grades	Polygonal ferrite + pearlite
1970	API X60 and X65	Ferrite + pearlite
End 1970	API X70	Acicular ferrite + bainite
1985	API X80	Bainite + fine ferrite
Currently under development	APIX100 and X120	Lath bainite + martensite/austenite islands (M/A films)

Gas Transmission System

The natural gas industry infrastructure is a complex system that includes compressor stations that pressurize the gas to keep it flowing, and transmission and distribution pipelines used to move the gas. The main differences between transmission and distribution systems, is that transmission lines are larger diameter pipelines designed to move large volumes of gas at high pressure (200-1500 psig), primarily higher strength steel grades are used, such as API 5L grades X52, X56, X60, X65, X70, and X80 [15,39]. On the other hand, distribution lines are usually operated at lower pressures (below 100 psig) and the typical steel grades used include A, B, X42, and X46 [39]. Table 3 presents the typical chemical composition for the aforementioned steel grades [40]. Additionally, about 1400 compressor stations maintain the gas pressure and flow. Parkins et al. reported that majority of IGSCC failures occur within 10 miles from the compressor stations [41] where the temperature (100-120 ^{o}F) and the pressure are higher [39]. Higher temperatures usually provide a contributing factor in terms of coating degradation which leads to the development of the cracking environment [42]. Higher pressure produces higher hoop stresses and higher driving forces for SCC damage. The coincidence of SCC appearing outside of discharge stations is not a requirement for the near-neutral SCC as this form of SCC appears to exhibit a lack of correlation with temperature [13].

Table 3. Gas Transmission Pipeline Steel Grades

Grade	*C (max)*	*Mn (max)*	*P (max)*	*S(max)*	*Minimum Yield Strength (MPa)*
A	0.22	0.90	0.03	0.03	207 (30 ksi)
B	0.26	1.20	0.03	0.03	241 (35 ksi)
X42	0.26	1.30	0.03	0.03	290 (42 ksi)
X46	0.26	1.40	0.03	0.03	317 (46 ksi)
X52	0.26	1.40	0.03	0.03	359 (52 ksi)
X56	0.26	1.40	0.03	0.03	386 (56 ksi)
X60	0.26	1.40	0.03	0.03	414 (60 ksi)
X65	0.26	1.45	0.03	0.03	448 (65 ksi)
X70	0.26	1.65	0.03	0.03	483 (70 ksi)

Service Failures

SCC has been observed in a wide range of pipeline steel compositions, welding methods, coating materials [41], and soils [4]. However, some materials appear to have higher susceptibility to SCC; while steel grade X-65 has been reported to be very susceptible to TGSCC [43], most IGSCC failures have occurred in the X-52 grade [41], and grade X70 appears to be prone to both SCC forms [44]. Moreover, SCC has been observed in an extensive array of pipeline strengths and dimensions (diameters and wall thicknesses). IGSCC service failures have occurred in pipes with diameters ranging from 203-762 mm (8-30″), walls thicknesses between 4.5 to 12.7mm (0.18 to 0.5″) and at 46 to 76% of the minimum yield strength of the pipes [41]. TGSCC failures have occurred in pipelines having diameters 114-1067mm (4.5-42″), wall thickness 3.2-9.4mm (0.12-0.37″), and strength from 241Mpa to 448Mpa (35-65 Ksi) [45].

2.2 STRESS CORROSION CRACKING

SCC can be defined as the initiation and propagation of cracks due to the combined action of a specific environment and tensile stress on a susceptible material [12,18,40,46]. The required tensile stress can arise from the manufacturing process and/or from the pipeline operating conditions [47]. According to Review et al., there are four main sources of stress: internal pipe pressure (hoop stress)—usually the highest stress [4]; operating pressure fluctuations (cyclic); soil movement or localized pipe bending (axial); and residual stresses from pipe manufacturing [48]. The pipeline operating pressure is determined by a percentage of the minimum yield strength (SMYS) and despite the fact that the maximum operating pressure allowed is about 80-40% SMYS, SCC failures have been observed in the 46-77% range [4]. It is worth mentioning, that higher operating pressures are used mainly in rural or sparsely populated areas (class 1) [4].

Buried pipelines are protected from corrosion by the application of a coating and cathodic protection (CP). However, holidays or defects in the coating lead to coating disbondment which allows for moisture and residual content (CO_2) to flow and interact with the pipeline surface and therefore to general corrosion, pits, and cracking [49]. Additionally, a disbonded coating shields the CP current to flow to the pipeline leaving the material vulnerable [49]. Consequently, the performance of the coating is a critical factor in the development of SCC; an intact coating will prevent the interaction between the steel

and the electrolyte and thus the development of SCC [4]. The environments that can lead to SCC are alloy specific; for instance, carbon steels are known to be susceptible to SCC passivating environments such as hot nitrate, hydroxide, phosphate, and carbonate/bicarbonate solutions, while aqueous electrolytes have been involved in the SCC failure of high-strength steels [4,12]. Furthermore, a relationship between environment, oxide thickness, and SCC was found by Poulsom and coauthors, who reported that the in annealed steels the environments that promote the formation of a thick oxide layer such as nitrate, hydroxide, and carbonate lead to intergranular SCC (IGSCC); while, those leading to the formation of a thin film such as liquid ammonia result in trangranular cracks [50]. A schematic diagram of the required conditions for the development of SCC [48] and details of factors affecting SCC are presented in Figure 5 and Figure 6, respectively. A contributoring factor to the complexity of this form of corrosion is that changes to any of the aspects shown in Figure 5 can change the material's response to SCC [12], for example it has been reported that wet-dry cycles can alter the soil resistivity which in turns alters the SCC response [4].

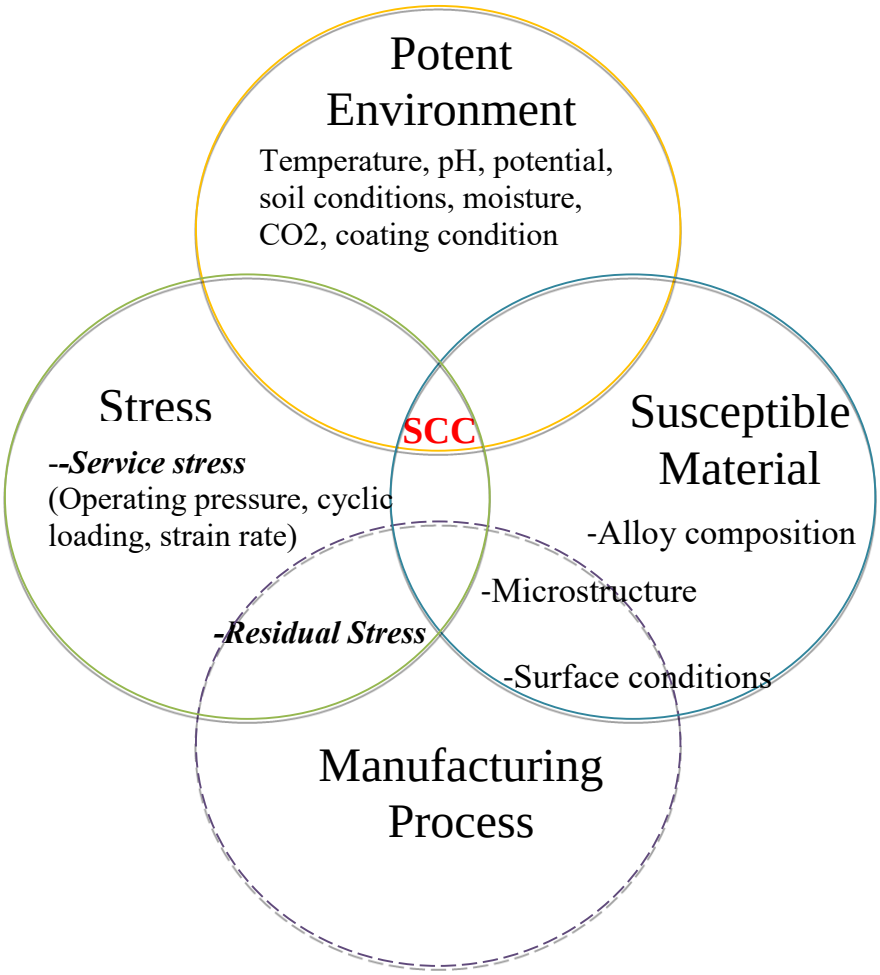

Figure 5. Stress Corrosion cracking required conditions.

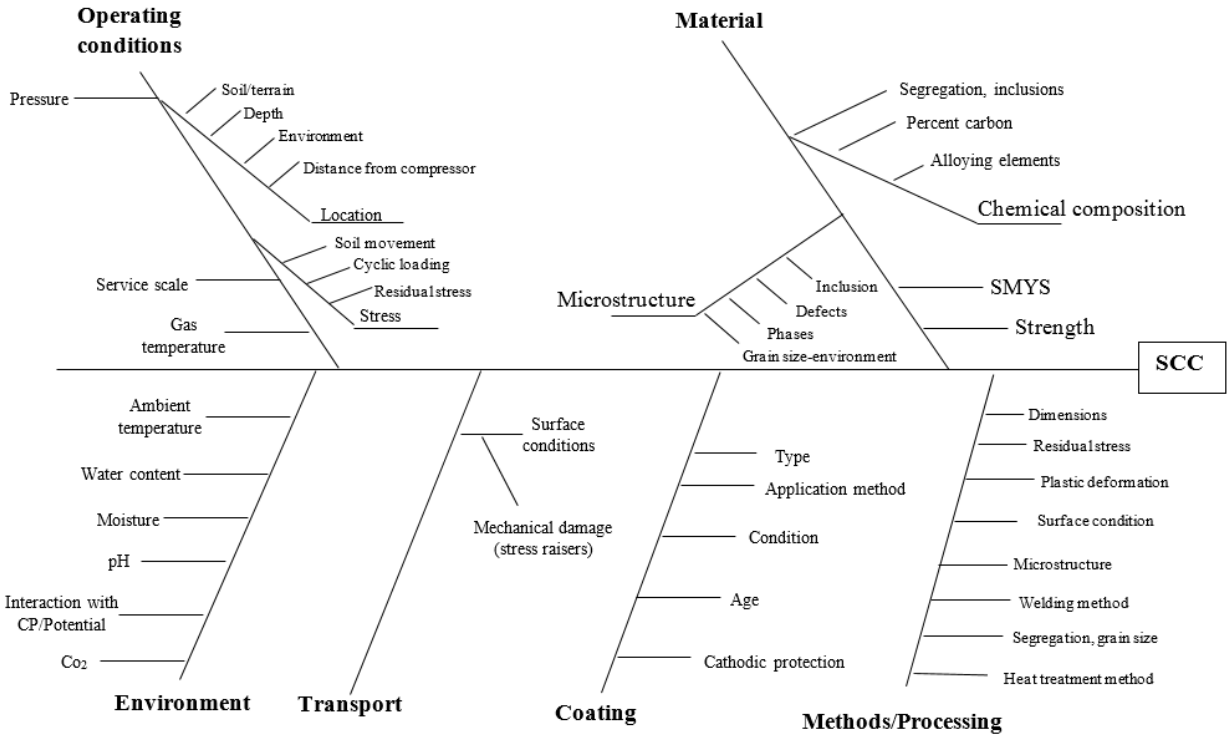

Figure 6. Detailed schematic diagram of factors affecting to SCC.

Stress Corrosion Cracking Process

The SCC process is divided into four stages, shown in Figure 7 [42]. During stage I, the required conditions for the development of SCC—such as coating deterioration which allows the material to interact with the electrolyte—originate at the outside surface of the pipeline. Once the cracking conditions are met and if the appropriate stressing conditions and susceptible materials are present cracks will initiate in stage II [51]. Discontinuities at metal surface such as scratches, grooves, or dents; metallurgical defects (inclusions, grain boundaries, dislocations, and voids); and corrosion pits can act as possible crack nucleation sites [4,52].

During stage II, the crack growth rate diminishes until it reach a steady-state growth (stage III). However, in some cases the crack growth rate can drop to zero leading to the formation of non-propagating

cracks “dormant cracks” [51] that can become active again through the interaction with active cracks [42]. Throughout stage III, cracks will continue to initiate, grow, and coalesce; eventually exceeding K_{ISCC}—stress that needs to be exceeded in order for the cracks to continue to grow [42]—which leads to an increase in the crack growth velocity. To-date the K_{ISCC} threshold stress has been difficult to define as real service conditions are more complex than lab reproduced SCC [4]. Lastly, in stage IV final failure takes place when a number of sufficiently large cracks coalesce and thus exceed the K_{IC} resulting in catastrophic fracture [12-13,40-42,53].

Crack coalescence takes place when two cracks in different planes grow until their tips pass each other and turn, eventually joining due to the overlapping of their stress fields [51]. Therefore, the distance between adjacent cracks dictates the interaction among them, as separation increases cracks are less likely to coalesce because the interaction between their stress fields will not take place [42]. Additionally, the geometry and location of the SCC colony also plays a key role in crack coalescence and growth [4]. Longitudinal, narrow, and long cracks have been reported to be more detrimental to the pipeline integrity then those with similarities in length and width [4]. Additionally, cracks in the middle of the colony tend to became dormant as they are shielded from stresses [4]. Nevertheless, crack coalescence accounts for significant crack length expansion exceeding normal stress corrosion crack growth kinetics, as the crack growth rate for individual cracks tends to decreases with time [42]. The approximate crack growth rate for both IGSCC and TGSCC has been estimated to be about 10^{-8} mm/s (stage 1-3) [51]. Furthermore, if no crack coalescence takes place stage II will continue eliminating the tendency to leak or fracture [51].

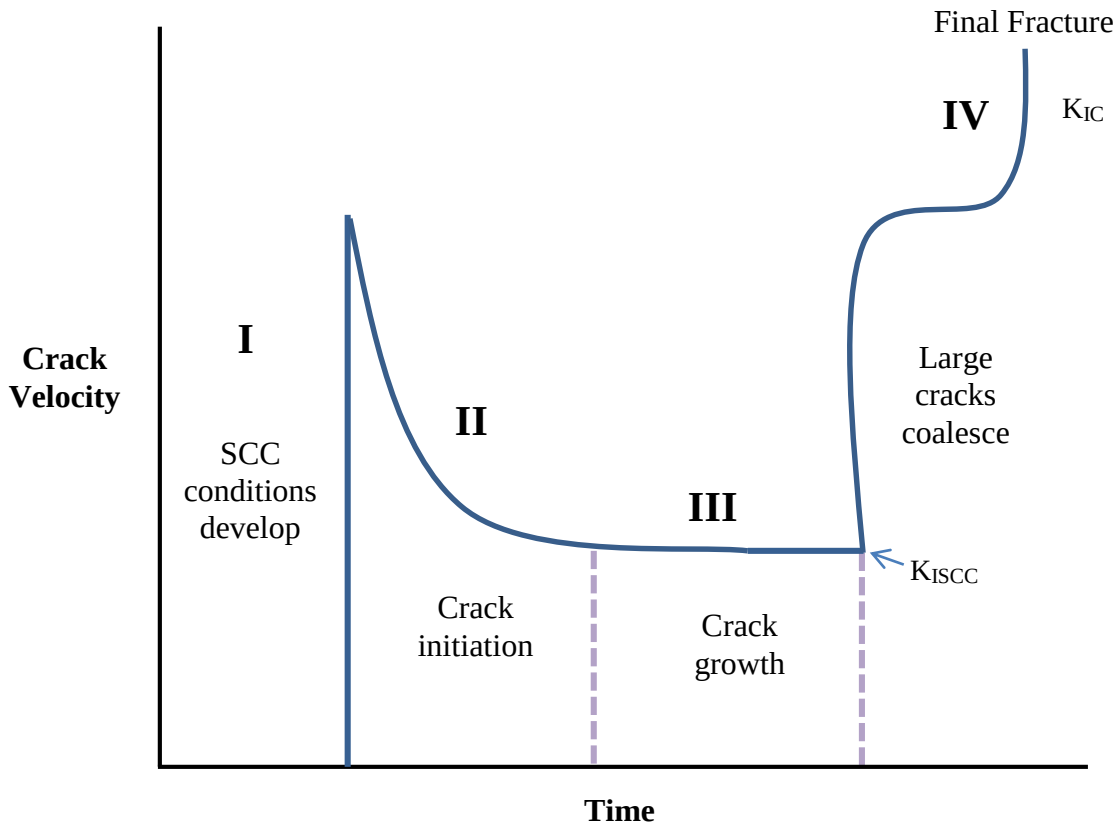

Figure 7. Stress corrosion cracking process stages.

Types of SCC

Underground pipeline steels are mainly susceptible to two forms of SCC, high-pH (classical SCC or IGSCC) and near-neutral pH (TGSCC). However, until recently a third form of SCC was reported, SCC in acidic soil [4]. It is important to keep in mind that the crack environment dictates the pH level for the type of SCC, and not necessarily the soil environment [4]. High-pH was the only known form of SCC until mid-1980 when near-neutral SCC was discovered during the TransCanada Pipeline failure [18,54] in fact most of Canada's pipeline failures have been attributed to near-neutral mode [13]. These two forms of SCC exhibit some similarities; colonies of cracks are usually formed on the outside surface, primarily at the bottom of the pipeline in the longitudinal direction [55]. Nevertheless, their crack morphology, growth mechanisms, and conditions are different [42].

High- pH (classical) SCC

Classical-SCC is also known as high-pH because it occurs at relative concentrated carbonate-bicarbonate solutions with an alkaline pH of 9.5-10 over a distinct electrochemical potential. The corrosive environment responsible for this form of SCC is believe to be the result from the interaction between the hydroxil ions from the cathodic protection-pipe reaction and the carbon dioxide in the soil from the decay of organic matter [4]. In the event of coating disbondment the cathodic current will increase the pH of the trapped electrolyte which then dissolves the carbon dioxide producing a concentrated carbonate/bicarbonate solution with a high pH [4]. High-pH SCC exhibits temperature sensitivity—as temperature decreases crack growth rate decreases exponentially [13,40,42]. This form of SCC has been typically observed within 20 km downstream of compressor stations [42]. Moreover, it is believed that warmer pipes could lead to soil water evaporation and therefore to the generation of the cracking electrolyte [4]. The average age of pipelines that developed this form of SCC was reported to be about 22.9 years [16]. High-pH stress corrosion cracks are thin, narrow, branched, and with little evidence of general corrosion on the crack walls. The cracks are frequently found in regions containing pits, however cracks have also been observed in areas with no obvious pitting [55-56]. Classical-SCC cracks follow an integranular path hence it is also referred as intergranular SCC (IGSCC) [42]. It has been reported that in steels with a mix ferrite/pearlite microstructure SCC cracks propagate mostly along ferrite:ferrite (α:α) grain boundaries [57] rather than ferrite:pearlite [58] and when the crack meets a pearlite colony it can be deflected or propagate in a transgranular mode in the pearlite colony [57] if the lamellae is oriented parallel to the crack path [59] leading to a mixed propagation mode [60].

The generally accepted IGSCC mechanisms are passive film rupture and anodic dissolution at the crack tip [23,61]. The protective film formed on the pipeline surface ruptures as a result of the localized plastic deformation at the crack tip, whereas in regions away from the crack the film remains intact leading to the formation of an electrolytic cell where the anode is the bare metal at the crack tip and the cathode the unbroken film [62]. The anodic dissolution depends on the repassivation rate; if repassivation rate is too high crack growth does not occur due to insufficient corrosion and if repassivation rate is too slow to much corrosion would take place and thus crack blunting and some form of pitting will take place instead of crack propagation [63], therefore SCC has been linked to an intermediate repassivation rate [62,64].

The segregation of alloying elements, impurity atoms, and the formation of precipitates at the grain boundaries evidently play a key role in IGSCC, as they can lead to electropotential differences between the grain boundary and the matrix [65-66] which can enhance the SCC susceptibility by providing a path for preferential dissolution. Parkins et al. concluded that the grain boundary regions containing precipitates can become anodic either because the precipitates are anodic or because the region in the vicinity of the precipitate is depleted of solute atoms making the grain boundary less noble (anodic) than the grain interior and therefore more susceptible to corrosion [67]. Sensitization in stainless steel is a typical example of preferential dissolution of the grain boundary as a result of chromium depletion in the region adjacent to the boundary [4]. Decreasing the carbon content in stainless steels decreases the tendency for sensitization [4].

Near-Neutral SCC (TGSCC)

Near-neutral SCC is associated with dilute groundwater containing bicarbonate and dissolved CO_2 [4,54]. The trapped electrolyte has a relatively low pH of 5.5-7.5. This form of SCC has mainly occurred when little or no cathodic protection reaches the pipeline [4]. Near-neutral SCC is characterized by transgranular, quasi-cleavage, wide cracks—hence also referred as transgranular SCC (TGSCC)—with little branching, and appreciable corrosion product within the crack walls [13,61,68]. Large amounts of white iron carbonate have been found near failure zones at pipeline surface [54,69]. Moreover, despite the fact that no apparent correlation between TGSCC and temperature has been determined (since it has been mainly detected far from compressor stations, about 67 km downstream) [42] a tendency to occur in a cold weather has been observed [4,16]. Furthermore, an apparent relationship between TGSCC and coating type has been suggested due to the fact that most of the near-neutral SCC failures in Canada have occurred on pipe with polyethylene tape coating, while less failures have happened on asphalt enamels and coal tar, and no cracks have been associated with fusion bonded epoxy or epoxy urethanes [28].

The mechanisms for TGSCC are not well understood [23] as some of the available data appears to be contradictory [70]. Currently, the most widely accepted TGSCC mechanisms are: anodic dissolution, hydrogen embrittlement, and the combined action of aforementioned mechanisms [2,18,23,54,71]. During SCC of the pipeline within a dilute aqueous environment hydrogen evolution takes place, the evolved

hydrogen can then diffuse into the steel into triaxially stressed sites such as the crack tip [72-73], enhancing the anodic dissolution rate and therefore the SCC intensity [74]. The hydrogen permeation to the material and dissolution of the crack tip and walls is enhanced by the lack of protective film formation in near-neutral environments [59]. Since hydrogen plays a key role in near-neutral SCC, the SCC susceptibility is strongly affected by any factors that alter the hydrogen permeation and adsorption (non-metallic inclusions, dislocation, grain boundaries, etc.) [4,75].

SCC in Acidic Environments

To date, little has been published about SCC in acidic environments, however, this type of SCC is particularly important for Southeast China, where extensive gas pipeline networks are located in the "red soil" region which exhibits acidic conditions with an approximate pH 3.5-6.0 [4,44]. Liu et al demonstrated the existence of a strong correlation between the SCC process and the applied potential [44]. As the potential was changed from less negative to more negative the fracture surface changed from ductile dimples, to transgranular, and lastly to brittle river-bed shaped fracture (more negative potential) [27,44]. This was attributed to the increased of hydrogen due to the decrease in potential [27,44]. The fracture surface in this environment exhibited a transgranular appearance with secondary internal cracks [27]. Furthermore, a bainitic structure exhibited higher SCC susceptibility in an acidic environment, while, a fine ferrite microstructure had the higher resistance [44].

Susceptible Microstructure

Despite the fact that a susceptible microstructure is one of the required variables for SCC to develop, what defines a susceptible microstructure remains ambiguous as SCC—in any of its presentations high-pH or near neutral pH—has been detected in a wide range of pipe steel grades, microstructures, grain sizes, pipe dimensions, fabrication methods, and manufacturers [2,4]. Baker et al. concluded that there was no strong evidence between the amount and type of micro-constituents and the promotion or inhibition of SCC [4,29]. Furthermore, to date no particular metallurgical features have been associated to SCC [4], leading to conflicting opinions on the effect of microstructure and microchemistry of pipeline steel in SCC occurrence. Although some authors believe these factors play a small role [76-77] others have concluded that alloy composition, microstructure, and heat treatment can strongly affect the materials' SCC behavior

[4,44]. Albeit, no definitive relationship between steel composition and structure and high or near-neutral SCC has been determined, some features that appear to play a key role in the SCC behavior have been found [4]. The following sections describe the microchemical and microstructural characteristics that have been linked to SCC.

Steel Strength

The introduction of modern manufacturing methods, such as thermo-mechanical processing (TMCP) and accelerated cooling after controlled rolling led to the introduction of steels with higher strength levels [1-2] and improved mechanical properties. Typically, high strength steels are characterized by a pearlite reduced structure and a low carbon content [32] which results in improved ductility, toughness, and weldability [78]. However, alloying elements such as Mn, Ti, Nb, and V must be added to improve the solid solution strengthening and disperse fine carbide structures [78]. On the other hand, lower strength steels featured a mix pearlite-ferrite structure and higher carbon [32,78-79]. Because of their unique characteristics high strength steels allow for reduced pipe wall thickness and lower costs, therefore they are very attractive to the gas transmission industry [4,80]. Nonetheless, the lack of sufficient evidence on the response of high strength steels to SCC [4,79] adds to the effect of strength on SCC response remaining ambiguous [32]. While some authors have reported that low strength steels are more susceptible to SCC [32] other investigations concluded that the SCC resistance decreases with strength level [79,81]. Moreover, Zhu et al determined that the strength—which is somewhat determined by the microstructure—not only influences the SCC behavior but also the mechanism [81]. In their investigation a high strength X80 steel with an acicular ferrite microstructure exhibited a mix propagation crack propagation mode in a high pH environment, while a low strength X80 steel with large polygonal ferrite microstructure cracked in an intergranular manner [81] raising more question on the role of strength and microstructure and SCC behavior and mechanism [81]. Lastly, it is a well-known fact that high strength steels are highly susceptible to hydrogen embrittlement (HE) [82] and that TGSCC is a hydrogen-dominated anodic dissolution process [74]. According to Galvale and coworkers alloys that show HE are one of the factors leading to SCC in metals [64].

Microconstituents

Pipeline steels are available in a range of microstructures [83] in which ferrite can assume different morphologies such as polygonal ferrite (PF), quasi-polygonal ferrite (QF), acicular ferrite (AF), and bainitic ferrite (BF) [84-85]. Polygonal ferrite (PF) occurs at the highest temperatures and slowest cooling rate and is characterized by equiaxed grains with straight, smooth, and continuous boundaries [86-87]. PF might be found in pipeline steels formed by non-controlled simply continuously cooled practice [88]. In contrast to PG, QF exhibits roughly equiaxed grains with irregular and jagged boundaries, high dislocation density, and subboundaries. QF transformation takes place through short range diffusion across ferrite/austenite boundary [86] due to rapid cooling [87]. The AF and BF morphologies have led to some confusion [89], while some authors have reported that they belong to the same family [87] others make a distinction between them [86] and classified AF as a mixture of QF, BF, few PF, and second phases (M/A islands) [86]. Nevertheless, both AF and BF occur at high cooling rates and exhibit elongated grains and high dislocation densities [86-87]. However, AF forms at an slightly higher temperature range than upper bainite and sometimes contains M/A constituents along the ferrite laths, while bainitic ferrite tends to be more elongated and has a higher dislocation density [80] and iron carbides [89]. The processing conditions dictate the different ferrite forms present in the final product which affect the strength level and consequently the susceptibility to SCC [86]. Cheng et al. suggested that the susceptibility to IGSCC is significantly influenced by metallurgical (microstructure from heat treatment) [4] and electrochemical variables [79]. Nonetheless, to date no obvious evidence between pipeline SCC failures (low pH and high pH) and steel grade and microstructure has been determined [90].

Among the metallurgical factors linked to SCC susceptibility are the differences in strength [70] and/or in electrochemical properties between the different steel phases and constituents [4]; these differences can lead to galvanic effects and to the formation and propagation of cracks [70]. It has been proposed that more uniform or homogenous microstructures such as those predominantly bainitic (quenched and tempered) have higher SCC resistance [76,90] as compared to those with mixed structures such as controlled rolled steels with ferrite-pearlite microstructure [43,70,90-91] and/or coarse grain structures [32]. Furthermore, while some authors have attributed the IGSCC susceptibility of quenched steels which are characterized by a martensitic microstructure to the high internal stresses in the martensite

and the excess carbon trapped interstitially [79] other authors believe that the SCC susceptibility depends not necessarily on quenching but on the quenching temperature [92]. On the other hand, in the case of mixed microstructure such as ferrite-pearlite microstructures carbon appears to play a key role; in a CO_2 environment carbon rich areas such as grain boundary carbides and pearlite act as cathodic sites which promote the dissolution of adjacent ferrite leading to crack propagation (TGSCC) [4,59,66,93].

Despite the fact that quenched and tempered steel with a fine bainitic structure or acicular ferrite exhibited higher resistance to IGSCC than controlled rolled steels with ferrite-pearlite microstructure [43,70,90-91], low temperature products such as bainite and tempered martensite are highly susceptible to hydrogen embrittlement (HE) [44,79] while pearlitic structures exhibit higher resistance [82]. This could be attributed to the fact that the sensitivity to HE is directly proportional to the steel strength [94]. Hydrogen has been linked to the degradation of the mechanical properties of steels [83] as it cannot only lead to HE but it can also increase the material susceptibility to near-neutral SCC [4,92]. Environmental degradation mechanisms such as SCC or HE compromise the electrochemical corrosion of the metal in which the electrons created by the anodic reaction are consumed by the cathodic reaction producing atomic hydrogen [94-95]. Consequently, depending on the environment-material combination the atomic hydrogen can penetrate into the steel, concentrate in the lattice defects (voids, vacancies, dislocation, inclusions), reduce the materials ductility, and induce cracking (if hydrogen threshold for cracking is reached) [83,95-96], or it can diffuse into the tip of the crack and promote crack propagation [44,94,97]. Since hydrogen can facilitate the initiation of SCC, SCC and HIC have been reported to be competing mechanisms, below certain pH or potential or if a certain hydrogen concentration is reached HIC becomes the dominating cracking process [74]. Among the factors that can influence the hydrogen diffusion into the steel are the phases present, grain boundaries, vacancies, dislocations, non-metallic inclusions, and precipitates [83], all of which can act as hydrogen traps and either reduce or increase the hydrogen diffusivity into the metal [83].

The relationship between microstructure and hydrogen trapping efficiency has been studied by different authors. Park et al. concluded that the trapping efficiency in an X65 steel increases in the following order; degenerated pearlite, bainite, and acicular ferrite [83]. Although AF has a higher

hydrogen trapping efficiency and therefore higher potential for cracking sites, the AF hydrogen induced cracking susceptibility is lower than that of bainite partly because its high toughness impedes crack propagation [96]. Likewise El-Danaf et al. reported that a pipeline steel with an acicular/ferrite microstructure and Nb additions exhibits good strength and toughness—two desirable characteristics for the pipeline industry [1,6,86]—due to the interconnecting characteristics of the laths and the presence of small carbonitrides and M/A films, these factors can inhibit dislocation movement and arrest/deflect cracks [88].

Grain Size

The effect of grain size on the corrosion resistance of an alloy appears to be strongly correlated to the environment-material combinations [98]. However, a complete understanding of its effects is still missing partly because as stated by Ralston et al. it is difficult to isolate this metallurgical feature from other microstructural characteristics in order to study its effect [99]. Therefore, some of the findings appear to be contradictory; a number of researchers have suggested that as the grain size decreases the susceptibility to corrosion decreases as well [99]. This theory is supported by Green et al. results, in which SCC cracks initiated more readily in a coarse grained 302 stainless steel (ASTM No.5) as compared to a fine-grained material (ASTM No.9) [100]. Contrary to these findings, other authors reported that decreasing grain size increases the corrosion susceptibility as finer grains can provide more sites for corrosion initiation [99]. Additionally, grain size can also influence the materials response to hydrogen absorption and therefore to TGSCC [101]. In their investigation Hag et al. found that smaller grains about 45 μm (ASTM G No. 5.5) were more efficient in trapping hydrogen at nodes and triple points and thus reducing the hydrogen mobility and diffusivity into the metal as compared to large polygonal ferrite grains (e.g. normalized microstructures) [83]. Nevertheless, trapped hydrogen increases the number of potential crack nucleation sites at the surface [96].

As mentioned before, the electrolyte exerts a strong influence on the effect of grain size on the corrosion response because of the unique electrochemical properties of grain boundaries and triple junctions [99] which can lead to preferential dissolution in specific electrochemical circumstances while remaining unaffected under other conditions [99]. Therefore, a fine grain structure has been reported to

be detrimental in electrolytes that promote active behavior while it can be beneficial in those that promote passivity, due to the fact that finer grains exhibit a more rapid repassivation rate and more stable films as compared to coarser grain structures [99]. Furthermore, grain refinement can reduce impurity segregation by reducing the compositional differences between the grain interior and the grain boundary. Texture is another characteristic that can have a direct influence on the SCC response [4,102]; it has been reported that deformed and elongated microstructures are more effective in deflecting crack growth and inhibiting crack propagation [4,103]. Furthermore, after hydrogen charging microcracks were observed in polygonal ferrite boundaries and sub-grain boundaries but not in those of acicular ferrite [81].

Other Metallurgical Features

Heterogeneous metallurgical features such as banding, mill-scale, and stress gradient-vacancy relationship can also influence the SCC response of a material [102]. Banding is a structural inhomogeneity characterized by alternating bands of different constituents, such as ferrite and pearlite [102]. The anisotropic behavior of this metallurgical feature has a significant influence on tensile ductility and fracture toughness [102]. Furthermore. it can facilitate the SCC rate if the cracks lie in the banding direction [102] and enhance the hydrogen degradation effect [104-105].

The incidence of corrosion product deposit and scale on the pipe surface has been also related to SCC of pipelines [4,97], studies have shown that surface scale leads to higher SCC susceptible as compared to a polished surface [32,90]. The porous structure of the corrosion deposit on the pipeline surface can lead to an electrochemical reaction which can result in serious pitting and the formation of crack initiation sites [4,97]. Additionally, applied stress can weaken the scale and increase the steel level of corrosion [106]. Another factor that can contribute to SCC is a decarburization layer at the rim [32]. Lastly, SCC crack propagation has also been attributed to the weakening ahead of the crack tip due to cavities produced by the agglomeration of vacancies at the crack tip as result of the stress gradients in this region [102].

Stress, and Plastic Deformation

Pipelines are subject to different conditions that can cause localized microplastic deformation below the yield stress of the steel which could significantly impact the material's response to SCC [75].

Some studies determined that surfaces with intense cold work stimulate the initiation of SCC [102]. During plastic deformation as the amount of deformation increases the number of defects increases as well. In materials with high stacking fault energy (SFE) primarily dislocations interact with secondary dislocations leading to the formation of dislocation loops, tangles, and eventually dislocation cells due to the easy of cross-slip; meanwhile, in low stacking fault materials where cross-slip is rather difficult, dislocations form planar arrangements even at high strains [107]. Since dislocations are an essential element in the deformation process, some authors have suggested that their behavior can qualitatively predict or affect the susceptibility to SCC [108]. Nevertheless, dislocation theories appear to mainly relate to TGSCC and not necessarily to IGSCC.

The surface layer of the pipeline has been reported to exhibit higher dislocation densities as compared to the core due to differences in cooling rate between rim and core [83], machining effects [102], and because the surface layer deforms before the bulk [75]. Furthermore, laboratory studies have reported crack initiation at the edge of the test specimens as a result of the low plastic deformation restrictions in the region [70]. Since dislocations can act as hydrogen trapping sites [83] a higher dislocation density implies a higher number of available hydrogen trapping sites, higher hydrogen adsorption coverage on the surface [75] and therefore higher number of potential crack nucleation sites [96]. Moreover, mobile dislocation can not only trap hydrogen but they can transport it to possible cracking sites reducing the SCC resistance [89]; this effect can be eliminated by the presence of small carbonitrides which can impede dislocation motion and thus block the hydrogen from potential sites [89,109]. However, if particles are too large (particles > 1 microns) they cannot pin the dislocations and the material becomes susceptible to hydrogen embrittlement [110]. Hydrogen can also reduce the atomic cohesion by expanding the lattice and therefore increasing the corrosion susceptibility [74] or migrate to the crack tip and promote anodic dissolution [97] and thus crack propagation [75]. Migration of hydrogen to crack tip is aided by the increased in the hydrostatic stress field around the crack tip caused by the increased in yield strength and decrease in ductility as result of large amount of cold work [75].

Other theories about the role of dislocations suggest that the strain energy stored in dislocations from the deformation process can promote the dissolution of specific sites as the corrosion of a stressed

metals can release energy [111]; that linear arrays of dislocations can act as stress concentrators and therefore induce localized cracking and TGSCC [112]; that dislocations can cause the crack tip to be film-free [113]; and that the coalescence of dislocations can aid to formation of corrosion tunnels [52]. On the other hand, Smith et al concluded that in aluminum alloys dislocations and dislocations pile-ups are not necessary for SCC [114].

Role of Inclusions

The pipeline surface condition—pits, non-metallic inclusions, scale, and persistent slip bands—play a key role on crack initiation during TGSCC [69-70]. Dissolution of or around non-metallic inclusions can lead to pit formation which can result in crack formation if an specific size is achieved (larger non-metallic inclusions result in larger pits in which cracks can form more readily) [70]. Furthermore, it has been suggested that the inclusions' chemical composition, morphology, and length are critical in determining their effectiveness as crack nucleation sites [4,44,80]. Contrary to this, the inclusion volume fraction appears to be non-significant to SCC [76].

Brittle and matrix incoherent particles such as Al enriched particles can successfully trap hydrogen at the matrix-particle interface voids and eventually form fissures and cracks [44]. In contrast, no cracking was associated to $Si0_2$ particles, presumably due to the fact that they can easily deformed and thus relieve residual stress [44]. Moreover, the role of manganese sulfides remains controversial; while in some studies no cracks where associated with elongated MnS inclusions [44,115] other investigations reported that typically MnS inclusions at the surface can lead to localized corrosion attack [72]. MnS can lead to corrosion attack because they can act as pit initiation sites in a chloride solution [116] and induce hydrogen induced cracking (HIC) as their morphology can reduce the fracture toughness of the material [95]. Therefore, MnS inclusions have been classified as one of the most detrimental pipeline inclusions [44].

Alloying Elements

Carbon and low alloy steels—main pipeline materials used—are susceptible to SCC in a wide range of environments [4]. Nevertheless, it has been reported that SCC is a system in which the environment, the alloying additions, and SCC are strongly correlated [4,50]. For example, additions of molybdenum to low alloyed steels improve the SCC resistance in carbonate/bicarbonate solution;

however, the effect is the opposite in a caustic environment [4]. In their investigation Poulson et al. analyzed the SCC fractography in carbon steels concluding that the crack path depends on heat treatment, environment, potential, and alloying elements [50]. The elements that are believed to have a significant impact in IGSCC are; sulfur (S), phosphorous (P), nitrogen (N), and carbon (C) [66]. Nevertheless, the role of this elements is complex and appears to depend on many factors. On one hand, it was determined that additions of C, N, or P to pure Fe increased its cracking susceptibility [66,113] and that the SCC propagation on an X52 steel was presumably influenced by P found near the crack tip where no grain boundary carbides were detected [59]. Other investigations have concluded that the segregation of S, P, and N were not likely to cause IGSCC as no segregation of this elements to the grain boundaries was found [117]. Furthermore, Grabke et al. determined that the role of P on IGSCC mainly depends on the corrosion conditions, potential, and electrolyte rather than on the amount of P [118], concluding that: P can lead to SCC of low carbon steels in caustic environment at oxidizing potentials, that it has no effect in caustic solutions at low potential, and has little to no effect on carbonate/bicarbonate solutions [4]. Additionally, under certain potentials (-300 to -100) P can aggravate the IGSCC in nitrates and hydroxide solutions [118]. Nonetheless, it was concluded that P segregation is not the origin of IGSCC [119]. The SCC behavior of pipe steels has also been associated to other elements such as titanium (Ti) which is believed to improve the resistance of ferritic steels to caustic SCC since Ti bonds to C and N, reducing the amount of free interstitial atoms and the electrochemical characteristics of steel [120]. Additions of chromium (Cr) and nickel (Ni) can also improve the resistance to SCC; however, this option may not be economically viable [4].

Carbon and nitrogen at the grain boundaries are critical elements for IGSCC, since very small amounts are required to cause SCC [4]. However, carbon might be the main reason for the IGSCC as compared to nitrogen [93]; as saturated grain boundaries with segregated N or S were not sensitive to intergranular corrosion in a hot nitrate solution [121]. Moreover, in another experiment as N content was increased no SCC susceptibility was observed [92]. Currently, there are many different theories about the role of C in IGSCC; while steels with a low C content have been reported to be more susceptible to SCC than those with high C content; higher carbon content is believed to facilitate transgranular cracking

[92,120]. Furthermore, Green et al. concluded that SCC cracking susceptibility of mild steels depends not only on the carbon content but on the carbon distribution as well [100] determining that up to 0.1% carbon content interstitial carbon or Fe_3C can segregate to the ferritic grain boundaries increasing the IGSCC cracking susceptibility. Nevertheless, it has been suggested that the effect of cementite in grain boundaries should be minimum due to its lack of continuity [122]. On the other hand, Tauber et al. believe that carbon at the grain boundaries—most likely present as fine cementite particles—was responsible for the intergranular corrosion of iron in a nitrate solution, as the carbides may have remain unpassivated [121].

The cracking resistance of a material was reported to increase as the carbon content was increase above 0.10% possibly because carbon formed pearlite colonies and therefore less carbon was available to segregate to the grain boundaries [100]. Parkins et al. determined that the dangerous carbon content ranges from 0.03%-0.2% [92] and other authors reported that in a hot NaOH solution there is a higher SCC sensitivity in the 0.009-0.05% C range [120] and that SCC is even possible below 0.001% carbon [92]. Furthermore, Wang et al. analyzed the C segregation to grain boundaries on X70 pipeline steel finding a relatively small carbon concentration which was determined to be insufficient to cause IGSCC, instead it was believed to be beneficial as it could cause some grain boundary strengthening making the material more resistant to deformation and therefore to cracking [123]. Other theories about the role of carbon state that C at the grain boundaries can lead to the absorption of species that reduce the surface energy which leads to the formation of microcracks, or that C lowers the grain boundary potential and gives rise to the anodic dissolution of the grain boundary and passivation of the grain [122]. Contrary to this finding, Flis et al concluded that interstitial constituents such as C and N appear to have no influence in enhancing the grain boundary reactivity, however preferential corrosion was observed with segregated substitutional constituents [124].

Lastly, the susceptibility of carbon steels to IGSCC has been attributed to the inability of the grain boundary to undergo passivation due to the grain boundary enrichment in carbon and other detrimental solutes [93,120]. Grain boundaries are regions with a higher free energy [92] and during processing if carbon content in the boundary becomes large enough carbide precipitation takes place; carbides then grow by the accumulation of more carbon, however if not sufficient carbon for carbide formation is

available interstitial carbon will segregate to the grain boundaries [93]. The existence of carbides and carbon at the grain boundary are believed to disturb the growth of the protective oxide film by introducing discontinuity [93]. Therefore, the grain boundaries will passivate less than the grain interior leading to anodic dissolution of the grain boundary [120]. Furthermore, ferrite is more prone to passivation in a high pH environment [93]. It has also been suggested that low carbon content steels are more prone to passivation deterioration in contrast to higher carbon content steels which can form a protective magnetite (Fe_3O_4) film [93,120].

Strain Aging

Strain aging is a time dependent diffusion process in which interstitial atoms such as carbon and nitrogen migrate to dislocations impeding their further movement and therefore increasing the steel resistance to plastic deformation [2,4,125] which leads to an increase in the yield strength and ultimate tensile strength, but to a decrease in elongation [4,125]. The migration of solute atoms to dislocations can occur while the metal is being deformed (dynamic) or after the application of plastic strain (static) [2,4], the latter usually occurs at room temperature while the former takes place at higher temperatures [4]. Over time more precipitates are formed and their size increases until they become so large that they can no longer impede dislocation movement (over-aging) leading to the softening of the material [2].

The main interstitial atoms involved in strain aging of carbon steels are carbon and nitrogen. These two elements exhibit high solubility in ferrite, high diffusion coefficient, and a strong capacity to block dislocation movement [2,4]. However, their effect is strongly affected by temperature; since nitrogen exhibits higher solubility in ferrite at lower temperatures as compared to carbon, below 150^{o}C nitrogen is the main strain aging contributor [2,4]. In order to prevent the migration of N and C; carbide (Mo, V, Nb) and nitride (Al, Ti, B, V, Nb) forming elements are added to diminish the amount of “free” nitrogen and carbon [2]. However, in the absence of these elements, only about 0.001% and 0.002% of C and N are required to cause strain aging [4]. Furthermore, the steel manufacturing process appears to play a role in strain aging, partially deoxidized steels exhibit higher susceptibility while fully deoxidized steels have a higher resistance [2]. The susceptibility to strain aging according to deoxidizing practice in deceasing order is: rimmed steel, semi-killed, silicon-killed, aluminum-killed, killed and microalloyed [2]. While

deoxidizing practice and chemical composition play a role in strain aging, steel microstructural constitutes such as ferrite, bainite, and martensite have no effect [4]. However, grain size does affect the materials response to strain aging due to the high dislocation density [4].

During pipeline operation, strain aging is a major concern [4] as temperature and plastic strains and long service terms are involved. The plastic strain required for aging can arise from steel manufacturing (rolling, forming, and welding) and from pipe operation (mechanical damage, ground movement, and bending) [2,4]. On the other hand, temperature can provide the necessary kinetic energy for interstitial atoms motion, therefore, the higher temperature near the compressor station 60ºC (140ºF) and/or from fusion bonded epoxy (FBE) coating application in which the pipe surface can reach about 250ºC (482ºF) could play a role in pipeline strain aging [4]. Despite the fact that steel pipe is subject to natural aging, and that it can be accelerated by the service conditions, [126] its effect on the degradation of pipeline service life and SCC susceptibility remains unclear. Kotrechko et al. studied the effect of long time service (30 years) on the mechanical properties of 17GS pipeline steel (0.14-0.20% C); in their investigation the pipeline experienced an increase in the yield strength and a decrease in ductility (base metal embrittlement), the rise in the yield strength was attributed to changes in the steel substructure due to aging [127]. Kotrechko el al. concluded that the main contributors for the decrease in toughness after long time service was the increase in yield strength [127]. During a laboratory investigation of grade X100 steel in diluted bicarbonate solution, results showed that under aging conditions the steel exhibits high susceptibility to SCC; an aging time of 6 days at 107ºC was found to be equivalent to 10 years of service at 40ºC for this grade of steel [4]. Accelerated aging at 250ºC for 1 h resulted in toughness deterioration of a low strength steel [126,128]. Contrary to this findings, other studies found no indication of detrimental impact of aging on fracture initiation and the longtime aging at room temperature (21 years) of an aluminum-killed steel which exhibited no significant changes in the mechanical properties [2].

Nevertheless, strain aging is a complex phenomenon in which the materials response depends on multiple factors such as the material's chemical composition, amount and direction of pre-straining, aging temperature and time, and the prior materials heat treatment [4]. Interestingly, the USA pipeline design code assumes that the material design properties remain constant during the pipeline service life [4].

Moreover, until recently the latest pipeline designs require three design codes some of which are applied to the SMYS to ensure that the pipeline remains in the elastic region during operation, however, early pipes (which constitute the majority of the current infrastructure) utilized only one design factor [4].

SCC Detection

Since the discovery of SCC much progress has been made towards a better understanding of this critical phenomena, however the prediction and location of SCC cracks on operational pipelines have not been fully developed [27] and can represent major financial and technical disadvantages [28]. The assessment of the SCC susceptibility must be a requirement for every segment of pipeline system [4] in order to ensure the reliable performance of the existing gas transmission pipes. Therefore, different techniques such as in-line inspection, direct assessment, and hydrotesting are available to gather information on the potential pipeline risk. Nevertheless, all of these techniques have some drawbacks and some degree of uncertainty [16,28,129]. Thus, the ultimate goal to prevent this insidious form of corrosion is to design steels resistant to SCC [32].

Research Plan

3.1 Research Objectives

The focus of this investigation is to gain insight into the metallurgical features of highly SCC susceptible pipeline materials by performing a systematic microstructural characterization to reveal not only the general microstructural features but also the metallurgical state of the region near the surface layer. This study will attempt to uncover the critical factors that are applicable across the different pipeline materials and therefore expand our understanding on what defines a susceptible microstructure. In this manner we can contribute in designing more SCC resistant materials. The specific objectives of this research are listed below:

- To identify the general microstructural features of gas transmission pipeline materials removed from service due to SCC.
- To compare the general microstructural features to those exhibited by an SCC-free pipeline removed from service due to pitting.
- To identify the sub-surface microstructural conditional state of highly SCC susceptible vintage pipelines and identify any trends.
- To establish thru-thickness hardness gradients in SCC and SCC-free pipelines which may be the result of residual deformation in order to understand its role on SCC susceptibility.
- To identify the chemical composition of SCC and SCC-free pipeline materials.

3.2 METHODS

3.2.1 Materials

Sections from different gas transmission pipelines containing stress corrosion cracks were used for the present investigation. It is important to note that all the investigated pipelines exhibited different chemical composition, dimensions, and service and processing conditions. Figure 8 to Figure 11 present the as-received sections from all of the investigated pipelines.

Figure 8. As-received sections from pipeline #1.

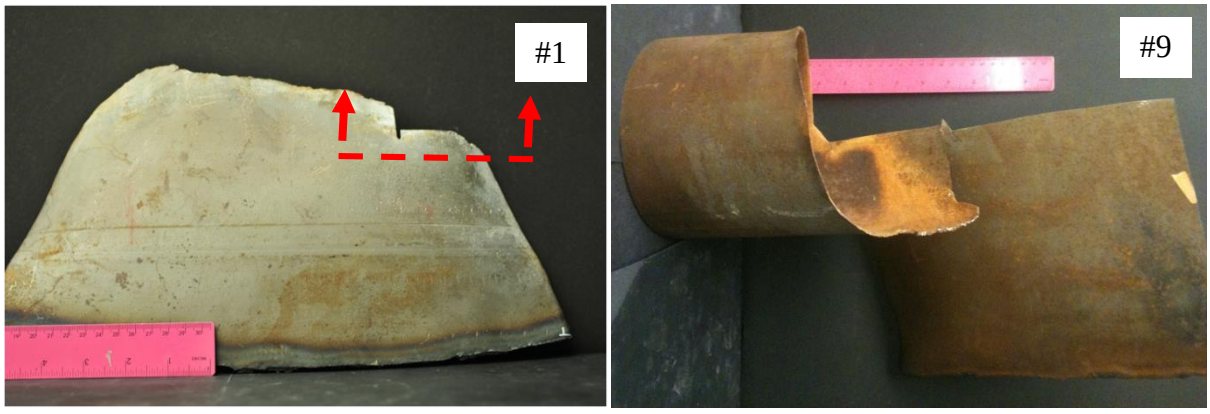

Figure 9. As-received sections from pipeline #2.

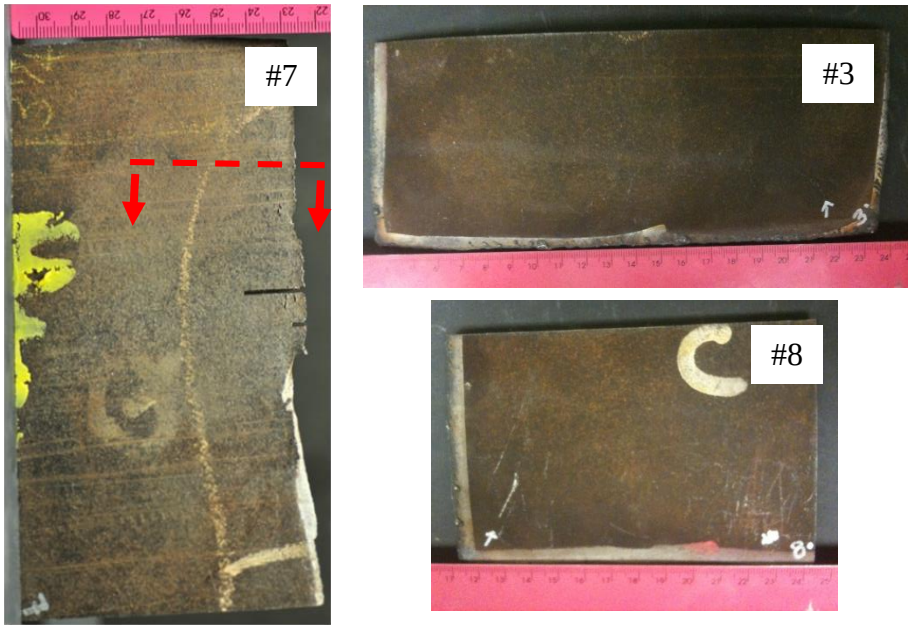

Figure 10. As-received sections from pipeline #3.

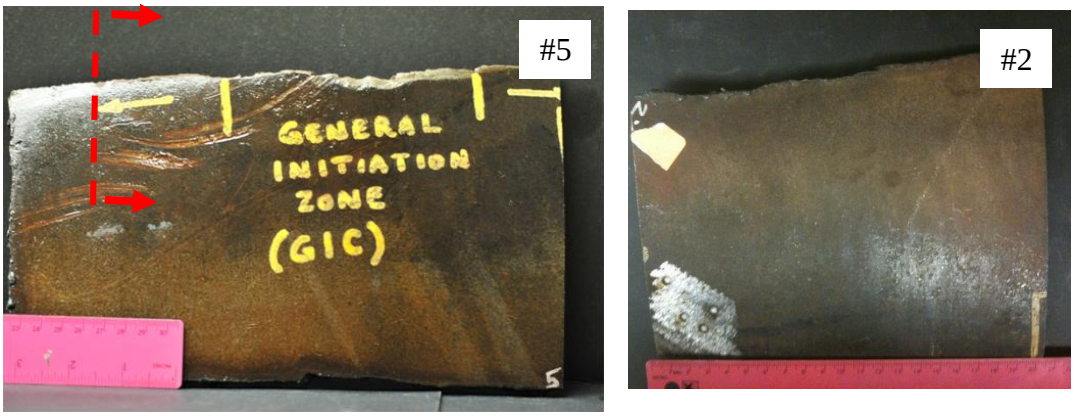

Figure 11. As-received sections from pipeline #4.

Figure 12. As-received sections from pipeline #5.

3.2.2 Non-Destructive Evaluation

Wet fluorescent magnetic particle inspection (WFMP) was performed on the as-received pipeline's sections to identify the pre-existing cracks. The samples were cleaned with solvent, to remove

oils, dust, dirt, and any other contaminants. Subsequently, the magnetic field was applied with a hand yoke and the parts were bathed with the suspension. Parts were then analyzed under a UV light. The observed crack colonies were photographed.

3.2.3 Chemical Analysis (OES)

OES was used to identify the pipeline material chemistry. Testing was performed in a region away from the cracks. The surface was prepared with an angle grinder grit 36. All of the received sections from the pipeline were tested. A minimum of three tests were performed per sample and an average calculated.

3.2.4 Chemical Analysis (EDS Mapping)

Elemental EDS mapping was performed in two distinct regions, close to the OD and in the middle section of each pipeline in order to get a general perspective of the distribution and concentration of different elements such as C, P, S, Mn, and Si, which are some of the elements that have been linked to SCC. Each chemical element is represented by a different colors and the concentration by the brightness [130]. Figure 13 represents the analyzed areas.

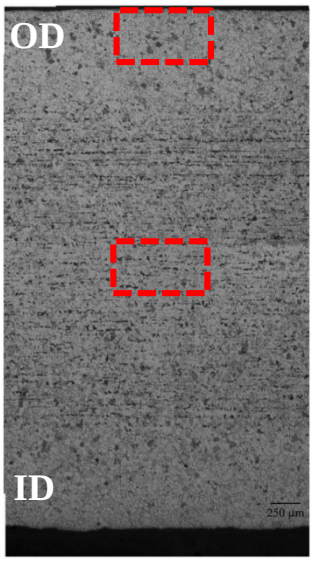

Figure 13. Elemental EDS mapping investigated regions indicated by the red box.

3.2.5 Microhardeness

Vickers microhardness testing was carried out at room temperature using a 500 g load. A hardness profile from the OD to ID was investigated in two sections; in an area adjacent to the SCC cracks and

away from the cracks. The surface was polished and etched prior to hardness testing. Tensile strength values (MPa) were estimated from HV results using the expression UTS= 3.2·HV, where 3.2 is a constant determined to be the optimal for carbon pipeline steels [131].

3.2.6 Microstructural Characterization

Optical Microscopy

For all of the provided pipelines microstructural characterization was performed in different cross-sections, on a crack containing region and away from the cracks. Figure 8 to Figure 11 indicate the sample preparation from crack containing regions. The material was sectioned in the appropriate direction with a water-cooled abrasive cut-off saw. Samples were then mounted, and polished following standard metallographic techniques. For optical microscopy after polishing, samples were etched with 2% Nital reagent (98 ml methanol and 2 ml nitric acid). Specimens were observed with a light microscope to determine the main microstructural characteristics in addition to SCC crack morphology. The grain size was measured by the linear intercept method and the corresponding ASTM G No. calculated per ASTM E112. The volume fraction of the different microconstituents was calculated by the systematic point count method (ASTM E562).

Transmission Electron Microscope (TEM)

Detailed microstructural characterization of the pipeline sub-surface state was achieved by means of the TEM. In order to observe the dislocation structures, grain boundary characteristics, and precipitates; thin foils were prepared from a section away from the cracks and close to the outside diameter. Samples were ground to 0.2 mm in thickness from the inside diameter, keeping the OD intact, as shown in Figure 14. Samples were then electropolished to perforation using a solution of 670 ml methanol and 330 ml nitric acid, at a voltage of 13.5V and a temperature of -15.5 ºC for pipeline #1. The rest of the investigated pipelines were electropolished utilizing a solution of 950 ml acetic acid and 50 ml perchloric acid, at a voltage of 40V and a temperature of 13.8 ºC. TEM samples were prepared parallel to the OD.

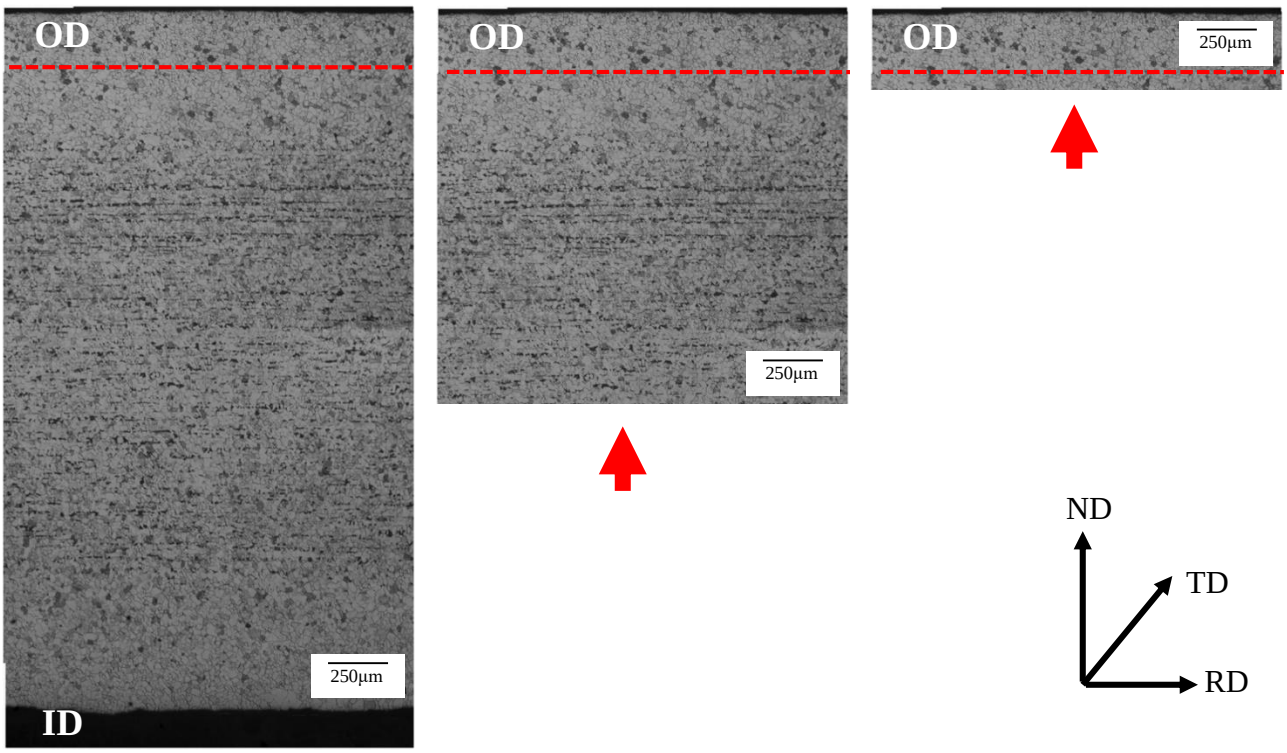

Figure 14. TEM sample preparation. The red arrow indicates the grinding direction and the red line the side view from the area that was analyzed. 2% Nital.

Results

This chapter presents the results from the microstructural and chemical characterization of vintage gas transmission pipeline materials that exhibit high SCC susceptible.

4.1 PIPELINE #2

4.1.1 Background Information

The pipeline #2 consisting of 15.2 cm (6 inch) OD, nominal wall thickness (wt.) of 3.76mm (0.148 in) was constructed by Newport Steel, it was installed in 1947 and hydrotested to 81% SMYS for 24 hours in 1967. This pre-1970 electric resistance welded (ERW) pipe (vintage) was built from grade A steel and was coated with a coal-tar enamel. No information regarding impressed-current cathodic protection (CP) was available. In July 1993 pipeline rupture occurred in NM; upon investigation it was determined that the primary fracture surface was axially oriented and contained numerous axial secondary cracks. The maximum crack depth was determined to be 79.4%. For purposes of this research this pipeline was identified as pipeline #2. Figure 9 presents the as-received sections of this pipeline and Table 4 summarizes the pipeline attributes and operating conditions.

Table 4. Pipeline #2 Attributes and Operating Conditions

Pipeline attributes and operating conditions			
Construction date	1947 installed	**Pressure @ failure**	5MPa (744 psig)
Failure date	1993 rupture	**SMYS**	208MPa(30000 psi)
Manufacturer	Newport Steel	**Classification**	Vintage
Outside diameter	152cm (6″)	**Location**	NM
Wall thickness	3.76mm (0.148″)	**Terrain/soil type**	Dry, red sand
Type of seam	ERW	**Distance-compressor**	n/a
Steel grade	Grade A	**Soil pH**	n/a
Coating	Coal-tar enamel	**CP**	n/a
Max crack length	79.4% wt.		

4.1.2 Non-destructive Evaluation

WMPI performed on section 1 from Pipeline #2, revealed multiple secondary cracks in the region adjacent to main fracture, as shown in Figure 15. Cracks exhibited multiple branching and were oriented perpendicular to the longitudinal axis.

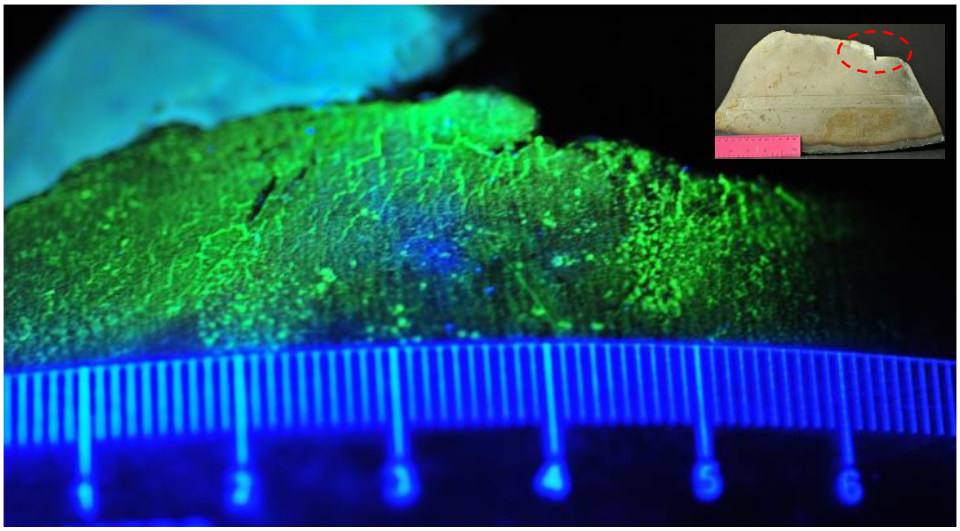

Figure 15. Wet fluorescent magnetic particle inspection revealed multiple cracks oriented perpendicularly to main fracture. Cracks exhibited extensive branching.

4.1.3 Chemical Analysis

Table 5 presents the chemical composition of each of the sections from pipeline #2. Chemical composition indicates that pipeline #2 was most likely made to a rimmed steel practice and was not made to Si or Mn deoxidation practice. Additionally, low Al and residuals also indicate that this steel was not manufactured to a fine grain practice.

Table 5. Pipeline #2 Chemical Composition

Pipeline #2											
Section	C	Si	Mn	Cr	Mo	Ni	Al	Co	Cu	Nb	Ti
1	0.03	0.005	0.32	0.008	0.003	0.031	0.01	0.008	0.06	0.002	0.001
9	0.02	0.003	0.30	0.009	0.004	0.035	0.01	0.009	0.06	0.002	0.001
Average	***0.02***	***0.004***	***0.31***	***0.01***	***0.004***	***0.03***	***0.01***	***0.01***	***0.06***	***<0.002***	***<0.001***

Pipeline #2					
Sample	V	W	Pb	Zr	Fe
1	0.001	0.023	0.01	0.001	Rem.
9	0.001	0.021	0.01	0.001	Rem.
Average	***<0.001***	***<0.02***	***<0.01***	***0.001***	***Rem.***

4.1.4 Elemental Mapping

Figure 16 and Figure 17 present the elemental mapping images from two distinct regions—an area adjacent to the OD and from the core region from pipeline #2. Each chemical element is represented by a specific color and the brightness corresponds to its concentration. The OD region exhibited some small carbonitrides aligned along the rolling direction (Figure 16) and less elongated MnS inclusions as compared to the core region (Figure 17). Furthermore, the OD region also exhibited an apparently slightly higher Si, Mn, and S content (Figure 17). Lastly, carbon content appears to be slightly higher near the core region, nevertheless no quantitative analysis was carried-out.

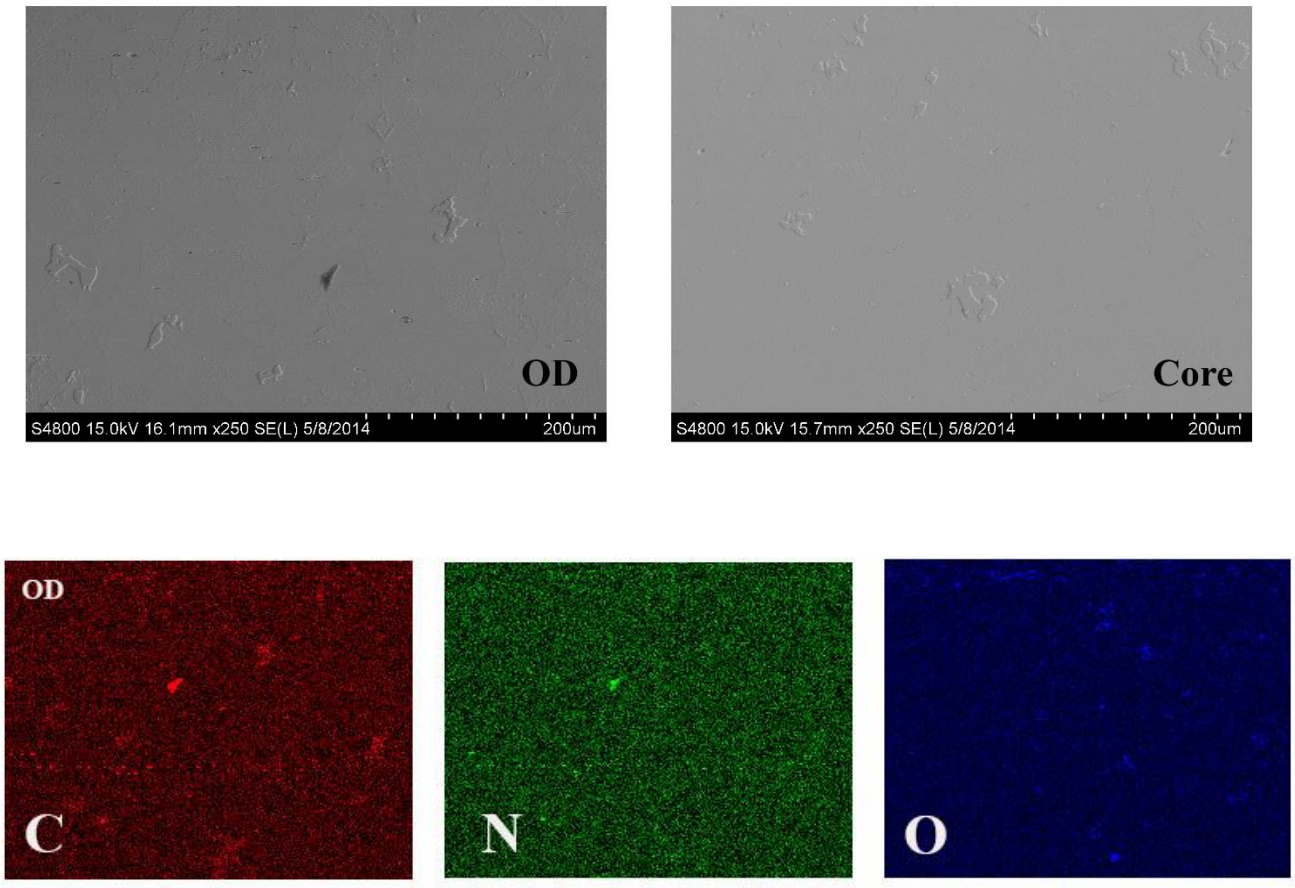

Figure 16. Elemental mapping from a region near the OD (left) and the core (right).

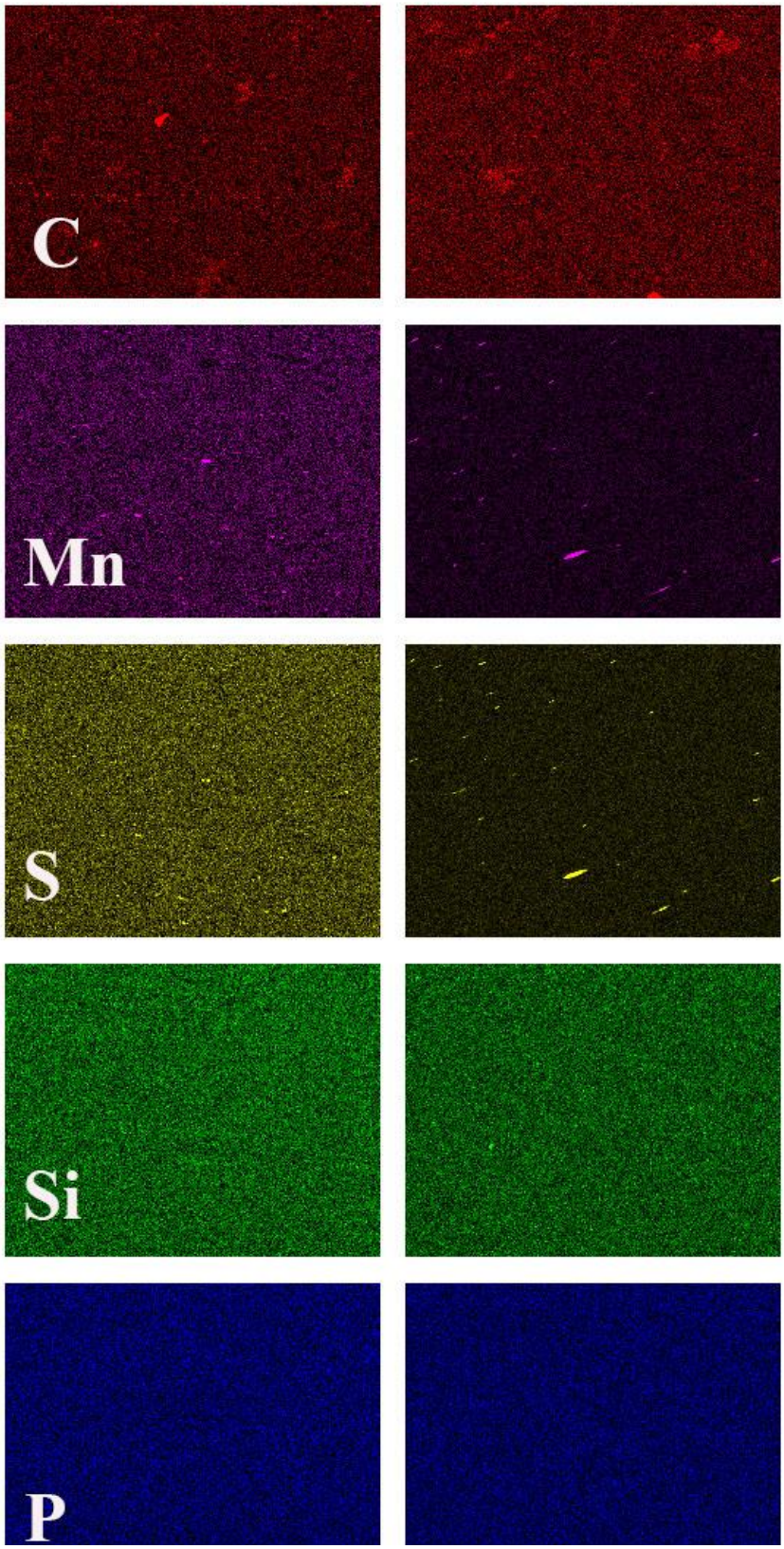

Figure 17. Elemental Mapping from a region near the OD (left) and the core (right).

4.1.5 Hardness

Figure 18 present the hardness profile from the OD to ID from crack containing and crack free regions from pipeline #2. The hardness profile from SCC and SCC-free zones exhibited a similar pattern with a lower hardness in the core region. Additionally, the region containing SCC cracks exhibited slightly lower values near the OD as compared to the SCC-free zone however, differences were minor. The average Vickers hardness and equivalent HRB and tensile strength for each of the analyzed sections are shown in Table 6.

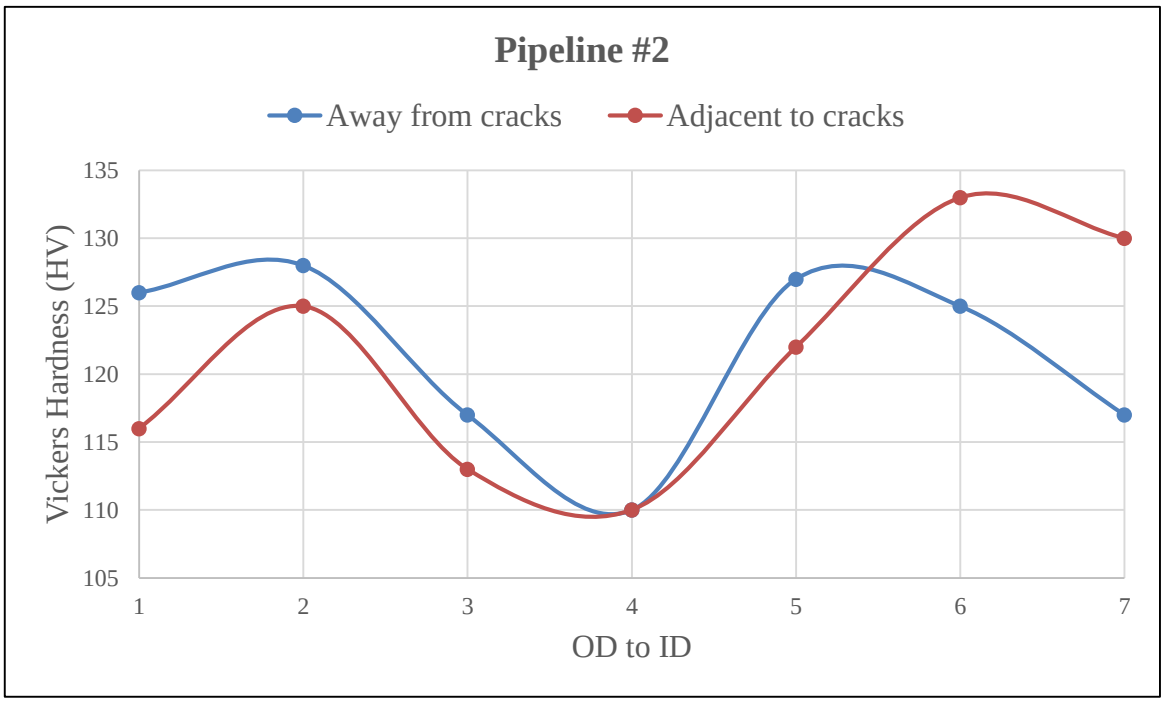

Figure 18. Pipeline #2 microhardness profile.

Table 6. Pipeline #2 Harness Testing Results

Region	Average Vickers (HV)	Converted Average HRB	Equivalent Tensile Strength MPa (psi)
Away from cracks	121	67	388 (56275)
Adjacent to cracks	121	67	388 (56275)

4.1.6 Microstructural Characterization

Crack morphology

The observed SCC in pipeline #2 shown in Figure 19 is characterized by very wide cracks with little branching, and predominantly intergranular cracking with what appears to be small amounts of transgranular attack. Furthermore, some grains appear to be missing (Figure 19 C-D).

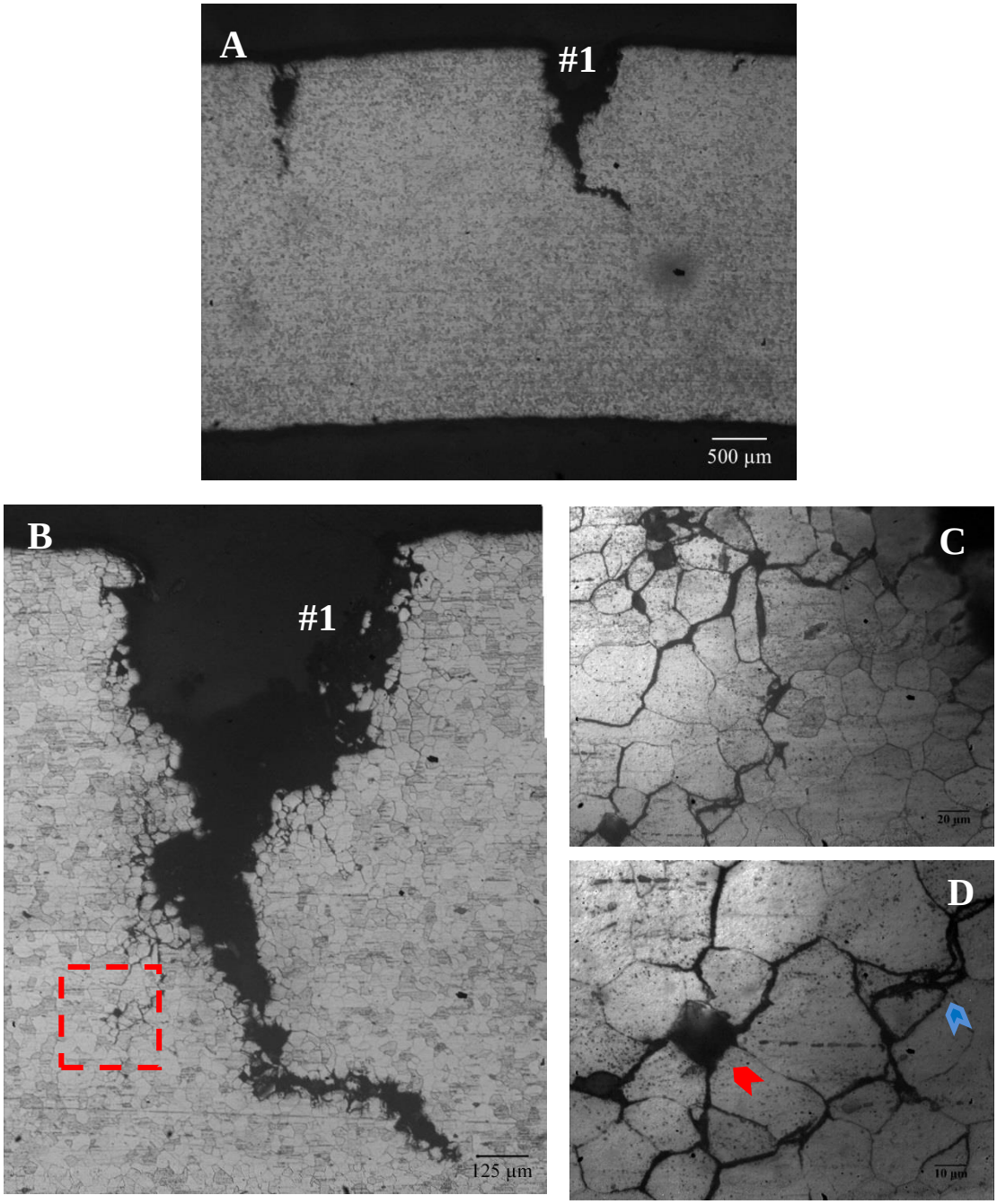

Figure 19. Optical micrographs showing stress corrosion secondary cracks for Pipeline #2. Higher magnification images indicate (B) extensive wall corrosion, (C-D) mix mode crack propagation (blue arrow) and what appears to be missing grains (red arrow). 2% Nital.

Microstructural Characteristics

The optical images (Figure 20) taken from pipeline #2 indicate that the primary microstructural constituents are polygonal ferrite (Figure 20A), cementite films at ferritic grain boundaries (Figure 20B), and small and random pearlite colonies—approximately 0.5-1% volume fraction (Figure 20C-D). The edge and centerline regions of this pipeline exhibited a uniform microstructure with no evidence of banding. Furthermore, the grain size was characterized by very fine grains surrounded by larger grains (Figure 20A). The average grain size was 20 μm (ASTM G No. 8) with no significant grain size differences between rim and core were detected. The microstructure also exhibited inclusions of varying sizes (Figure 20E-F) including smaller more globular inclusions; ogee-shaped and elongated manganese sulfides (MnS) with a maximum aspect ratio of 5 (observed in the core region), and disconnected inclusions (Figure 19D).

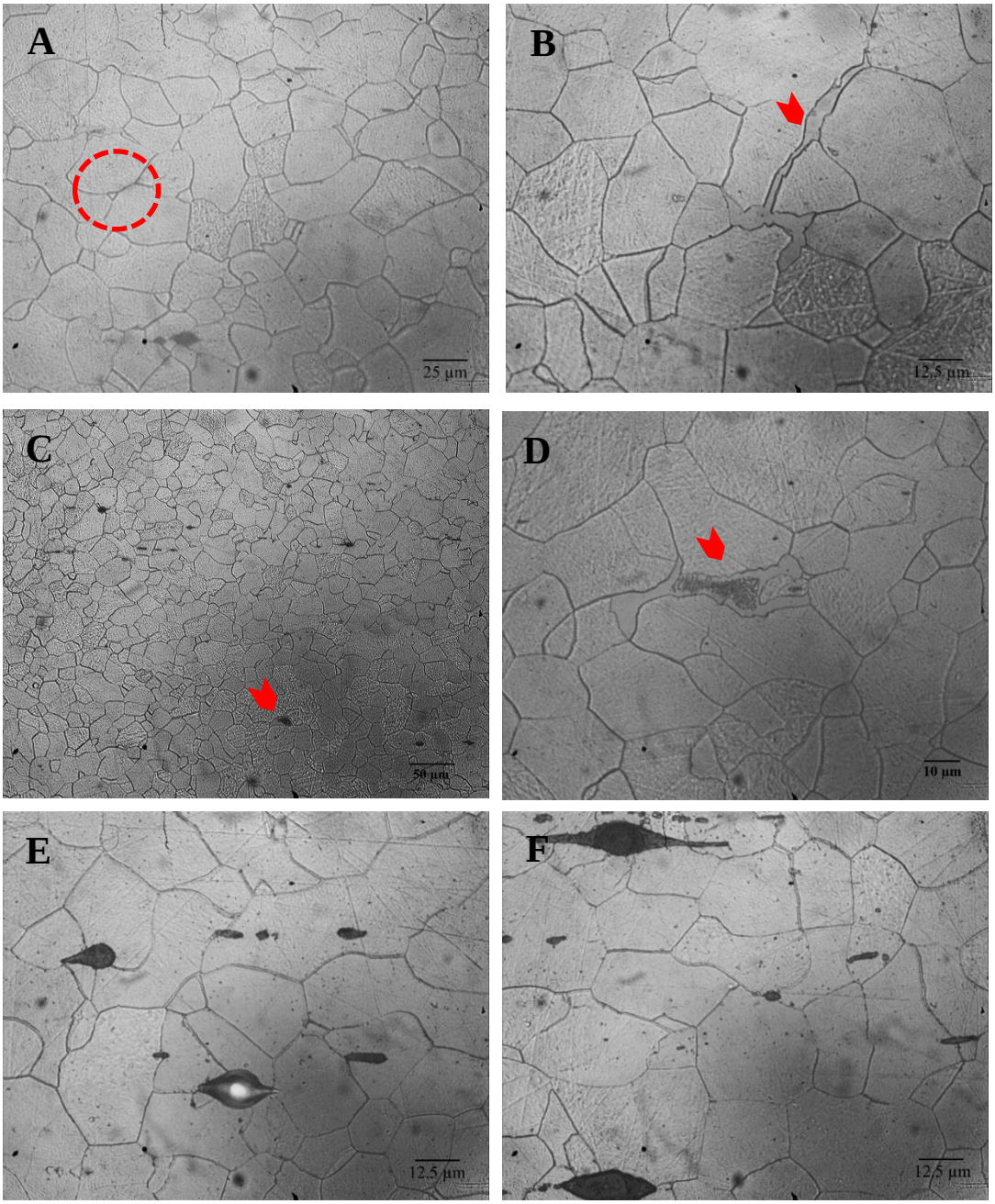

Figure 20. Light micrographs of the microstructural features of pipeline #2 showing (A) polygonal ferrite with a combination of small and large grains, (B) cementite films at ferritic grain boundary, (C-D) small and random pearlite colonies, and (E-F) elongated manganese sulfides. 2% Nital.

The representative bright field TEM images showing the general microstructure of pipeline #2 is presented in Figure 21. Micrographs exhibit what appears to be large polygonal ferrite (PF) grains with dislocation structures (Figure 21 C-D) and small amounts of lath-shaped ferrite. Additional images from the dislocation structure near the grain boundaries and within the ferritic grains are shown in Figure 22-Figure 23.

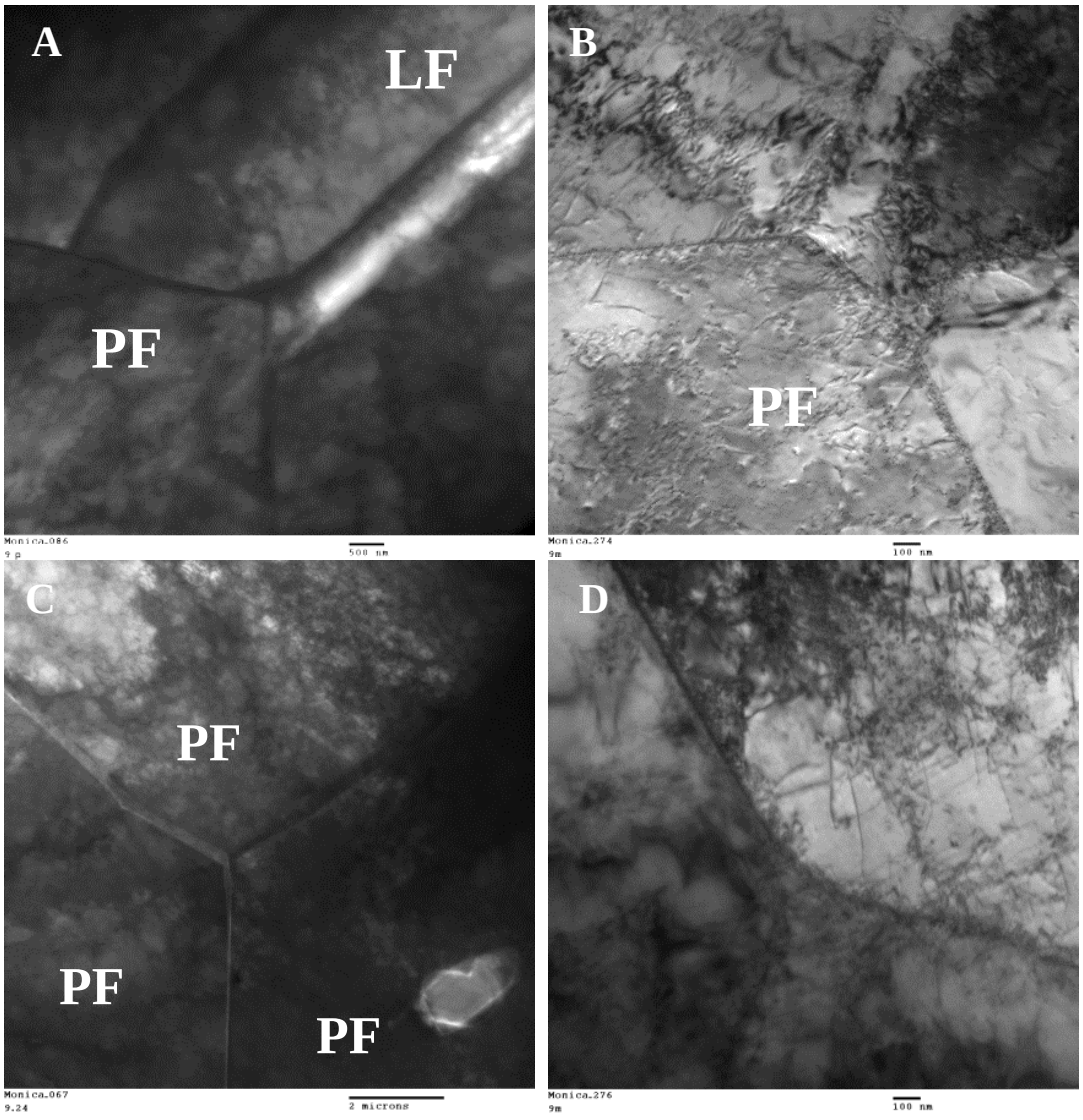

Figure 21. Bright field micrographs suggest that the microstructure is predominantly characterized by polygonal ferrite (PF) grains with dislocation structures.

Figure 22 presents TEM micrographs of ferrite grains that contained a significant number of dislocations in the vicinity of the grain boundary and what appears to be fine precipitation on dislocation lines (Figure 22C-D) and on some grain boundaries (Figure 22D). Figure 23 presents high magnification TEM images from dislocation cells within the ferrite grains. Two distinct dislocation cell morphologies were observed; larger dislocation cells with an approximate diameter of 0.70 µm (Figure 23A-B) and smaller cells with heavy walls (Figure 23C-D). Coarse cuboidal-shaped particles (~0.6-2 µm) were also observed within the ferrite grains (Figure 24).

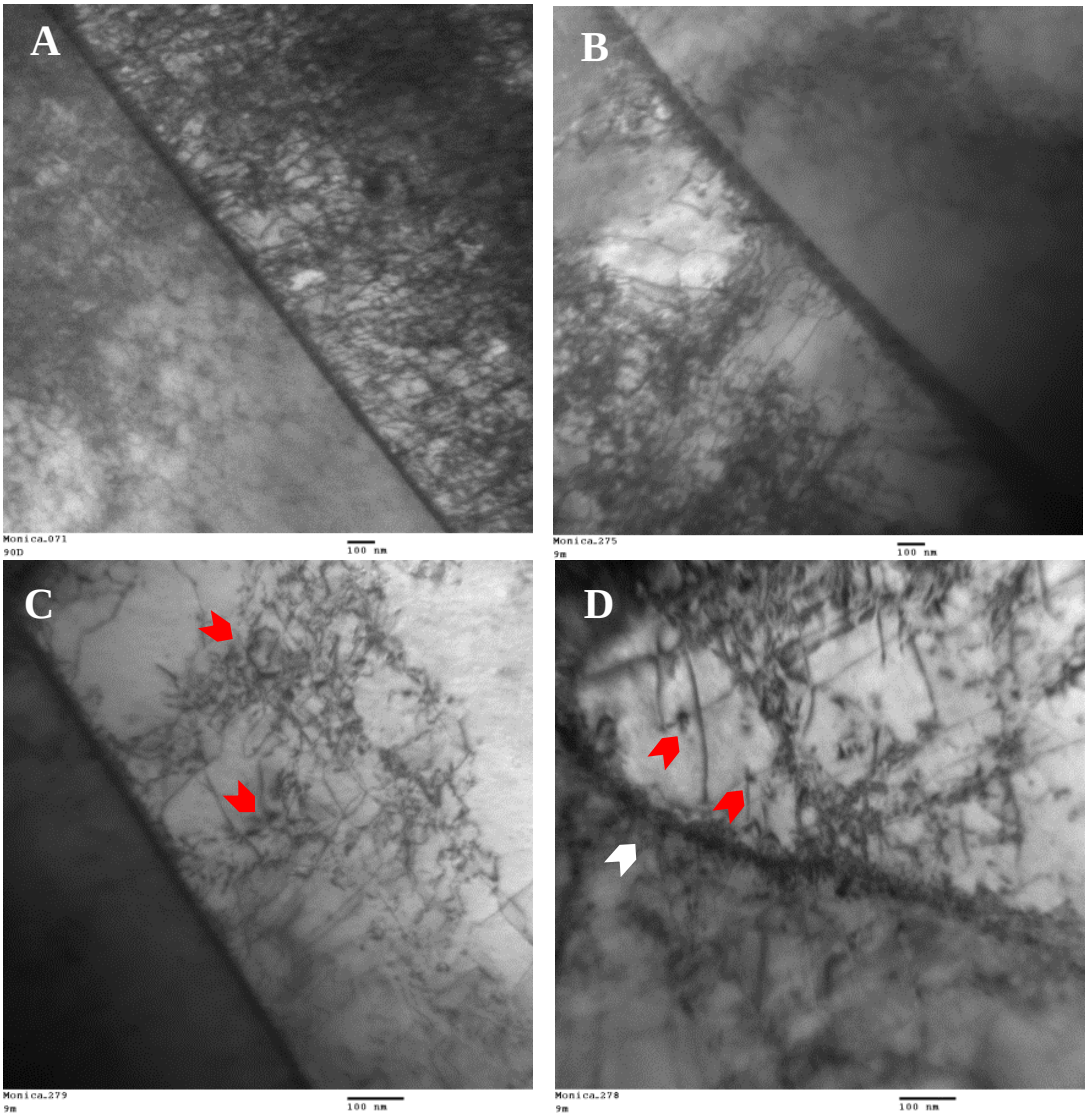

Figure 22. Transmission electron micrographs of pipeline #2 showing (A-D) dislocation near the grain boundary, (C-D) precipitation on dislocations (red arrow) and (D) on the grain boundary (white arrow).

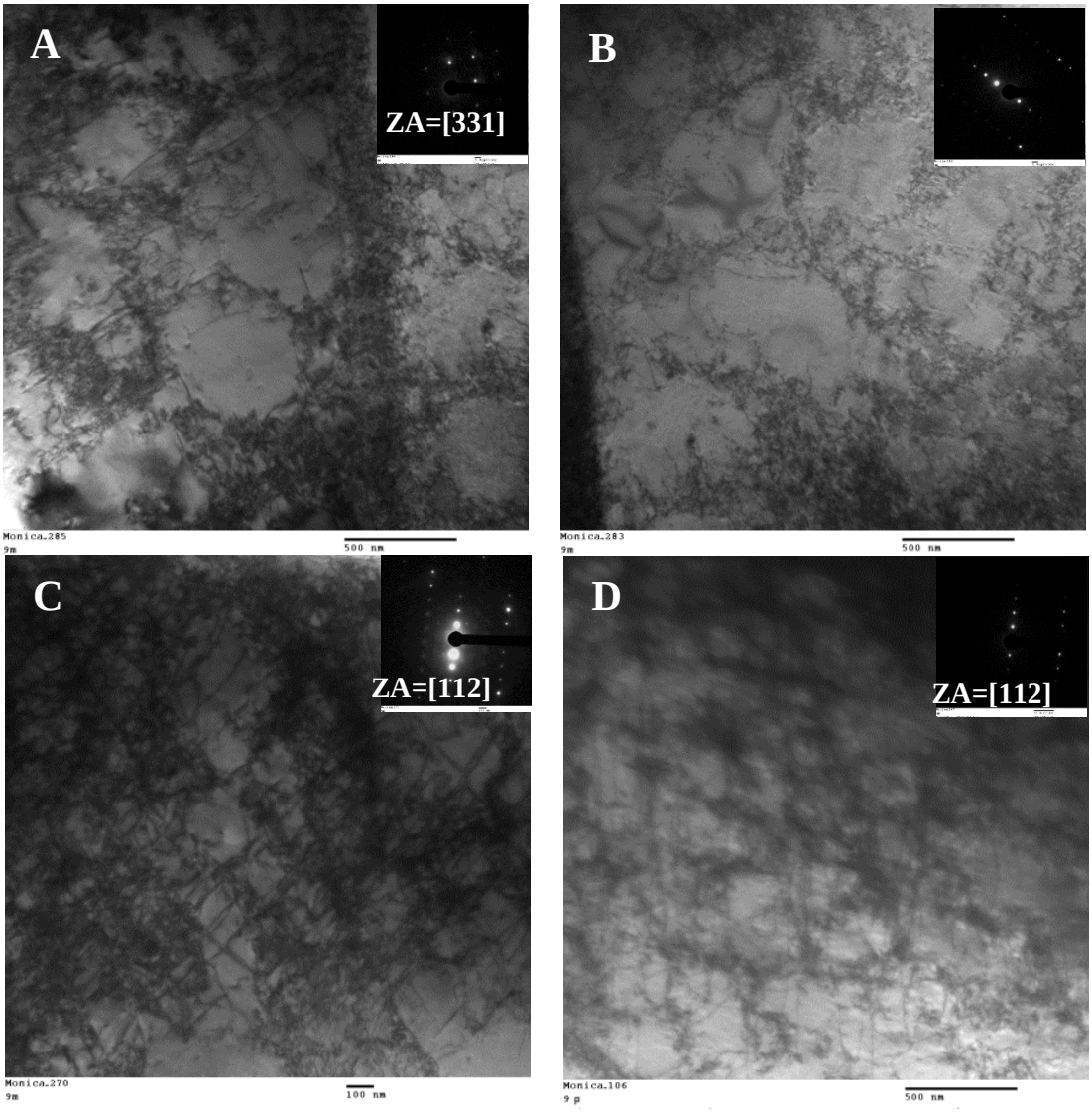

Figure 23. Transmission electron micrographs of pipeline #2 showing (A-B) dislocation cells (C-D) and cells with heavy walls.

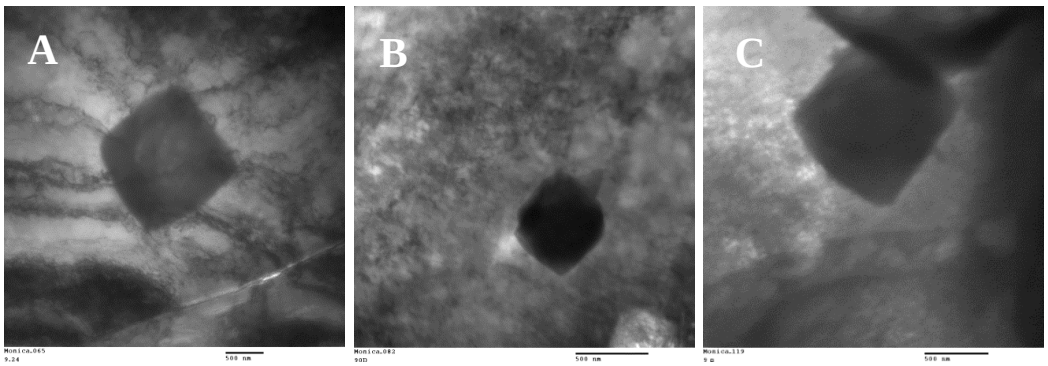

Figure 24. Bright TEM micrographs showing coarse cuboidal-shaped precipitates (A) 2µm, (B) 0.62µm, and (C) 1.3µm within the ferritic grains.

4.2 PIPELINE #1

4.2.1 Background Information

The pipeline #1 (Figure 8) was constructed to API Spec 5L requirements by Cal-Met in 1949; it was not hydrostatically tested during installation. This single submerged arc welded pipe was built from grade A steel, with a 220 mm (8 5/8″) O.D., a nominal wall thickness of 4.5 mm (0.180″), and a specified minimum yield strength (SMYS) of 208MPa (30,000 psi). Pipe was coated with coal-tar enamel, and impressed-current cathodic protection (CP) was applied. In 1991, multiple cracks were found in different sections of the pipeline, the maximum crack length measured 43 mm (1.7″) and the maximum crack depth was thru-wall. Analysis of the soil in this region revealed a pH of 9. For purposes of this research this pipeline was identified as pipeline #1, Figure 8 presents the as-received sections of this pipeline and Table 7 summarizes the pipeline attributes and operating conditions.

Table 7. Pipeline #1 Attributes and Operating Conditions

Pipeline attributes and operating conditions			
Construction date	1949	**Pressure @ failure**	n/a
Failure date	1991	**SMYS**	208MPa (30,000 psi)
Manufacturer	Cal-Met	**Classification**	Vintage
Outside diameter	220 mm (8 5/8″) OD	**Location**	AZ.
Wall thickness	4.5 mm (0.180″)	**Terrain/soil type**	Apparent moisture
Type of seam	SSAW	**Distance-compressor**	n/a
Steel grade	Grade A steel	**Soil pH**	High pH (9)
Coating	Coal-tar enamel	**CP**	Yes
Max crack length	100% wt.		

4.2.2 Non-Destructive Evaluation

As previously discussed, wet fluorescent magnetic particle inspection was carried-out in all of the received sections from the pipeline #1; revealing a longitudinal crack with extensive branching in sections 11 and 12 (Figure 25A-B), this crack was located adjacent to the weld seam. Furthermore, multiple SCC colonies demonstrating coalescence of cracks were observed in section 10 (Figure 25C). Cracks were oriented in both directions—longitudinally and circumferentially. It should be noted that many of these crack colonies were "non-classical" and apparently grouped in crack clusters with no particular orientation relative to the hoop stress imposed in service.

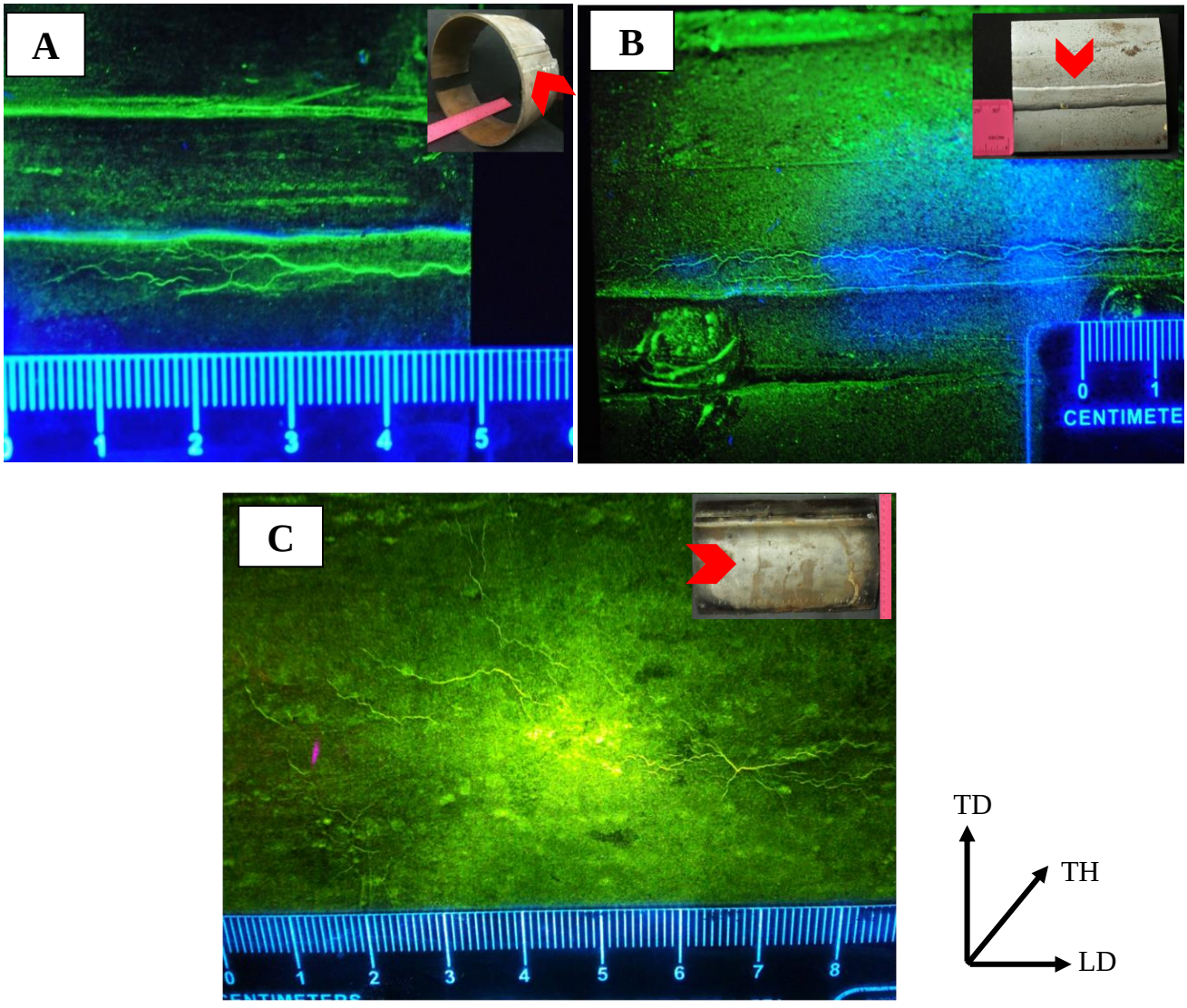

Figure 25. WMPI macrographs showing (A-B) longitudinal SCC cracks along weld seam and (C) "non-classical" SCC colony oriented in both the transverse and the longitudinal direction.

4.2.3 Chemical Analysis

The chemical composition of each section from pipeline #1 is presented in Table 8. Chemical results indicate that pipeline #1 was manufactured to a rimmed steel practice and was not made to Si and/or Mn deoxidation practice. Furthermore, the low residuals content (Al, Mo, Cu, Cr, and Ni) indicate that this pipeline was not made to a fine grain practice.

Table 8. Pipeline #1 Chemical Composition

Pipeline #1										
Section	C	Si	Mn	Cr	Mo	Ni	Al	Co	Cu	Nb
10	0.06	0.003	0.36	0.008	0.002	0.018	0.014	0.008	0.075	0.002
11	0.04	0.003	0.35	0.03	0.002	0.026	0.008	0.010	0.109	0.002
12	0.06	0.003	0.35	0.031	0.002	0.025	0.003	0.010	0.096	0.002
Average	***0.05***	***<0.003***	***0.35***	***0.02***	***<0.002***	***0.02***	***0.01***	***0.01***	***0.09***	***<0.002***

Pipeline #1						
Section	Ti	V	W	Pb	Zr	Fe
10	0.001	0.020	0.023	0.010	0.001	Rem.
11	0.001	0.027	0.027	0.010	0.001	Rem.
12	0.001	0.001	0.020	0.010	0.001	Rem.
Average	***<0.001***	***0.016***	***0.023***	***<0.010***	***<0.001***	***Rem.***

4.2.4 Elemental Mapping

Figure 26 and Figure 27 present the elemental mapping images from two different regions, near the OD (left column) and from the core region (right column). Each chemical element is represented by a specific color and the brightness corresponds to its concentration. Therefore, from Figure 27 it can be seen that the core area exhibits a slightly higher C and Si concentration as compared to the OD, as well as larger MnS non-metallic inclusions. On the other hand the OD was characterized by small particles containing Si and a higher concentrations of Mn and S. No significant differences were observed in the P content.

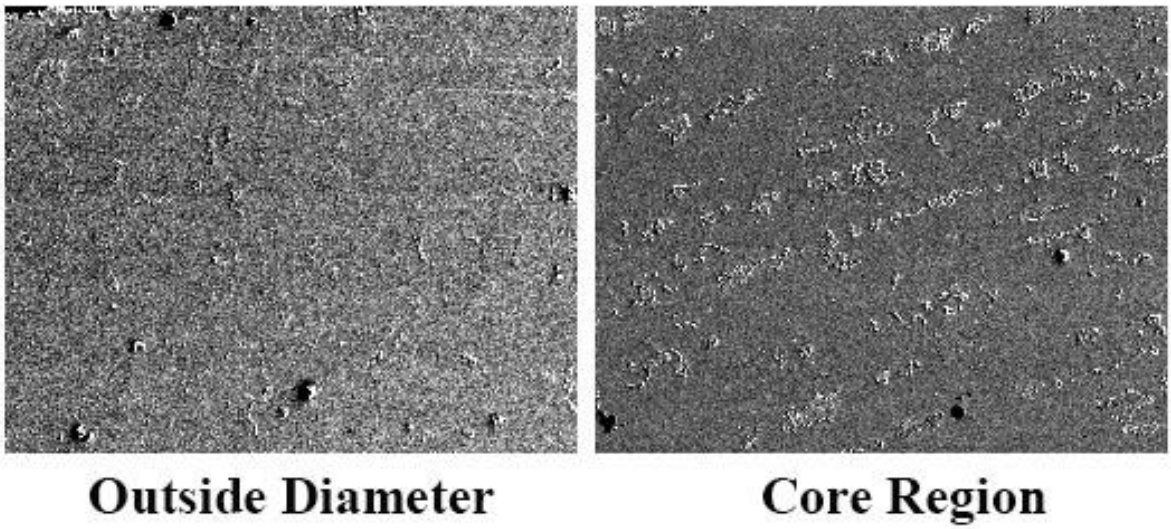

Figure 26. SEM image from OD (left) and the core region (right).

\

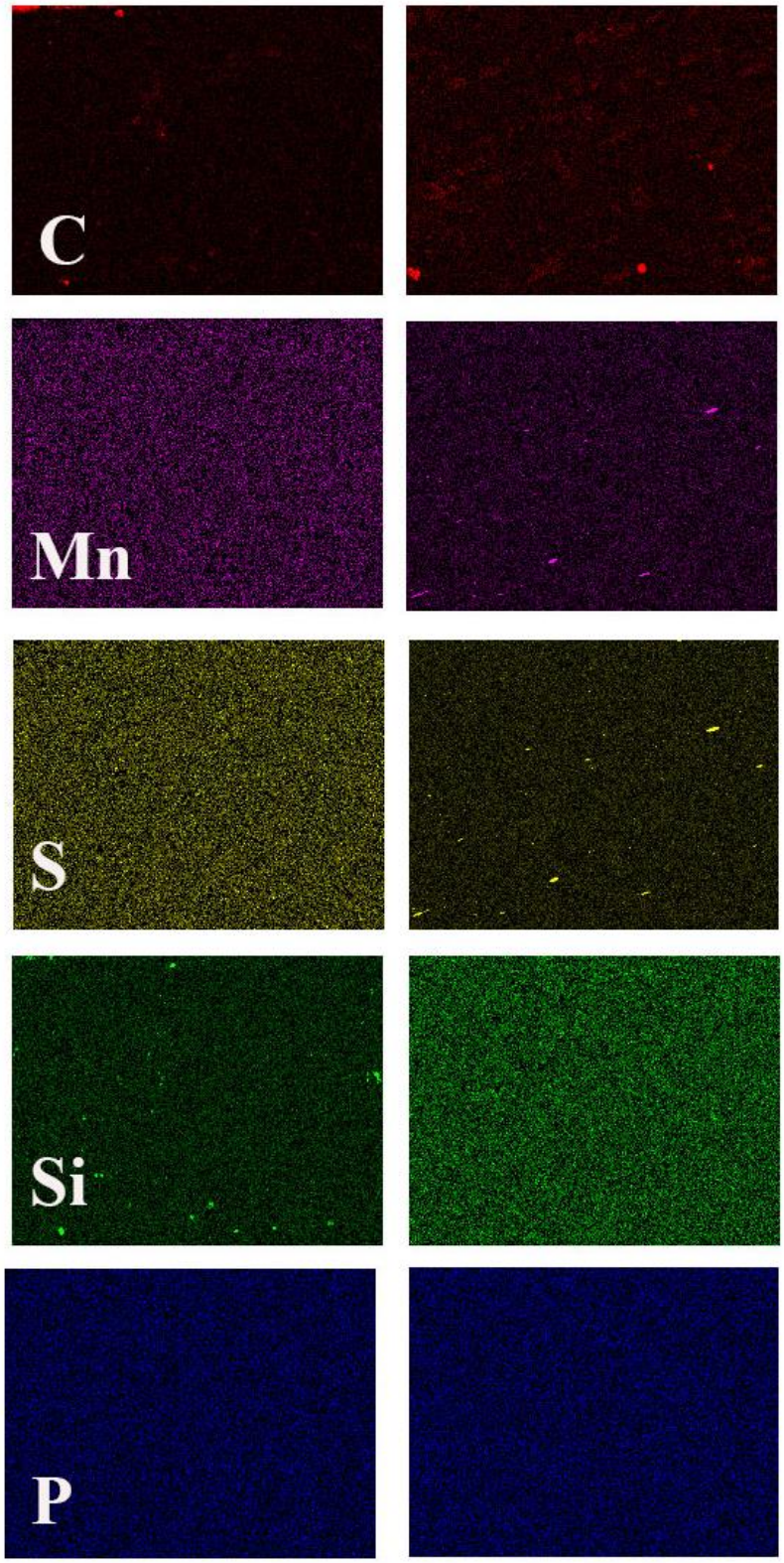

Figure 27. Elemental mapping from a region near the OD (left) and the core (right).

4.2.5 Hardness

Figure 28 present the hardness profile from the OD to ID from two crack containing sections—weld region and body of the pipe— and from a crack free zone. Table 9 the average Vickers hardness (HV) and equivalent HRB and tensile strength. Hardness results indicate that while SCC-free region exhibited slightly lower hardness than the weld-SCC zone the region in the body of the pipeline containing SCC cracks exhibited a significantly lower hardness profile. Additionally, all regions displayed a lower hardness in the core zone.

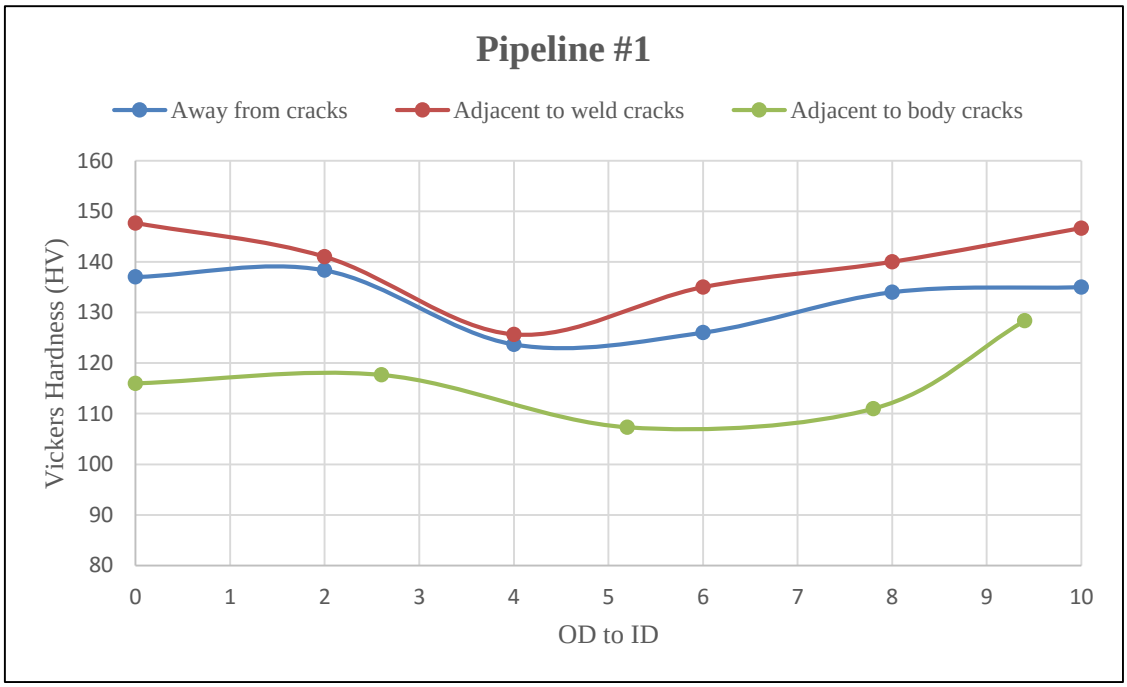

Figure 28. Pipeline #1 microhardness profile.

Table 9. Pipeline #1 Harness Testing Results

Region	Average Vickers (HV)	Converted Average HRB	Equivalent Tensile Strength MPa (psi)
Away from cracks	133	72	423 (61351)
Adjacent to weld seam crack	139	75	446 (64687)
Adjacent to body cracks	116	65	371 (53809)

4.2.6 Microstructural Characterization

Crack morphology

Light microscopy of the crack containing cross-section from section 12 (Figure 29) revealed multiple cracks of varying sizes on the O.D. The largest crack observed follows an intergranular path, exhibits extensive branching, and what appears to be crack wall corrosion. Furthermore, the inner diameter revealed evident pitting.

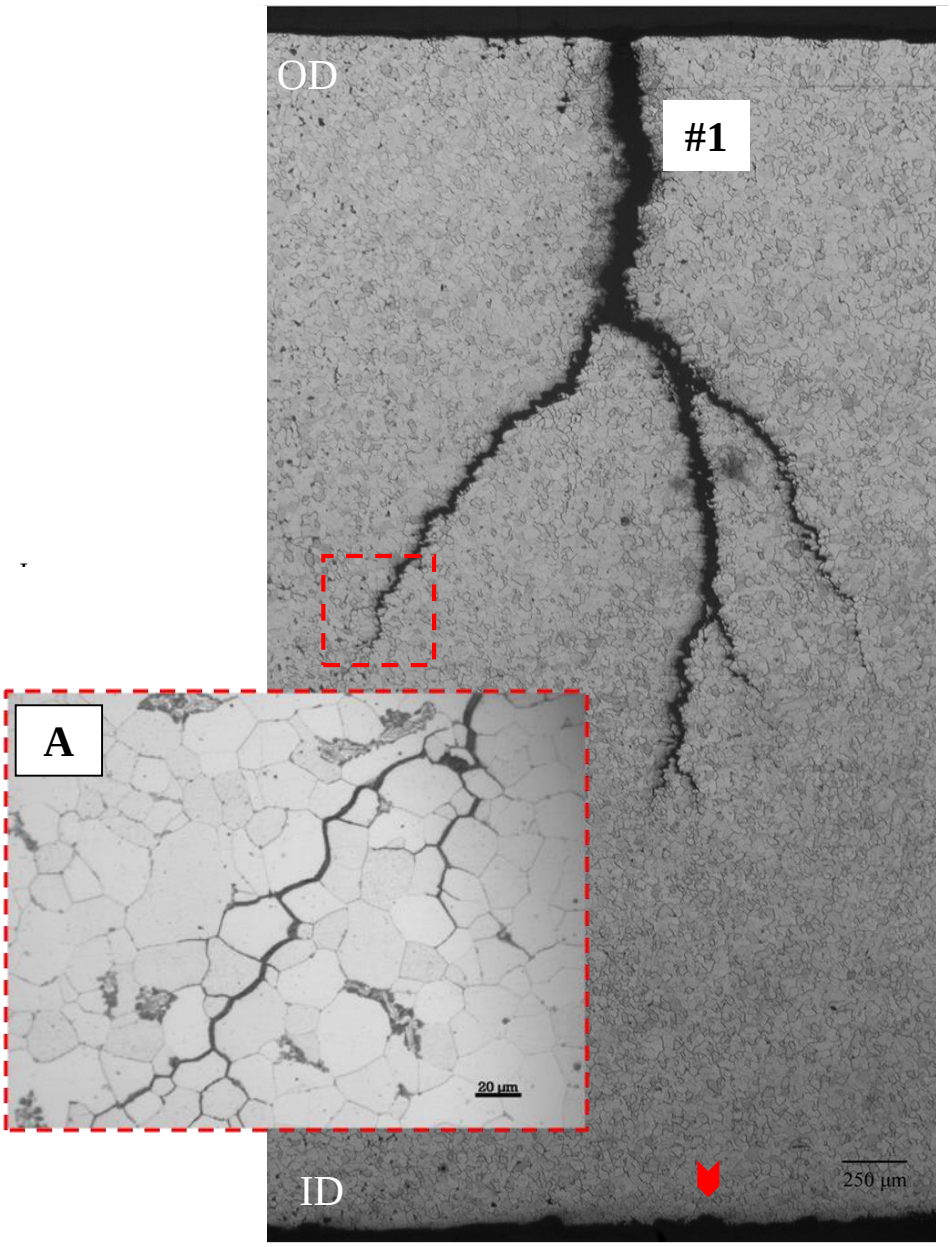

Figure 29. Optical view from intergranular SCC cracks along the weld zone. Crack #1 exhibited extensive branching and crack wall corrosion. A magnified view from one of the crack branches is shown in A. The arrow indicates pitting on the inner diameter. 2% Nital.

Microstructural Characteristics

The microstructure of pipeline #1 (Figure 30) exhibits polygonal ferrite grains with small and random colonies of pearlite (dark constituent) and cementite films at ferritic grain boundaries. Randomly distributed inclusions were observed within the ferrite grains and intersecting grain boundaries.

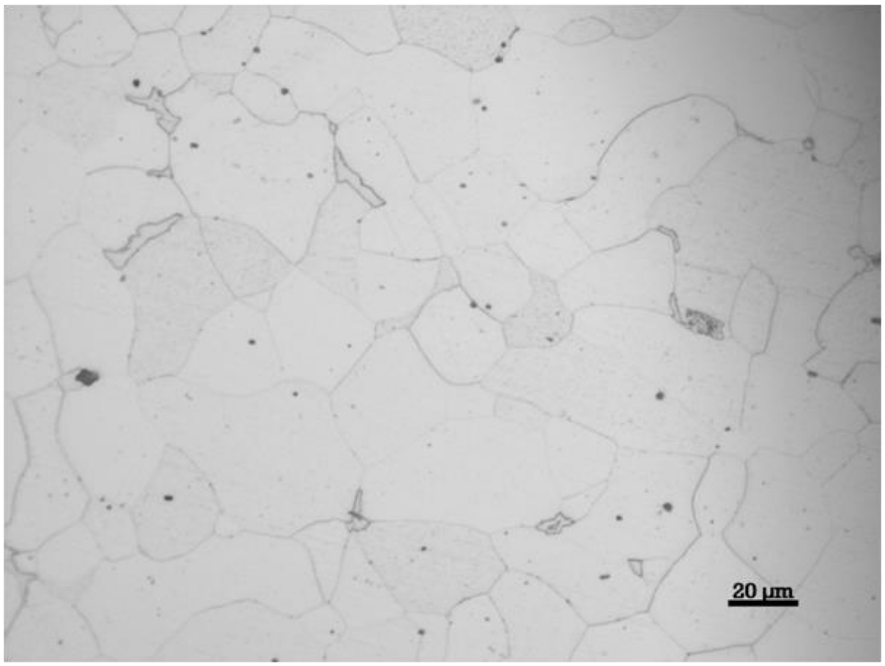

Figure 30. Microstructure of pipeline #1 showing a ferritic grain structure, cementite films, and small pearlite colonies. 2% Nital.

The core area from the base metal exhibited regions with a banded structure of alternating ferrite-pearlite bands (Figure 31). The pearlite volume fraction in the core region was about 5% as compared to 0.5-1% in the rim area. A closer examination of the OD, ID, and core microstructures (Figure 31B-D) revealed a bimodal grain size distribution in which fine and coarse grains were observed, this was more evident on the ID where the largest grain was approximately 10 times the average grain size which was about 22 µm (ASTM G No. 7.5-8). The centerline area also exhibited a higher volume fraction of gray and oblong shaped MnS inclusions (maximum aspect ratio 4).

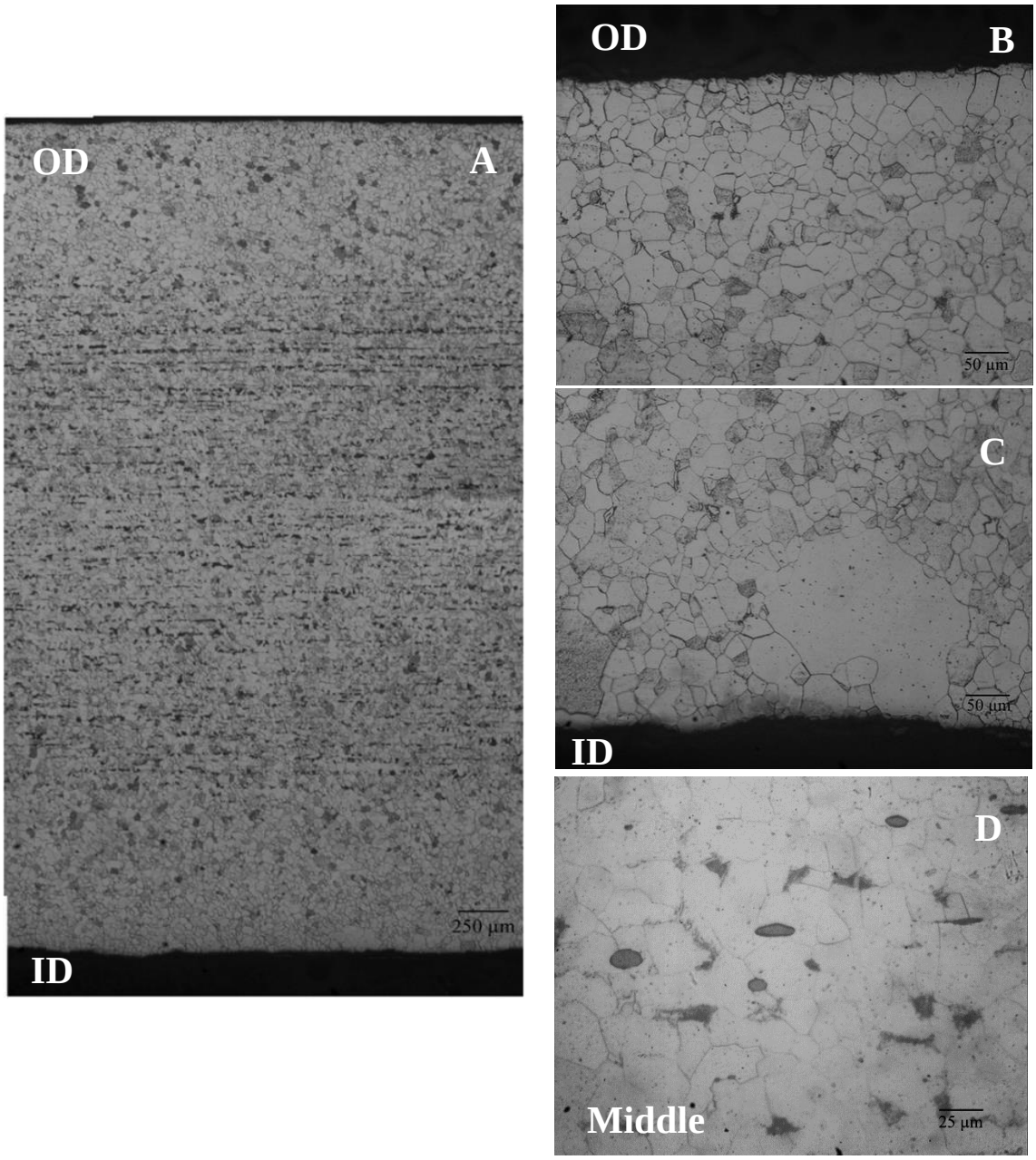

Figure 31. Light micrographs from the base metal showing (A) banding, (B-C) grain coarsening and (D) MnS in the core region. 2% Nital.

Bright field TEM micrographs near the OD of pipeline #1 suggest that the microstructure is characterized by polygonal ferrite grains (Figure 32), what appears to be grain boundary precipitation (Figure 32C), and dislocation structures (Figure 32D and Figure 33A). Nevertheless, some grains appear to be virtually dislocation free (Figure 32A). Furthermore, a grain boundary crack segment located near a large particle at a triple point junction is shown Figure 33C-D.

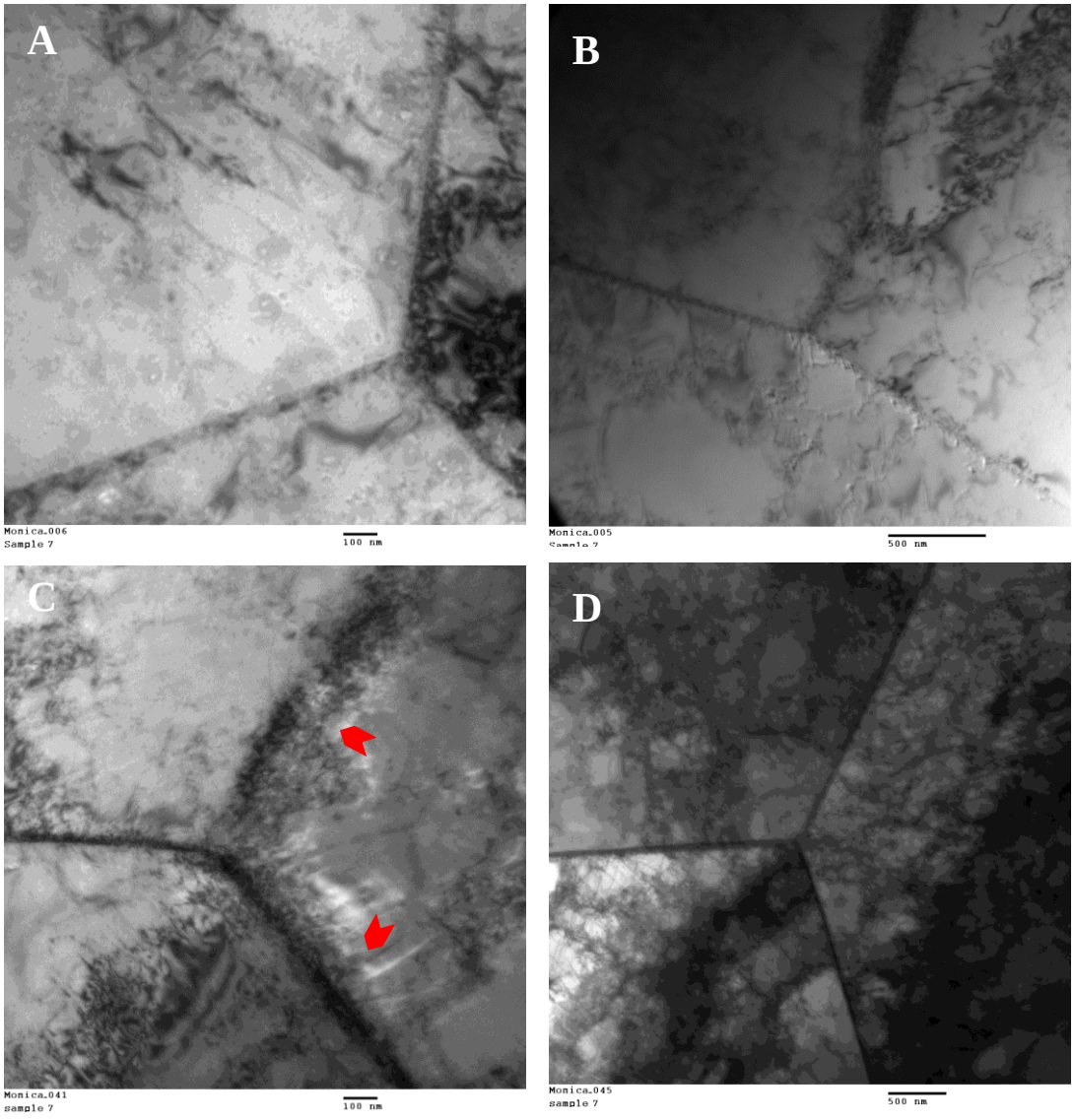

Figure 32. Bright-field micrographs of triple grain boundary junctions in pipeline #1. Fine grain boundary precipitation (arrow) (C).

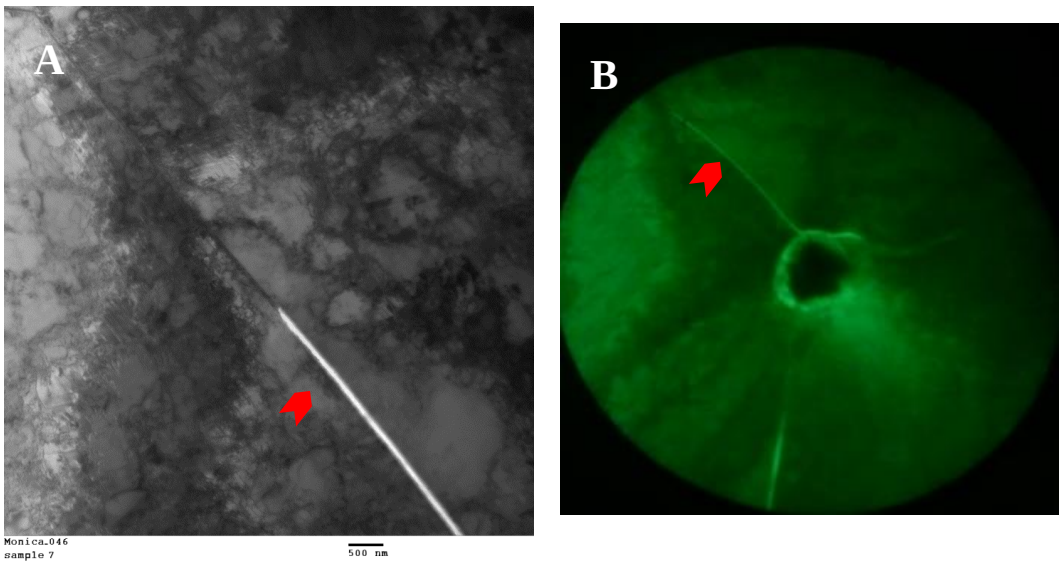

Figure 33. Bright TEM micrograph showing (A) dislocation structures and (A-B) an intergranular crack segment near a particle at a triple point grain boundary.

Higher magnification TEM micrographs revealed that the ferritic grains contained loosely formed dislocation cells (Figure 34A), dislocation cells with an approximate diameter of 0.80 μm (Figure 34B), and homogenous dislocations (Figure 34C-D). Homogenous dislocations exhibit a more uniform dislocation distribution; while, heterogeneous dislocations such as cells are characterized by mixed regions of high and low dislocation densities.

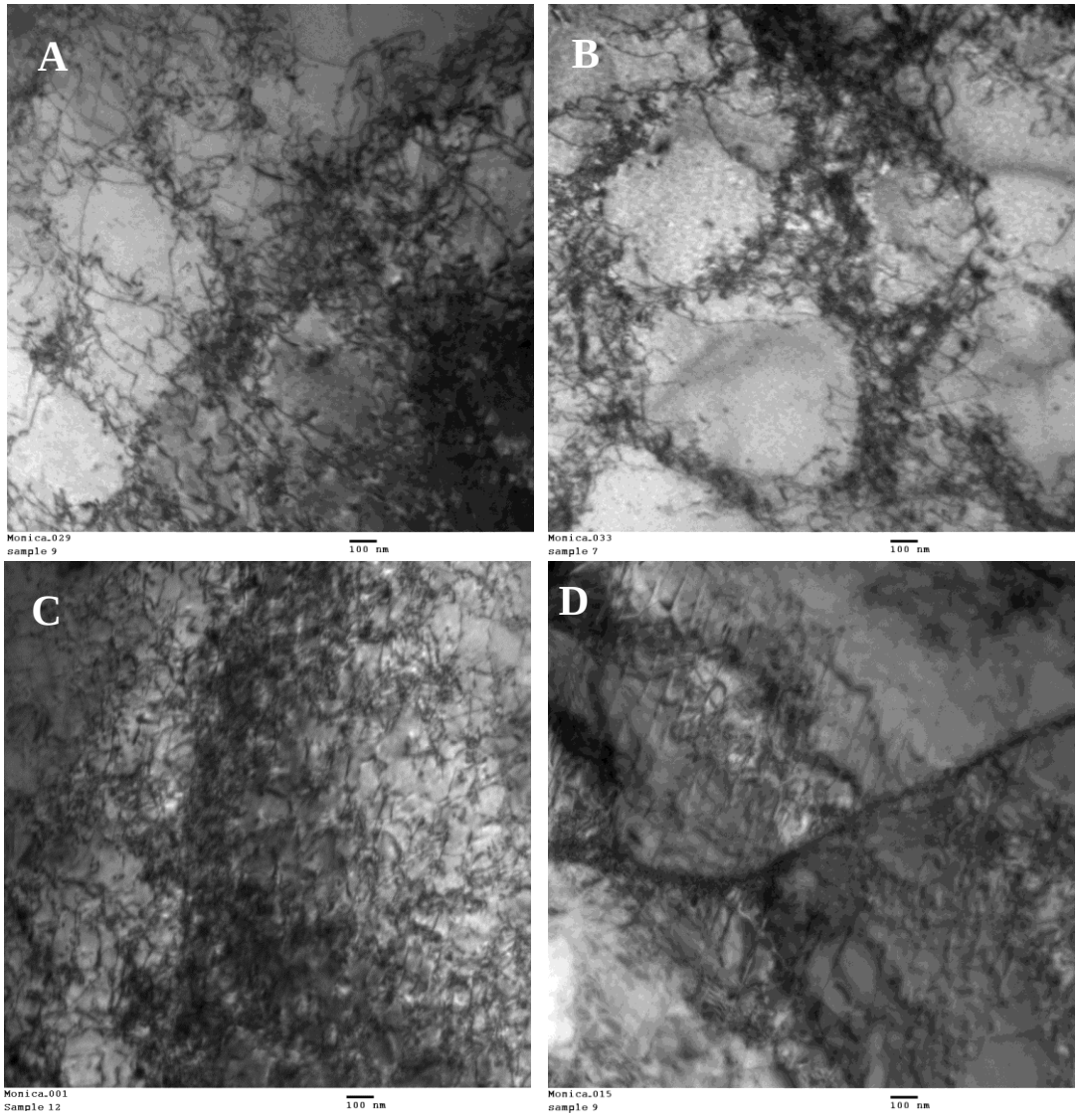

Figure 34. Bright TEM micrographs showing (A) loosely formed cells, (B) dislocation cells, and (C-D) homogenous dislocations.

4.3 PIPELINE #3

4.3.1 Background Information

On October 1994, sustained SSC damage over 7 miles was found in a natural gas transmission pipeline constructed in 1950 by Republic Steel to API Spec 5L requirements for grade X52 steel. This double submerged arc welded (DSAW) seam pipe had a 61 cm (24 inch) O.D. and a nominal wall thickness of 6.88 mm (0.271 inch). During failure investigation it was observed that the coal tar coating exhibited poor adhesion. A year from the first SCC failure, on October 1995, a hydrostatic test rupture was generated at a pressure of 99% of SMYS, SCC was determined to be the cause of failure. During this investigation sections from the hydrostatic test failure were analyzed. The general attributes and operating conditions for pipeline #3 are presented Table 10.

Table 10. Pipeline #3 Attributes and Operating Conditions

Pipeline attributes and operating conditions			
Construction date	1951	**Pressure @ failure**	8MPa (1160 psi)
Failure date	1995	**SMYS**	423MPa(6135 psi)
Manufacturer	Republic Steel	**Classification**	Vintage
Outside diameter	61cm (24″)	**Location**	AZ
Wall thickness	6.88mm (0.271″)	**Terrain/soil type**	Dry/brown/sandy
Type of seam	DSAW	**Distance-compressor**	n/a
Steel grade	X52 grade steel	**Soil pH**	High
Coating	n/a	**CP**	n/a
Max crack length	67% wt.		

4.3.2 Non-destructive Evaluation

Wet magnetic particle inspection revealed multiple stress corrosion cracks with little branching. Cracks were oriented parallel to a main fracture surface, as shown in Figure 35.

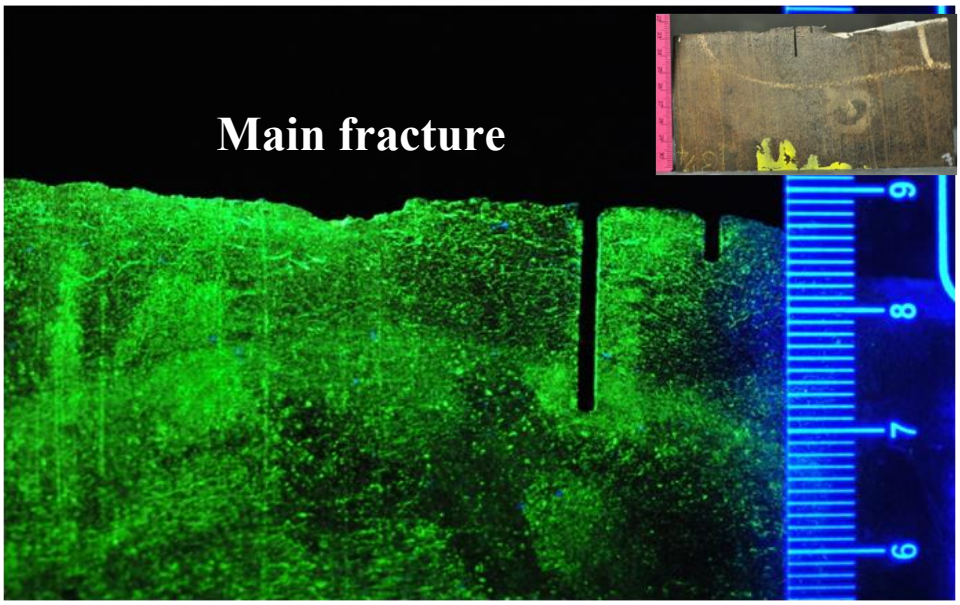

Figure 35. Presence of SCC adjacent the fracture interface revealed by WMPI.

4.3.3 Chemical Analysis

The chemical composition of each section from pipeline #3 are presented in Table 11. Chemical results indicate that pipeline #3 was manufactured to a semi-killed steel practice product of partial deoxidation. Furthermore, low residuals (Ni, Mo, Al, and Cr) indicate that this pipeline was not manufactured to a fine grain practice. Nevertheless, this pipeline exhibited a higher Cu content.

Table 11. Pipeline #3 Chemical Composition

Pipeline #3											
Section	C	Si	Mn	Cr	Mo	Ni	Al	Co	Cu	Nb	Ti
3	0.14	0.03	0.77	0.005	0.003	0.053	0.004	0.02	0.213	0.002	0.001
7	0.15	0.034	0.84	0.005	0.002	0.053	0.002	0.021	0.228	0.002	0.001
Average	***0.14***	***0.03***	***0.80***	***0.005***	***0.003***	***0.05***	***0.003***	***0.02***	***0.22***	***<0.002***	***<0.001***

Pipeline #3					
Section	V	W	Pb	Zr	Fe
3	0.002	0.02	0.01	0.001	Rem.
7	0.001	0.02	0.01	0.001	Rem.
Average	***0.001***	***<0.02***	***<0.01***	***<0.001***	***Rem.***

4.3.4 Elemental Mapping

The EDS elemental mapping images from pipeline #3 are presented in Figure 36 and Figure 37. The left column corresponds to an area adjacent to OD while the right column corresponds to the core region. During this analysis the core region exhibited more elongated MnS inclusions as compared to the rim as well as some silicon-containing particles. No qualitative significant differences were observed in the C, Mn, S, Si, and P content between rim and core.

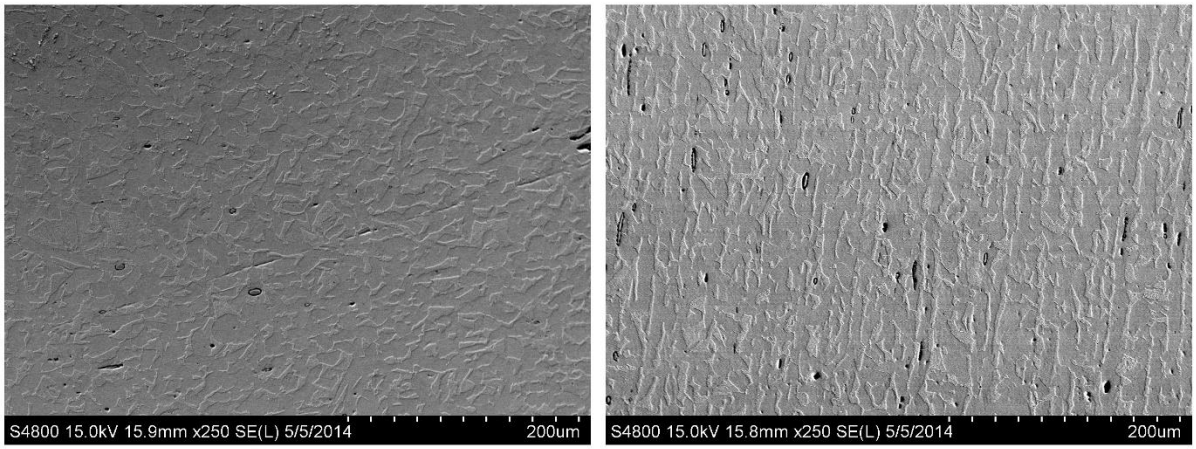

Figure 36. SEM images from an area near the OD and the core where elemental mapping was performed.

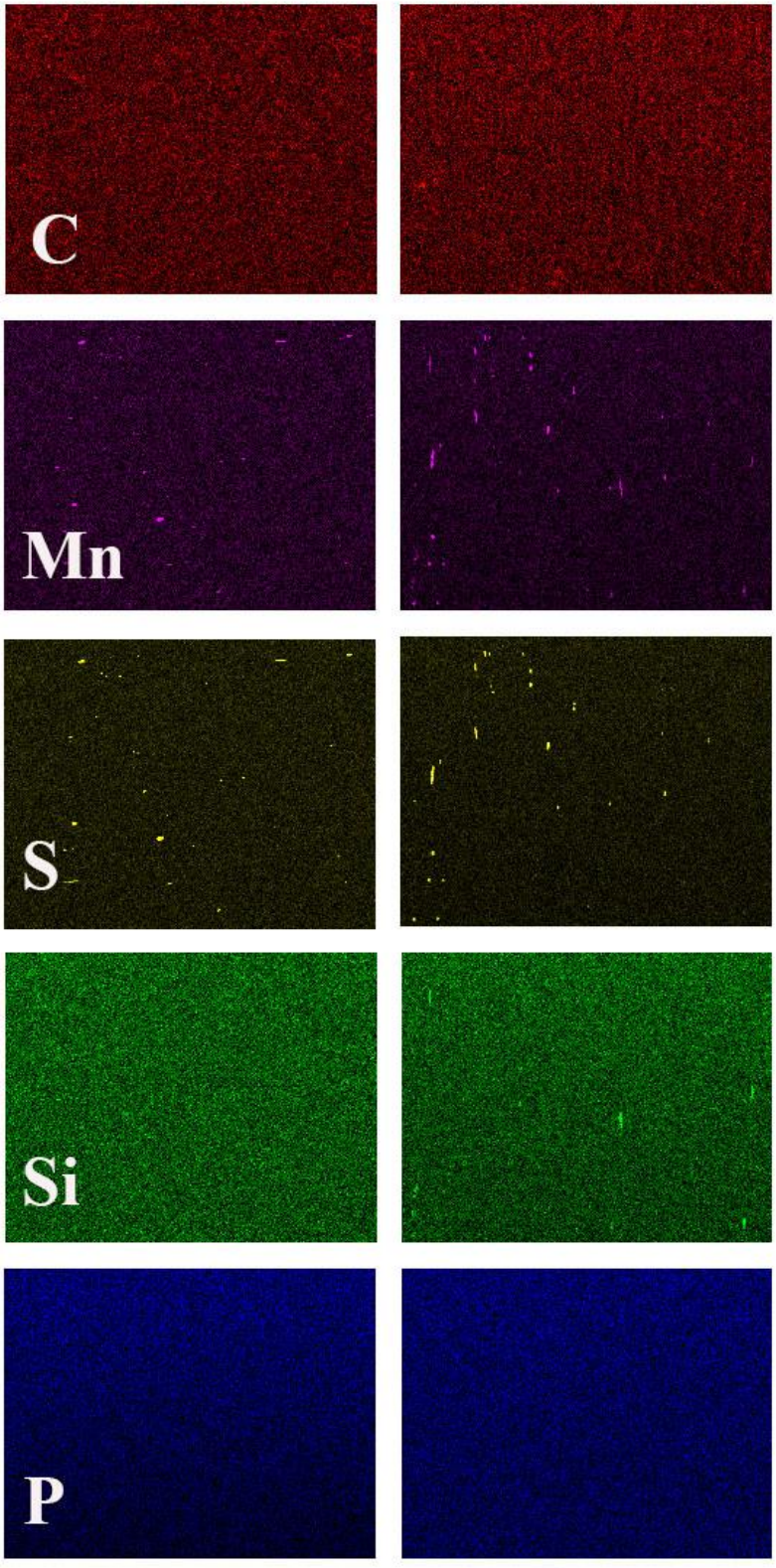

Figure 37. Elemental mapping from a region near the OD (left) and the core (right).

4.3.5 Hardness

Figure 38 present the hardness profile from OD to ID from crack containing and crack free regions and Table 12 shows the average Vickers microhardness and the equivalent HRB and tensile strength. The thru-thickness hardness profile from SCC and SCC-free zones exhibited a similar pattern with the lowest hardness observed in the core region. However, the crack containing region exhibited a higher hardness as compared to the SCC-free zone.

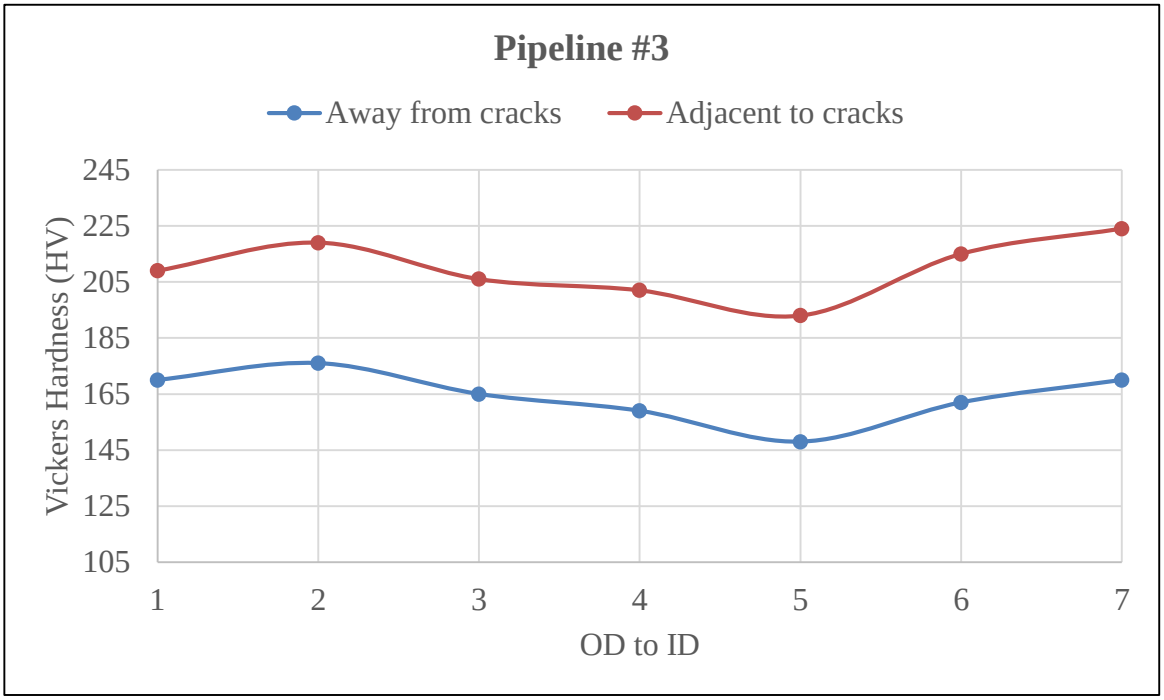

Figure 38. Pipeline #3 hardness profile.

Table 12. Pipeline #3 Harness Testing Results

Region	Average Vickers (HV)	Converted Average HRB	Equivalent Tensile Strength MPa (psi)
Away from cracks	164	83	526 (76289)
Adjacent to cracks	210	93	668 (96885)

4.3.6 Microstructural Characterization

Crack morphology

Light microscopy from a transverse cross sectional area containing cracks shows multiple very wide cracks on the OD, very wide cracks are a typical feature of a hydrotest failures (Figure 39). The crack morphology is not evident due to the large width of the cracks, nevertheless cracks appear to follow a predominantly intergranular path with small amounts of transgranular fracture.

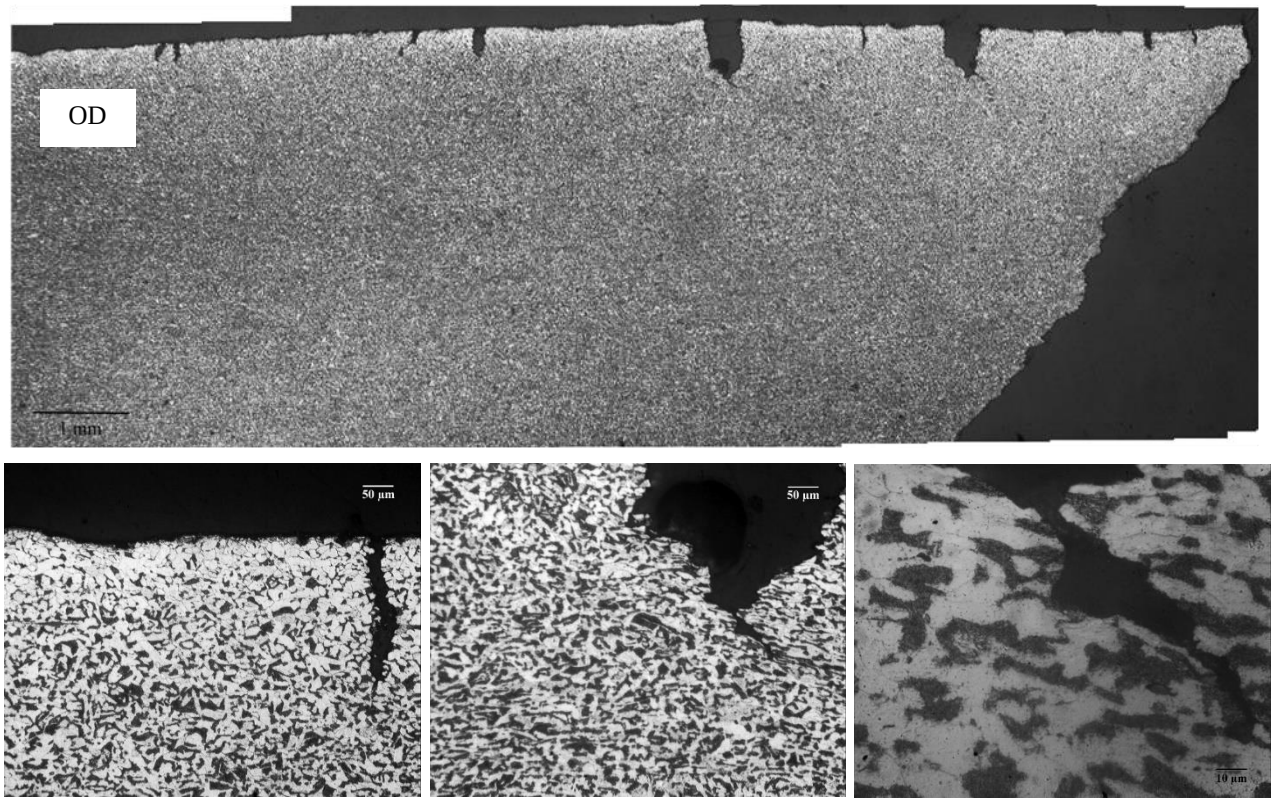

Figure 39. Light micrographs showing very wide stress corrosion cracks (result of hydrotesting) on pipeline #3 samples.

Microstructural Characteristics

Optical microstructure shown in Figure 40 reveals ferrite bands (white) with elongated and disconnected inclusions (aspect ratio 8 or more) (Figure 40B), and pearlite bands (dark constituent)— the pearlite volume fraction was approximately 24%. The ferritic grain structure was characterized by polygonal and/or quasi-polygonal ferrite with some needle-shaped ferrite (Figure 40C). The average grain size calculated by the linear intercept method is 12 µm (ASTM G No. 9.5); no significant differences between rim and core grain size were observed. Furthermore, what appears to be a decarburized layer near the OD is shown in Figure 40D.

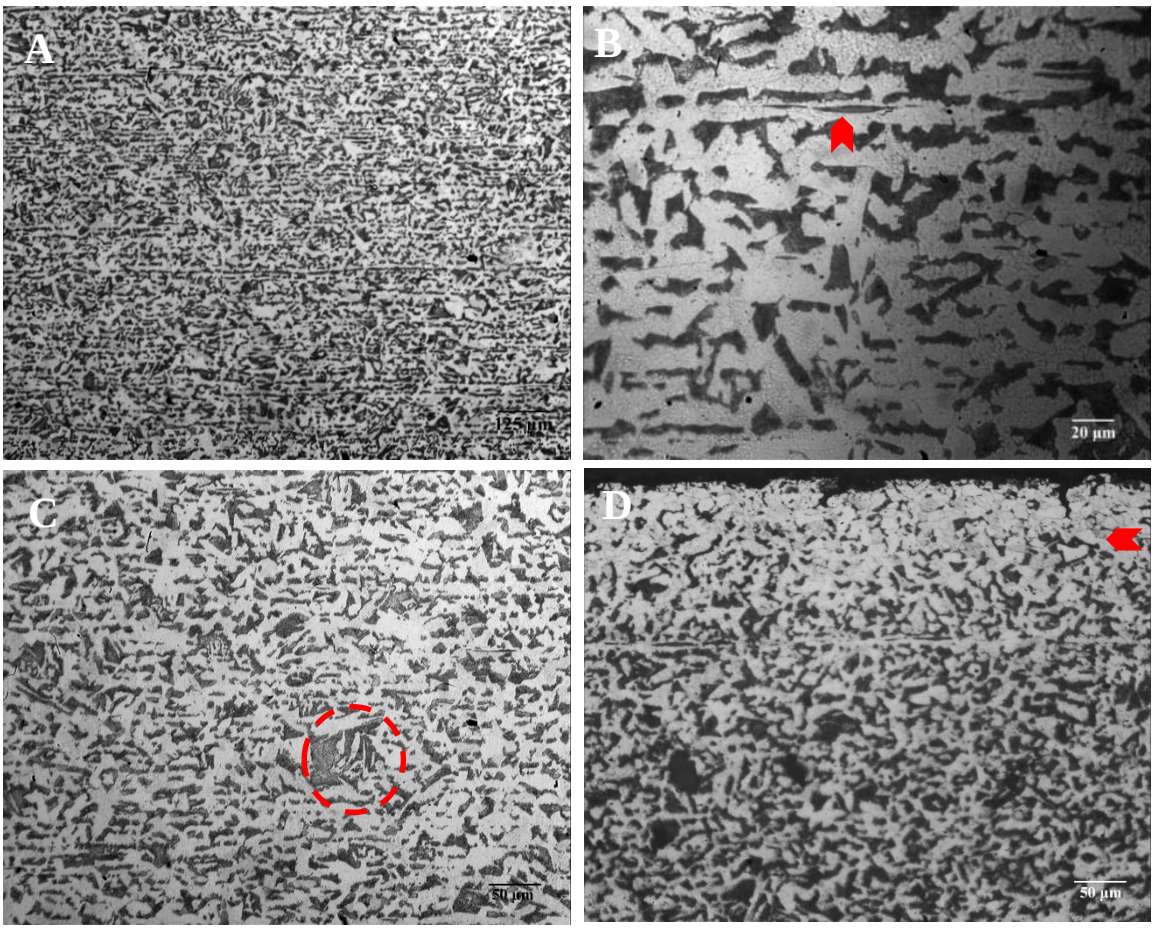

Figure 40. General microstructure of the pipeline #3 indicate (A) banding, (B) elongated inclusions, (C) mixed ferrite morphologies, and (D) a narrow decarburized layer near the outer diameter (arrow). 2% Nital.

Representative bright field TEM micrographs of the region near the OD from pipeline #3 are presented in Figure 41 and Figure 42. The microstructure was a combination of ferrite, grain boundary carbides, and pearlite colonies. The ferrite grains were predominantly polygonal (Figure 41A-B) and were characterized by dislocation structures (Figure 42C). Relatively straight dislocation lines are visible in Figure 42B and precipitation of fine particles within grain interior are noticeable in Figure 42A.

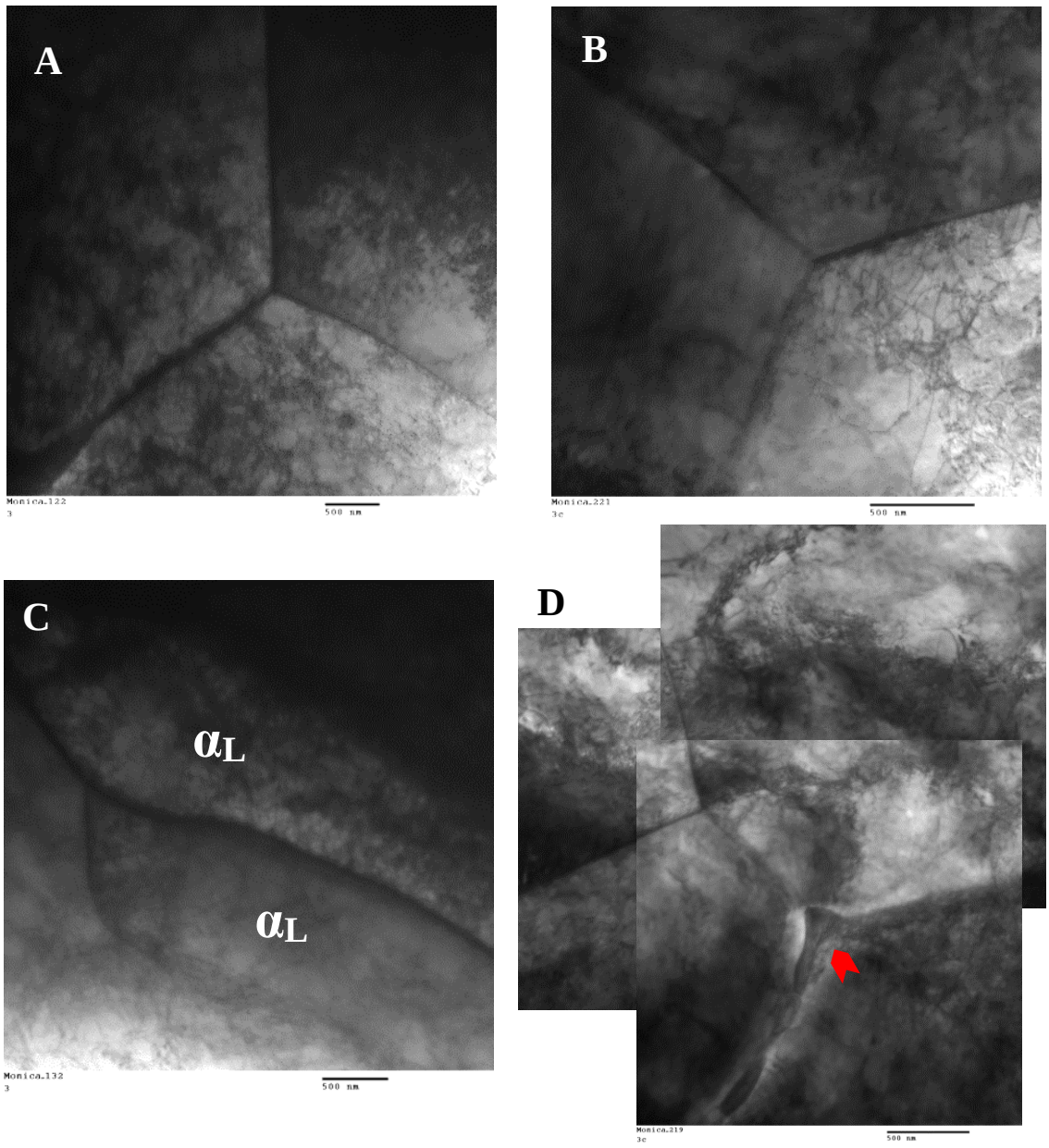

Figure 41. Bright TEM micrographs from pipeline #3 show what appears to be (A-B) polygonal ferrite structure, (C) lath-shaped ferrite, and (D) grain boundary carbides.

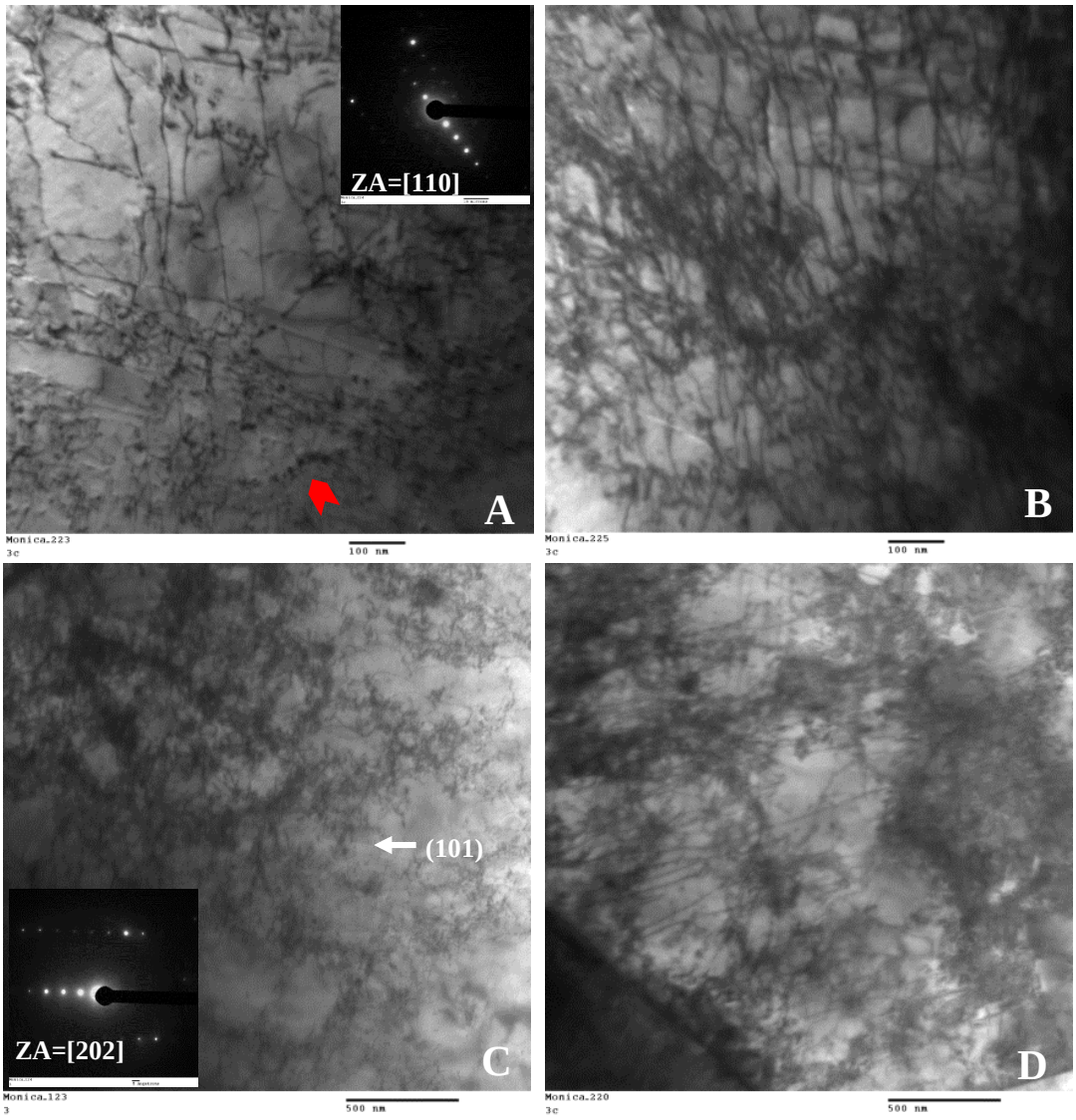

Figure 42. TEM micrographs showing dislocation structures in the body of the ferritic grain and fine precipitation within the grain (red arrow).

Figure 43 show representative TEM bright field images from the pearlite colonies observed in pipeline #3. Figure 43A-B exhibit a more degenerate pearlite morphology characterized by an irregular lamellar structure with broken-up, mostly non-parallel cementite platelets, and some roughly spheroidal cementite particles. Furthermore, Figure 43B also exhibits “bulged-pancake” cementite (grain boundary allotriomorph) and cementite with a dog-bone termination. A more lamellae pearlite structure is presented on Figure 43C.

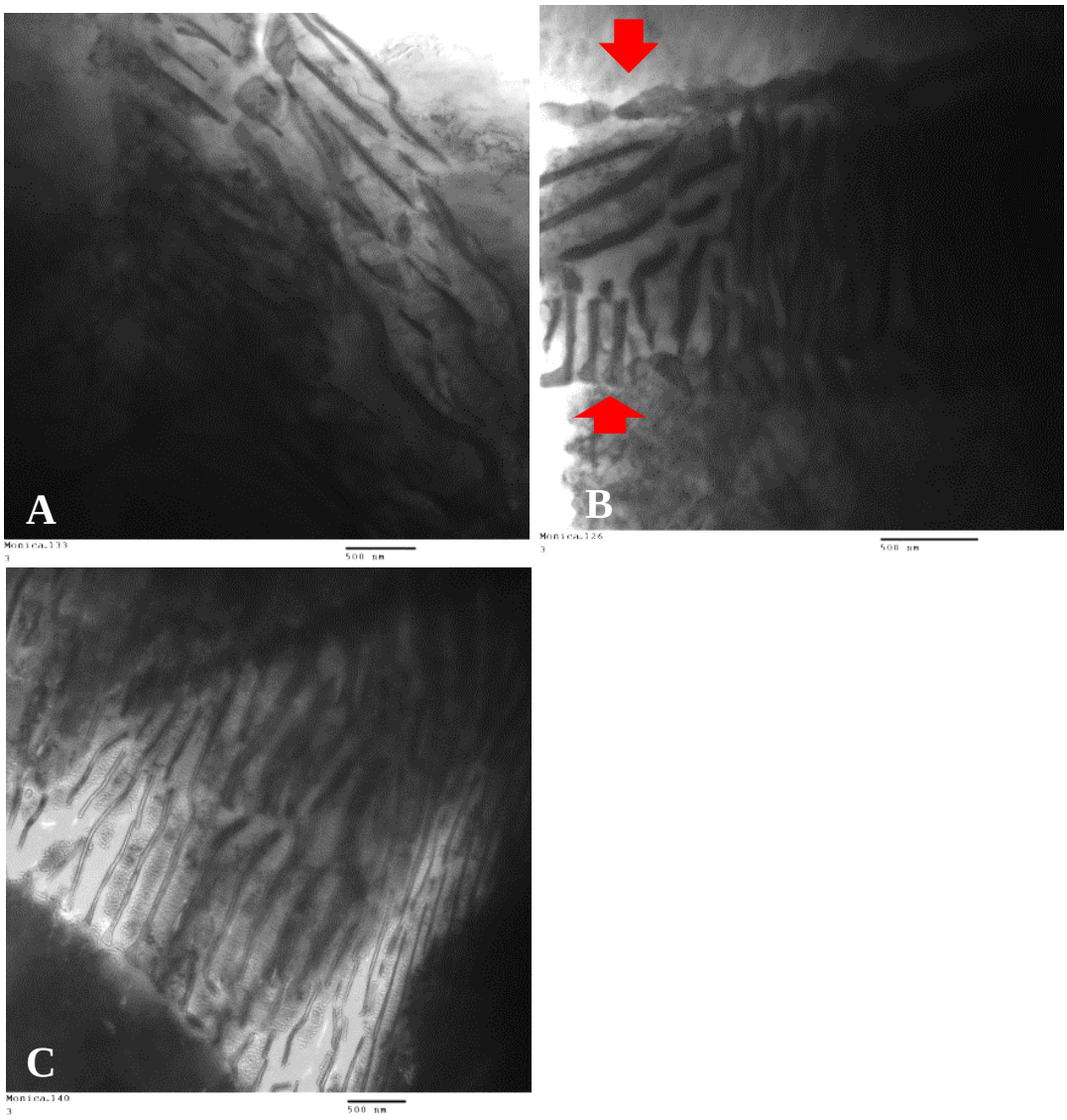

Figure 43. Bright field TEM micrographs showing (A-B) degenerated pearlite and (C) lamellae pearlite in pipeline #3. (B) Arrows indicated “bulged-pancake” cementite and cementite with a dog-bone termination.

4.4 PIPELINE #4

4.4.1 Background Information

The 76 cm (30”) OD pipeline with nominal wall thickness of 8.22 mm (0.324”) experienced SCC damage downstream from the compressor station. Therefore, after an operational SCC leak in 1967 a hydrotest program was installed, from which many hydrostest ruptures were reported in the subsequent years. Pipeline #4 was among the ones that experienced SCC hydrotest leaks. This DSAW pipeline consisted of an A.O. Smith pipe constructed to API 5LX specifications for grade X52 and a coal tar enamel coating. In 1954 cathodic protection was applied. The general pipeline attributes and operating conditions for pipeline #4 are presented Table 13

Table 13. Pipeline #4 Attributes and Operating Conditions

Pipeline attributes and operating conditions			
Construction date	1947-1950	**Pressure @ failure**	n/a
Failure date	1967	**SMYS**	423MPa(6135 psi)
Manufacturer	A.O. Smith	**Classification**	Vintage
Outside diameter	76cm (30″)	**Location**	n/a
Wall thickness	8.22mm (0.324″)	**Terrain/soil type**	No clay
Type of seam	DSAW	**Distance-compressor**	n/a
Steel grade	X52	**Soil pH**	High (7.4-8.8)
Coating	Coal tar	**CP**	n/a
Max crack length	50% wt		

4.4.2 Non-Destructive Evaluation

The observed SCC colony on section 5 (Figure 44) from pipeline #4 exhibited axially oriented cracks with fairly dense spacing and little branching.

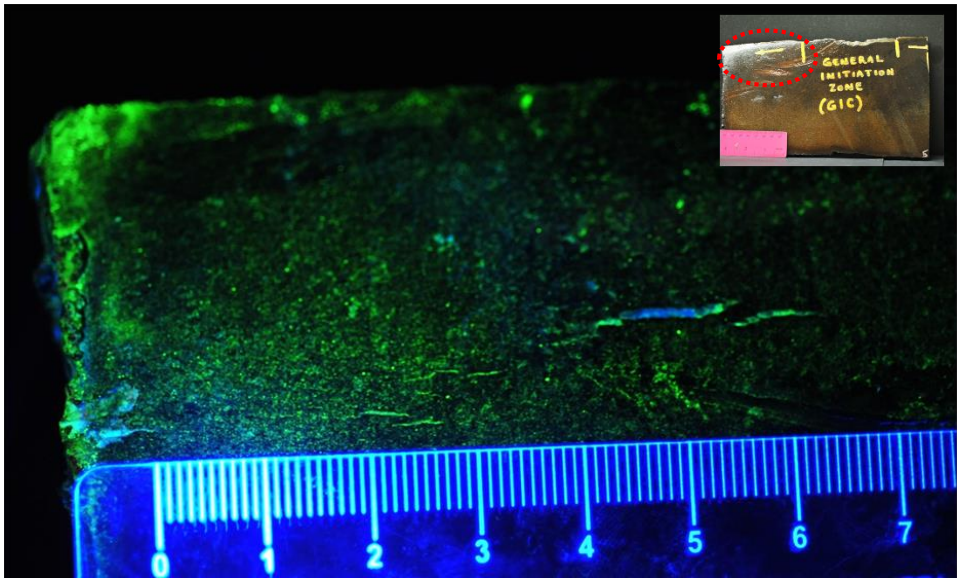

Figure 44. WMPI revealed multiple axially oriented stress corrosion cracks with little branching.

4.4.3 Chemical Analysis

The chemical composition of each section from pipeline #4 presented in Table 14 revealed that this pipeline was manufactured to a semi-killed (partial deoxidation) or killed steel practice product of full deoxidation. Furthermore, Al content indicates that this pipeline was made to a fine grain practice.

Table 14. Pipeline #4 Chemical Composition

Pipeline #4											
Section	C	Si	Mn	Cr	Mo	Ni	Al	Co	Cu	Nb	Ti
5	0.18	0.018	1.19	0.002	0.002	0.004	0.021	0.009	0.019	0.002	0.004
2	0.19	0.02	1.3	0.002	0.002	0.004	0.029	0.007	0.014	0.002	0.019
Average	***0.19***	***0.02***	***1.3***	***0.002***	***0.002***	***0.004***	***0.03***	***0.01***	***0.02***	***0.002***	***0.012***

Pipeline #4					
Section	V	W	Pb	Zr	Fe
5	0.002	0.031	0.01	0.001	Rem.
2	0.002	0.02	0.01	0.002	Rem.
Average	***0.002***	***0.03***	***0.01***	***0.002***	***Rem.***

4.4.4 Elemental Mapping

Figure 45 and Figure 46 present the SEM and elemental mapping images from a region adjacent to the OD (left column) and the core region (right column) from pipeline #4. The EDS mapping revealed subtle differences between the analyzed areas. The carbon concentration appears to be slightly higher in the OD region as indicated by the color brightness. In addition, the OD exhibited a qualitative slightly higher concentration of Mn, S, Si, and P. Si enriched round particles were observed in the core. Lastly, elongated manganese sulfides (MnS) were observed in both areas with a seemingly higher volume fraction near the OD.

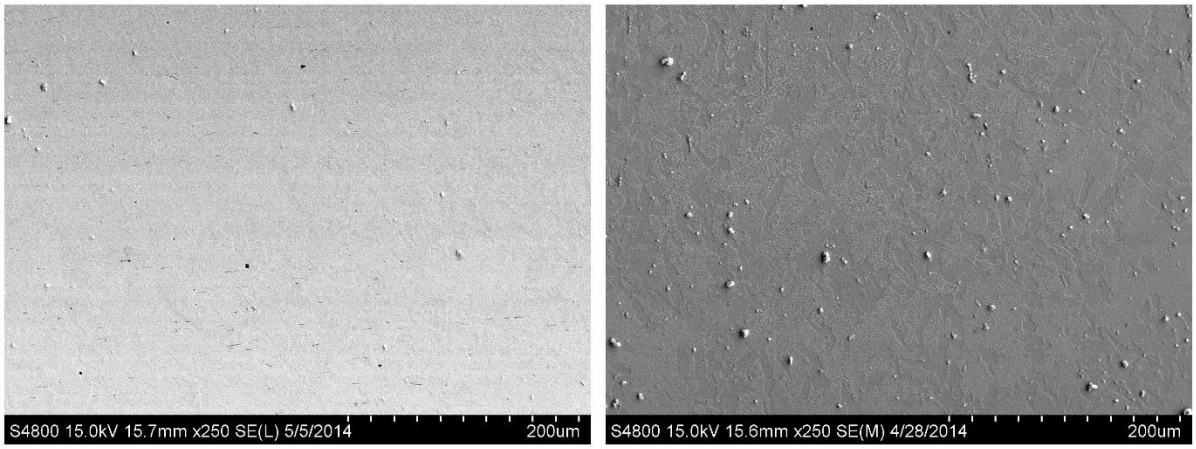

Figure 45. SEM images from a region near the OD and the core where elemental mapping was carried-out.

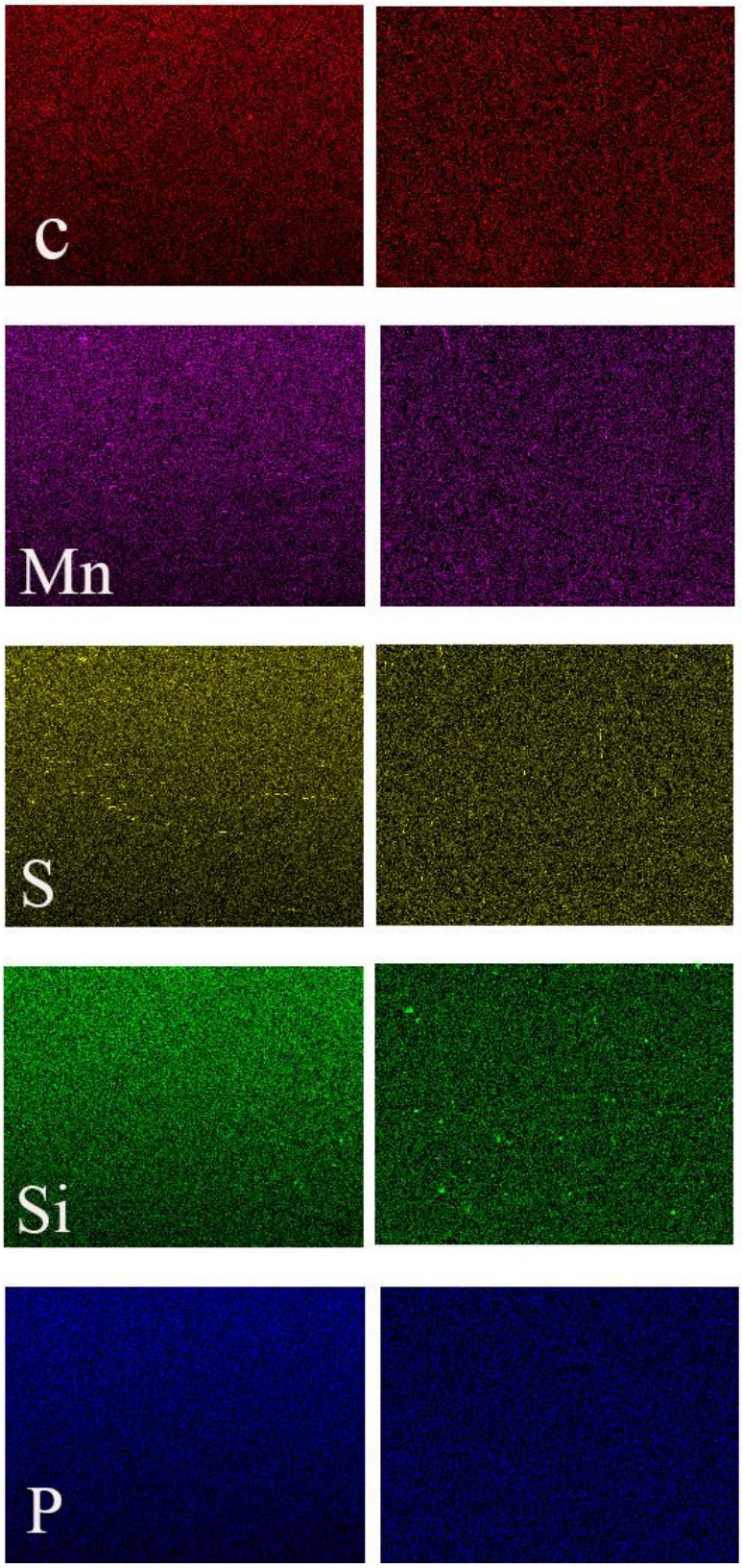

Figure 46. Elemental mapping from a region near the OD (left) and the core (right).

4.4.5 Hardness

Figure 47 present the hardness profile from the OD to ID from crack containing and crack free regions and Table 15 the average Vickers microhardness and equivalent HRB and tensile strength. The hardness profile from both areas followed a similar pattern with a slightly higher hardness in the SCC crack containing region. Additionally, the region close to the OD exhibited higher hardness values for the SCC-crack containing zone.

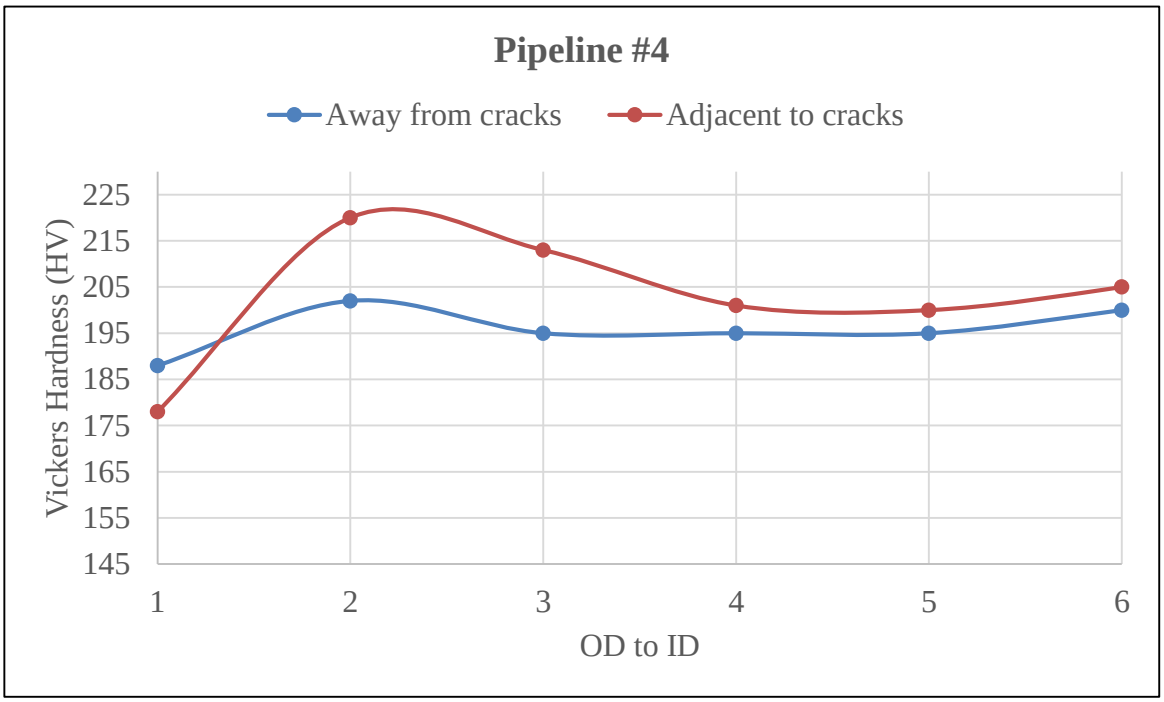

Figure 47. Pipeline #4 harness profile.

Table 15. Pipeline #4 Harness Testing Results

Region	Average Vickers (HV)	Converted Average HRB	Equivalent Tensile Strength MPa(psi)
Away from cracks	196	91	627 (90939)
Adjacent to cracks	203	92	649 (94129)

4.4.6 Microstructural Characterization

Crack morphology

Representative light micrographs from crack containing cross-section revealed various cracks of different sizes (Figure 48) and evident pitting on the OD (Figure 48E-F). The observed stress corrosion cracks exhibited a wide appearance and followed a mixed propagation mode—integranular and transgranular attack (Figure 49).

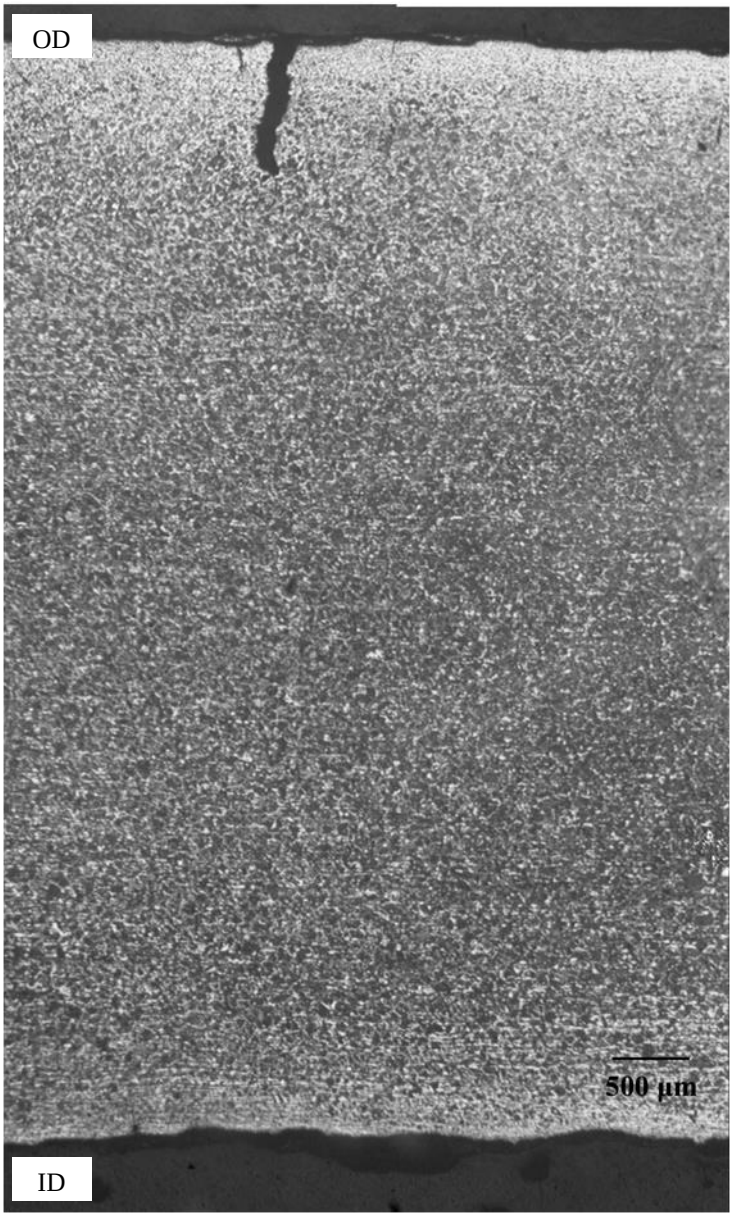

Figure 48. Light micrographs showing SCC cracks on pipeline #4. 2% Nital.

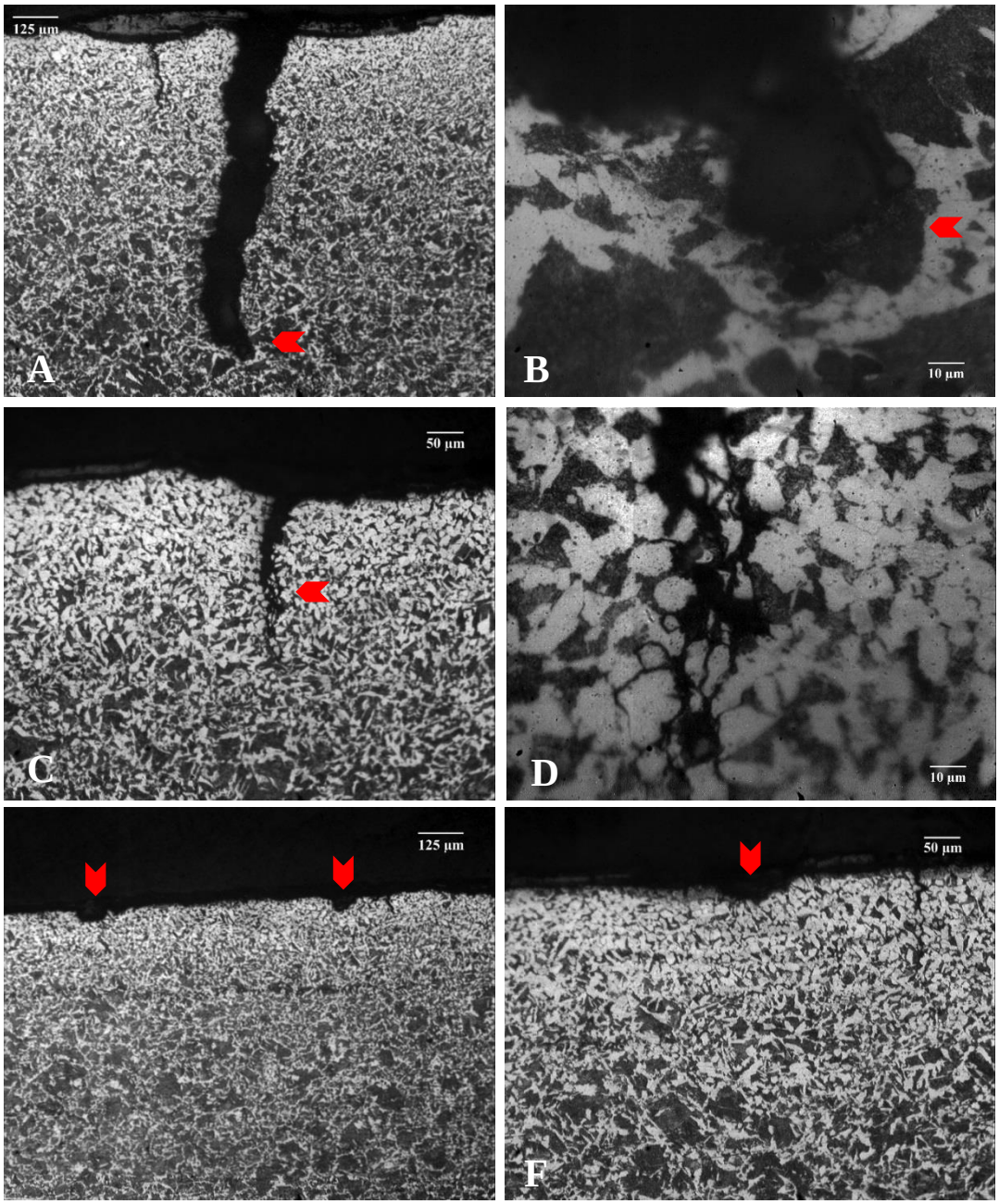

Figure 49. Details on SCC crack morphology on pipeline #4 revealed (A) very wide cracks (C-D) with a mix mode crack propagation, and (E-F) evident pitting on the OD. (B) Detail of crack tip, which appears to terminate in a pearlite colony. 2% Nital.

Microstructural characteristics

The microstructure of pipeline #4 exhibited what appears to be a decarburized layer near the OD (Figure 50A-B) and a banded structure (Figure 50C-D) characterized by alternating layers pearlite (dark microconstituent) and ferrite with elongated inclusions (some with aspect ratios greater than 20) (Figure 50E-F). The banded structure was more evident in the core region and near the ID (Figure 50B and D).

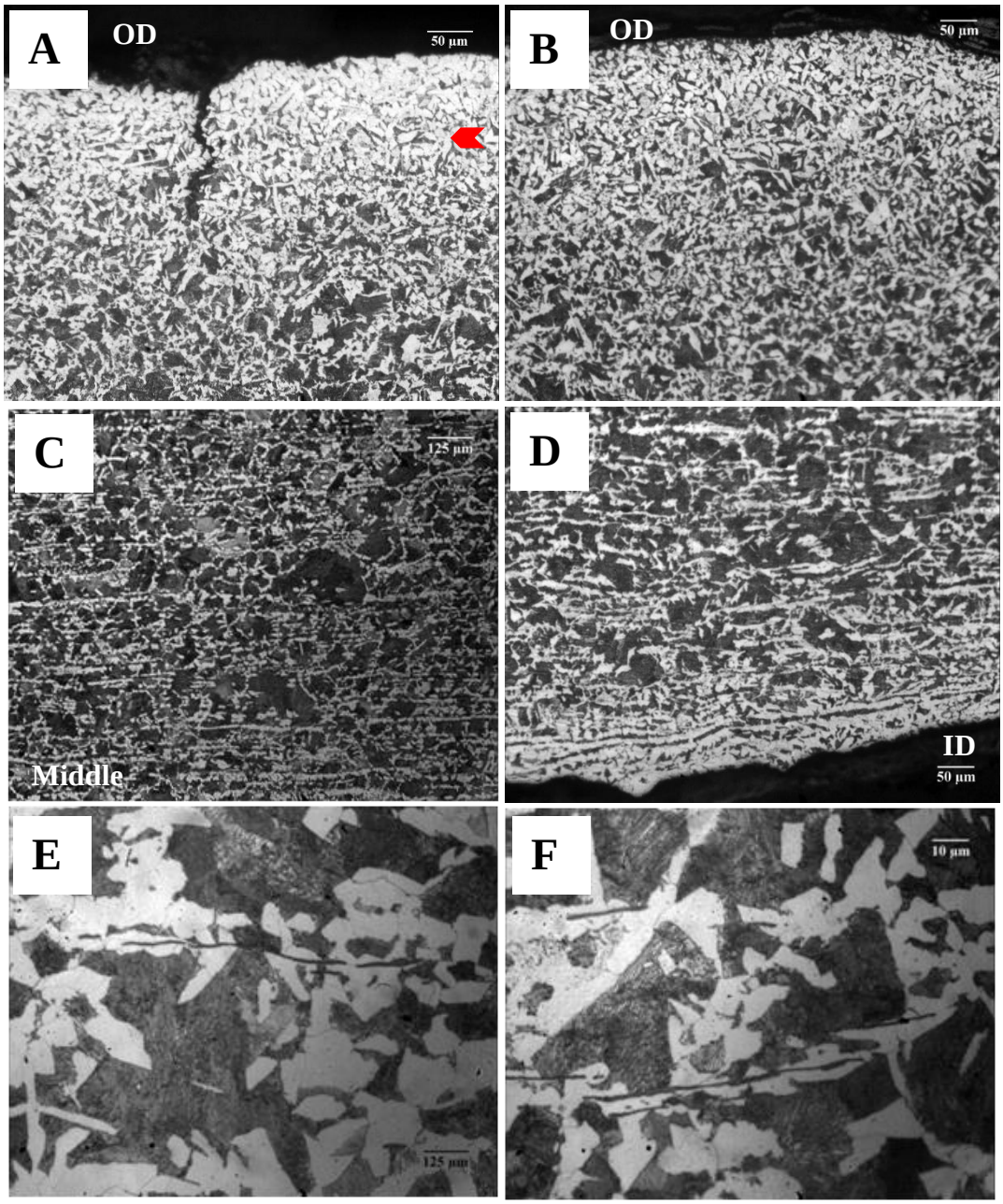

Figure 50. Light micrographs of the general microstructure of pipeline #4 showing (A-B) a narrow decarburized layer on the outer diameter, (C-D) evident banding on the core region and inner diameter, and (E-F) elongated inclusions. 2% Nital.

Furthermore, the microstructure near the OD exhibited a more needle-shaped ferrite and smaller pearlite colonies as compared to the core region which was characterized by polygonal or quasi-polygonal ferrite and coarser pearlite colonies. The core grain size calculated by the linear intercept method was about 12 µm (ASTM G 9.5), while that on the OD was 9 µm (ASTM G 10.5). The microstructural difference between rim and core is shown in Figure 51.

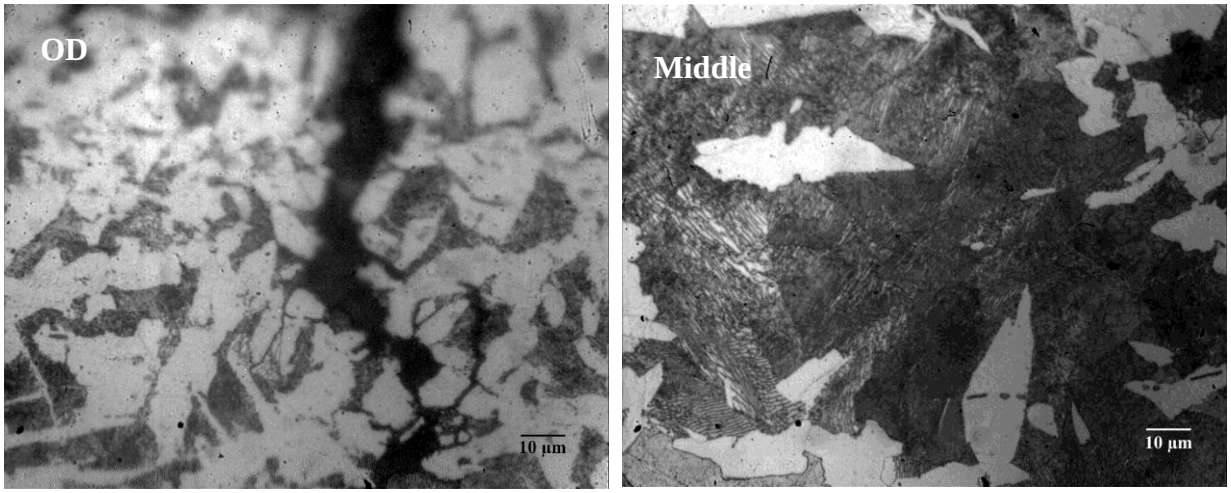

Figure 51. Light micrographs exhibiting the differences in ferrite and pearlite morphology and size between rim and core region. 2% Nital.

TEM bright field images from pipeline #4 clearly show the presence of ferrite grains (Figure 52), dislocation structures (Figure 53), pearlite colonies (Figure 54), and particles with different morphologies and sizes (Figure 55 to Figure 56). Micrographs in Figure 52 suggest that the ferrite morphology is characterized by polygonal or quasi-polygonal ferrite (Figure 52A-C) and what appears to be some lath-type ferrite (Figure 52C). Furthermore, ferrite grains exhibit high dislocation density.

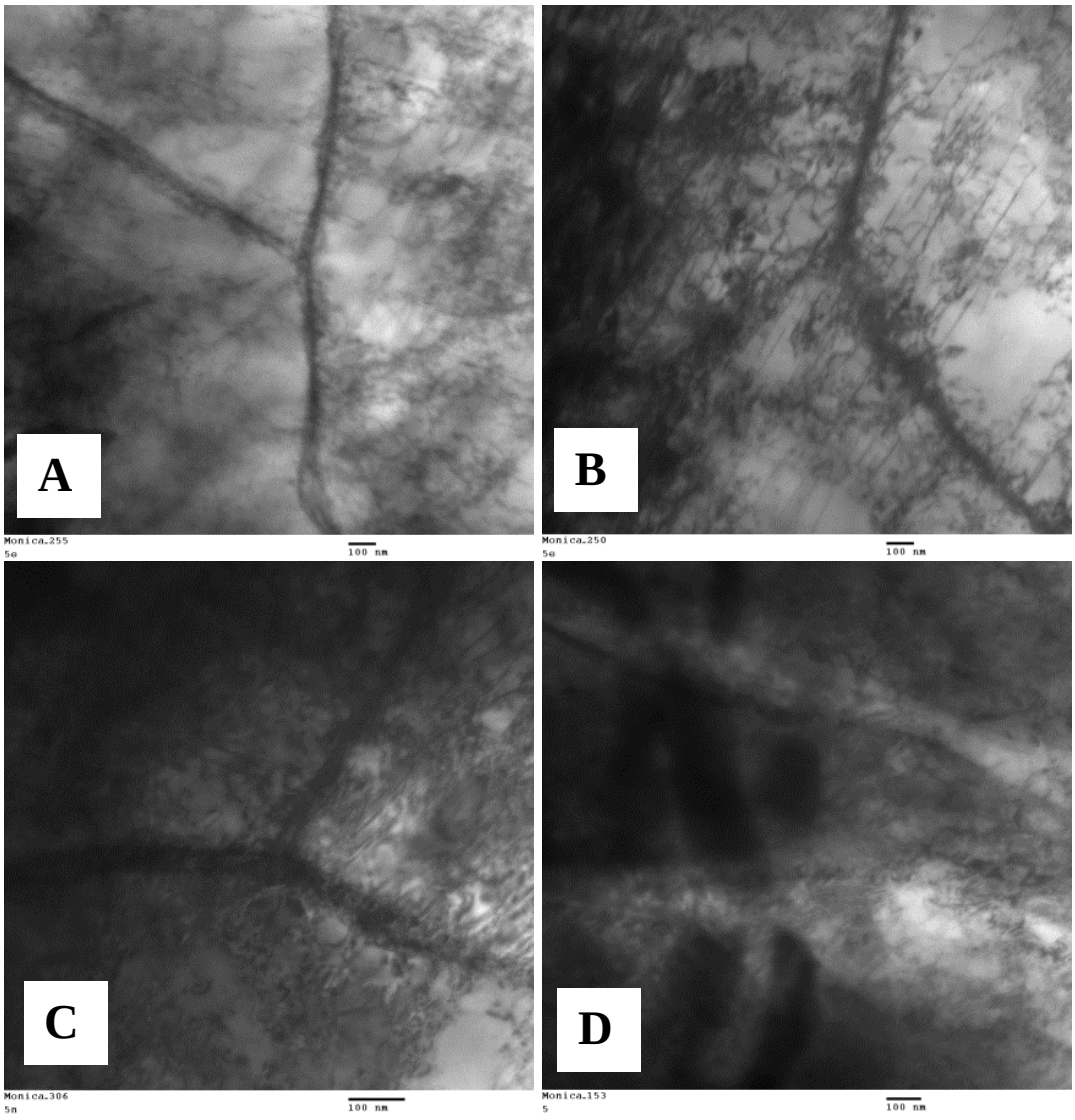

Figure 52. TEM micrographs illustrating the general microstructure of pipeline #4; (A-C) suggest the presence of polygonal or quasi-polygonal ferrite with (B-C) straight dislocations, and (D) what appears to be needle-shaped ferrite with large carbides.

Dislocation structures within the ferrite grains are presented in Figure 53. Dislocation loops are shown in Figure 53A, some relatively straight dislocations in Figure 53B, and dislocation cells in Figure 53C-D.

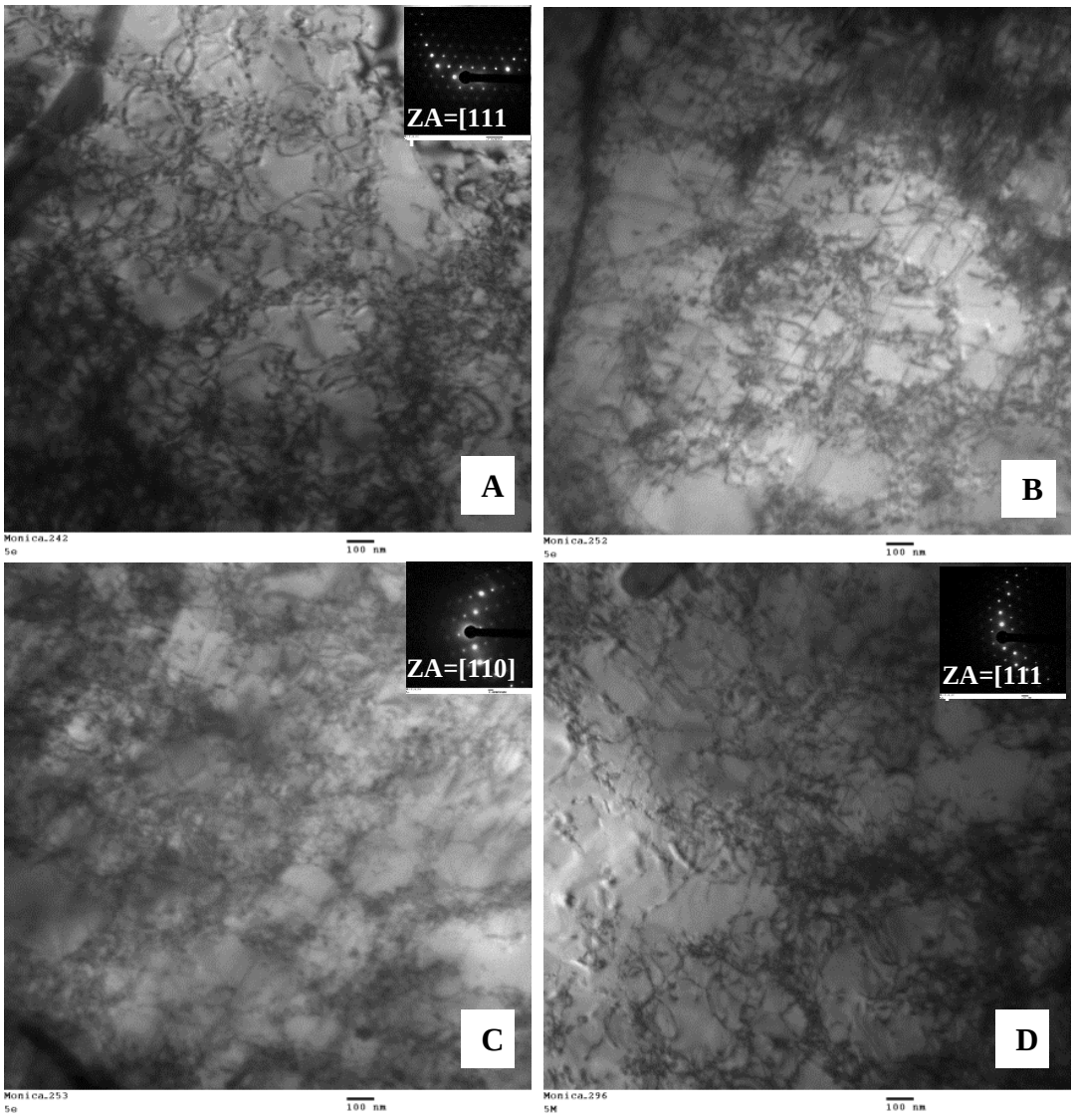

Figure 53. Bright TEM micrographs illustrating dislocation structures within the ferrite matrix with (A) dislocation loops, (B) relatively straight dislocations, and (C-D) cells.

Another microstructural constituent present in this pipeline steel is pearlite. While pearlite colonies presented in Figure 54A-D suggest a lamellae structure with continuous and nearly parallel cementite platelets, Figure 54E-F show broken-up pearlite with morphology of degenerated pearlite.

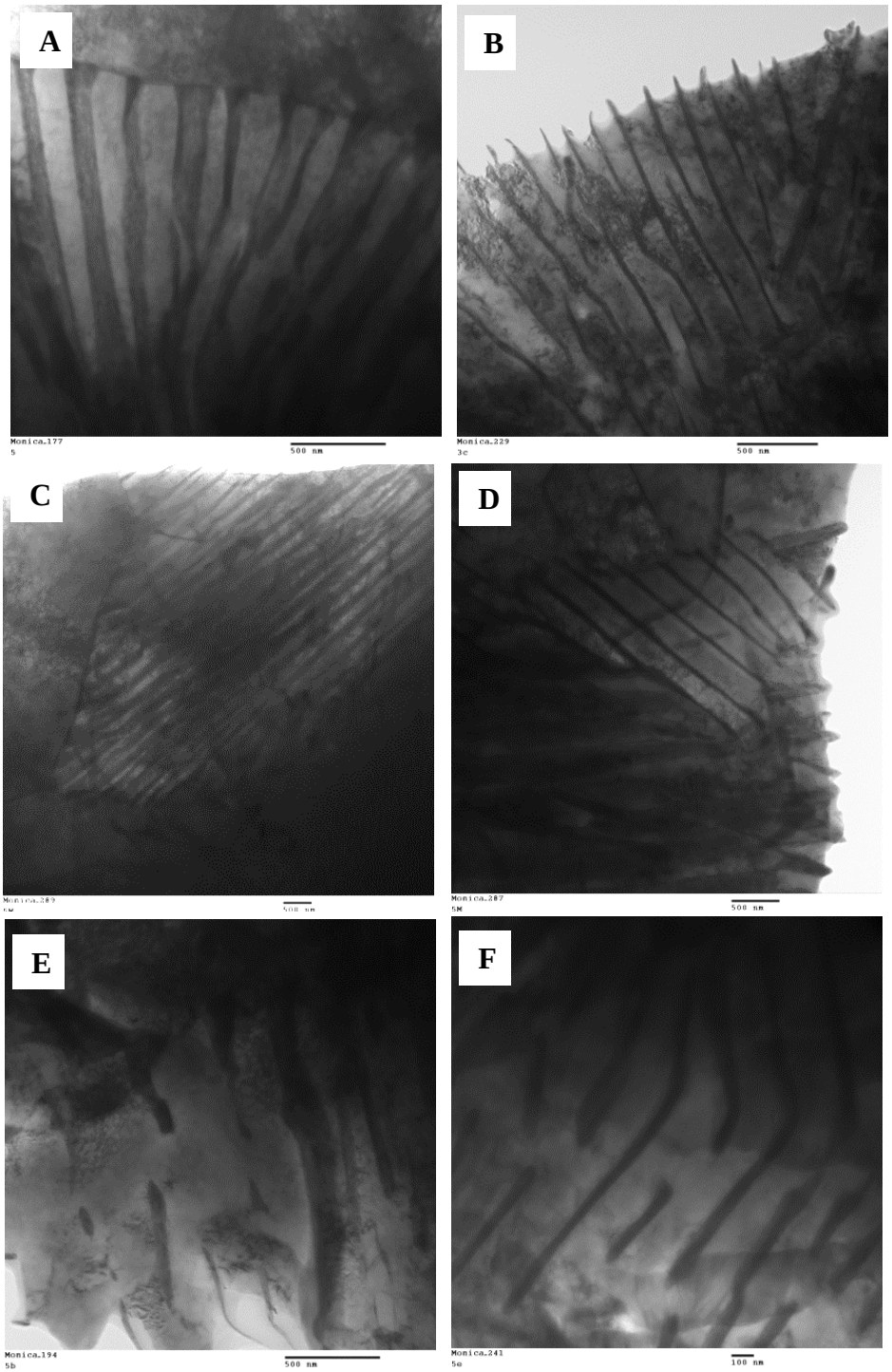

Figure 54. TEM micrographs showing (A-D) pearlite colonies and (E-D) degenerated pearlite

Particles with different morphologies within the ferrite grains are presented in Figure 55 and Figure 56. Figure 55 shows cuboidal shaped particles (~0.07-0.3 µm) and Figure 56 illustrates large nearly circular (~0.2 µm) and elongated particles (Figure 56A-B), and cementite at the ferrite grain boundary (Figure 56C-D).

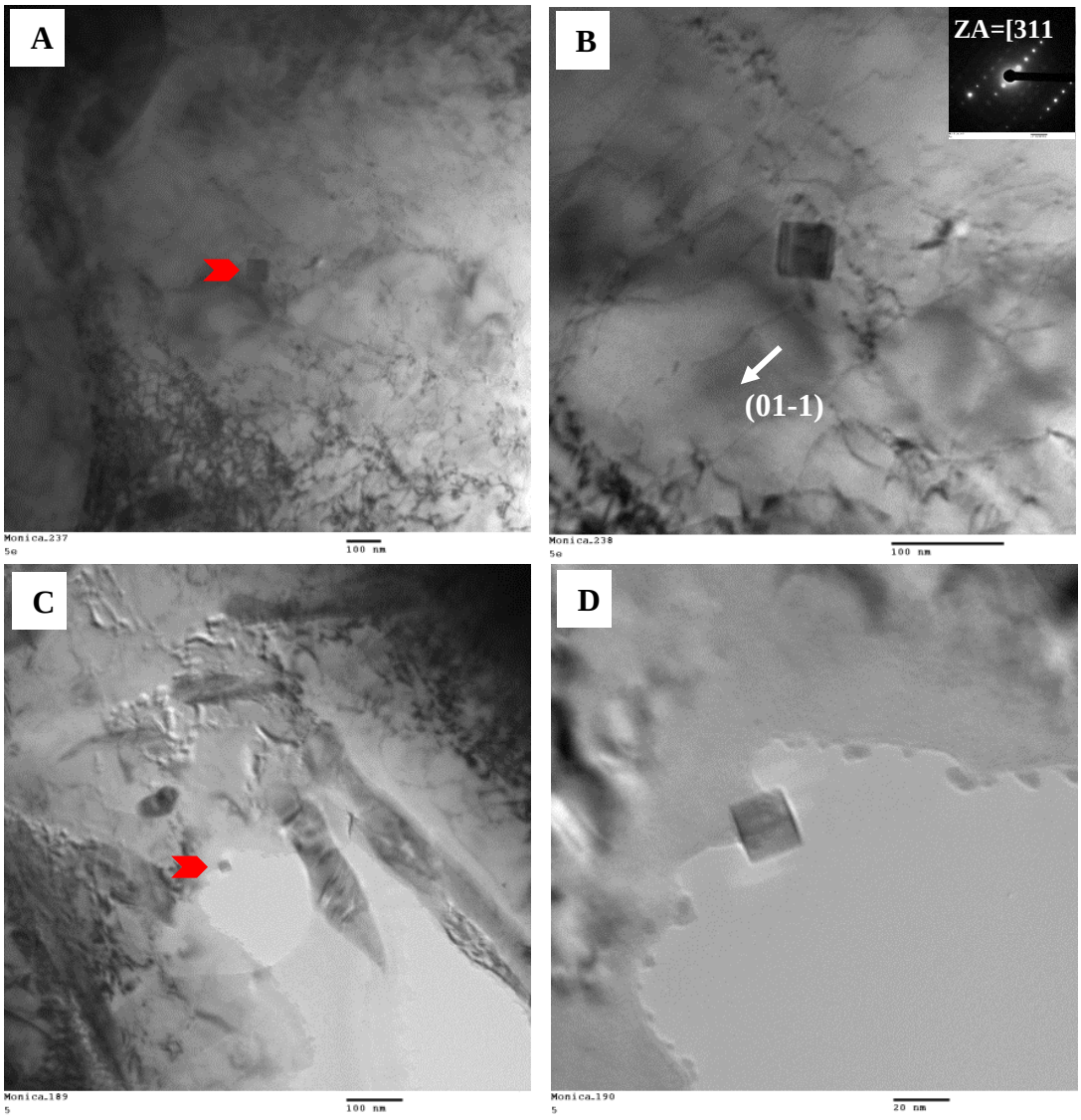

Figure 55. Bright field TEM micrographs showing cuboidal particles (A) (0.07 µm) and (C) (0.3 µm) (B) and (D) are higher magnification images from (A) and (C) respectively. Straight dislocation in the (01-1) direction are observed in (B).

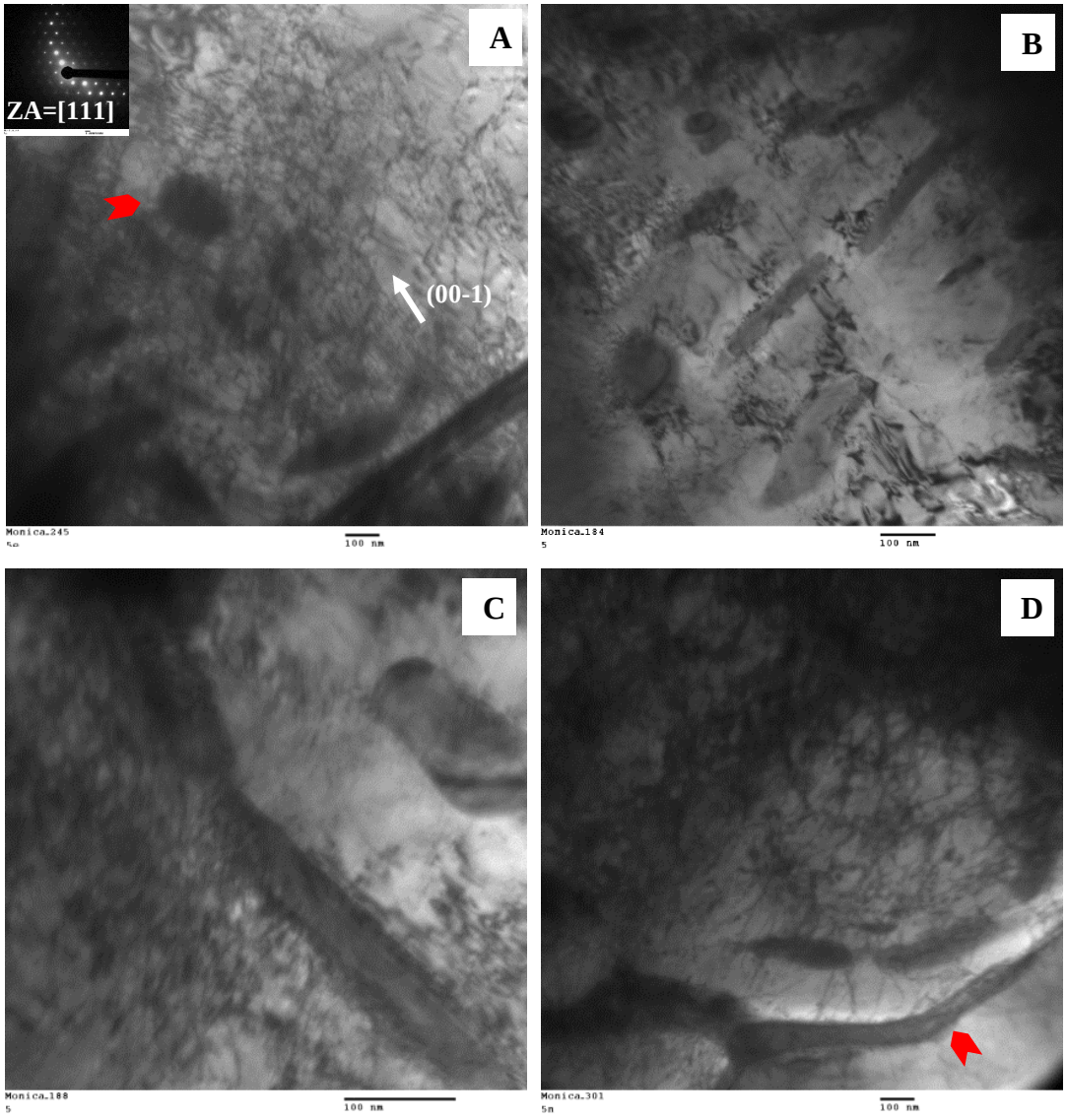

Figure 56. Bright field TEM images showing (A) a large (~0.2 µm) nearly circular particle and dislocations in the (00-1) direction. (B) Carbides and (C-D) cementite at ferritic grain boundaries and dislocation tangles.

4.5 PIPELINE #5

4.5.1 Background Information

Pipeline #5 was constructed by Lone Star and installed in 1966. This long seam (ERW) pipe was built from X52 grade steel, with a 406 mm (16″) O.D. and a nominal wall thickness of 7.14 mm (0.281″). A coal-tar enamel and impressed-current cathodic protection (CP) were applied. In 2011 a "smart pig" detected pitting; therefore, the pipeline was removed from service. Figure 12 presents the as-received sections from this pipeline and Table 16 summarizes the pipeline attributes and operating conditions.

Table 16. Pipeline #5 Attributes and Operating Conditions

Pipeline attributes and operating conditions			
Construction date	1966	**Pressure @ failure**	n/a
Failure date	2011	**SMYS**	423MPa(6135 psi)
Manufacturer	Lone Star	**Classification**	Vintage
Outside diameter	406 mm (16″)	**Location**	TX
Wall thickness	7.14 mm (0.281″)	**Terrain/soil type**	n/a
Type of seam	ERW	**Distance-compressor**	2.5 miles
Steel grade	X52	**Soil pH**	n/a
Coating	Coal tar + CP	**CP**	n/a
Max crack length	n/a		

4.5.2 Non-Destructive Evaluation

During wet magnetic particle inspection some surface discontinuities were revealed. Nonetheless, no indication of stress corrosion cracking was found, as shown in Figure 57.

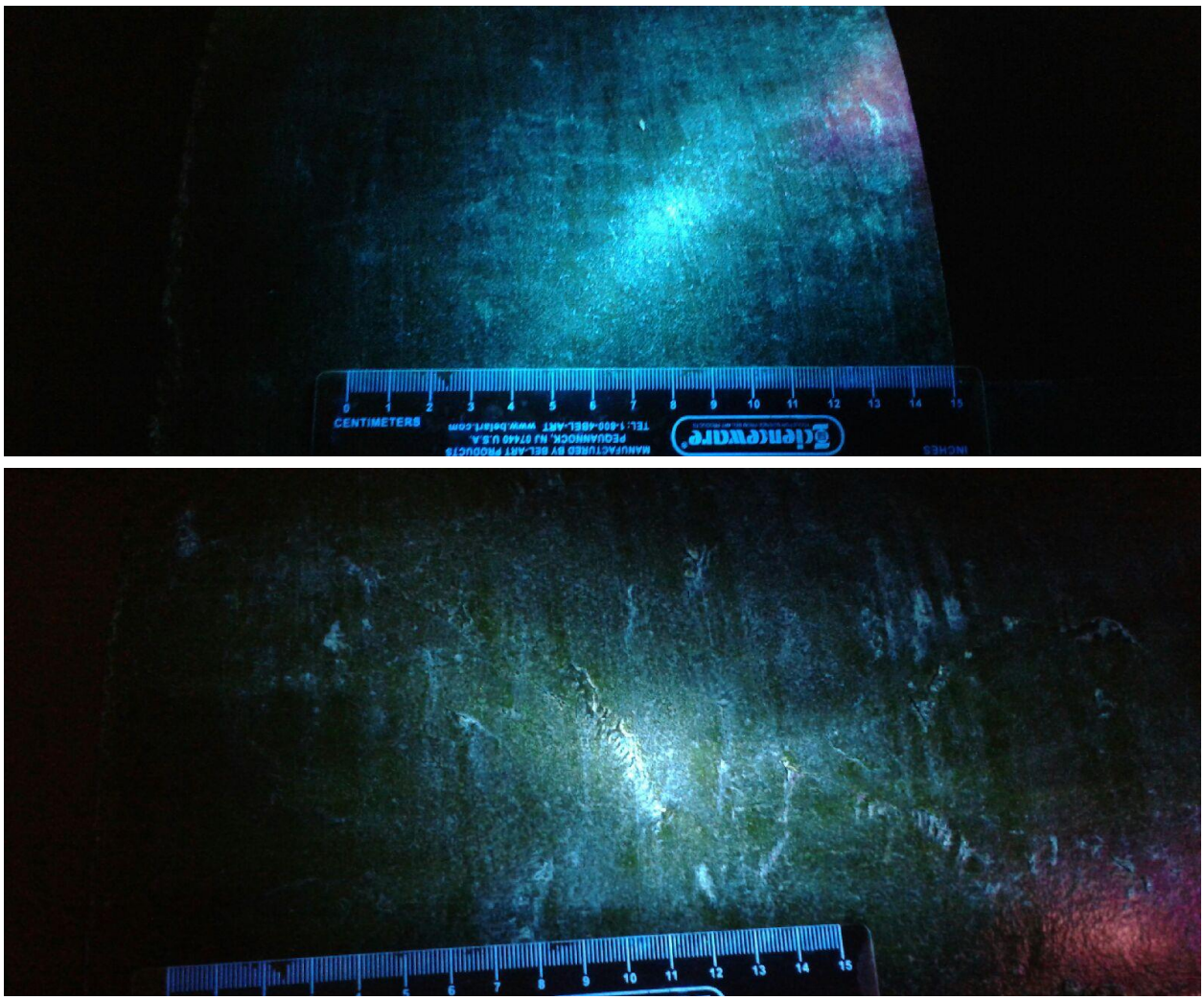

Figure 57. Wet magnetic particles inspection revealed some surface discontinuities on pipeline #5 but no evidence stress corrosion cracks.

4.5.3 Chemical Analysis

Table 5 presents the chemical composition of pipeline #5. Chemical analysis revealed that this pipeline was manufactured to a semi-killed or killed steel practice product of partial or full deoxidation as indicated by the Mn content. Furthermore, this pipeline was made to a fine grain practice as revealed by Al content.

Pipeline #5										
C	Si	Mn	Cr	Mo	Ni	Al	Co	Cu	Nb	Ti
0.27	0.006	1.5	<0.002	<0.002	<0.0035	0.02	0.004	0.02	<0.002	0.003

Pipeline #5				
V	W	Pb	Zr	Fe
<0.001	<0.02	<0.01	0.004	***Rem.***

4.5.4 Elemental Mapping

Figure 58 and Figure 59 presents the SEM and elemental mapping images from a region adjacent to the OD (left column) and the core region (right column) from pipeline #5. The EDS mapping revealed subtle differences between the analyzed areas. The OD exhibited a slightly higher concentration of Mn and S as indicated by the color brightness. Contrary to this, Si concentration was higher on the core. The presence of MnS sulfides was observed in both regions, however, the MnS in the core exhibited a more elongated appearance. No significant differences were observed in the C and P concentration.

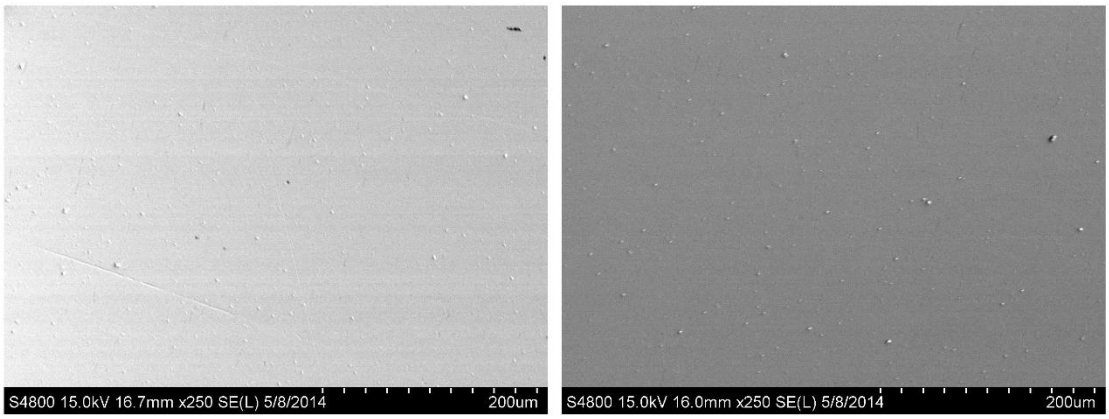

Figure 58. SEM images from the OD and the core region.

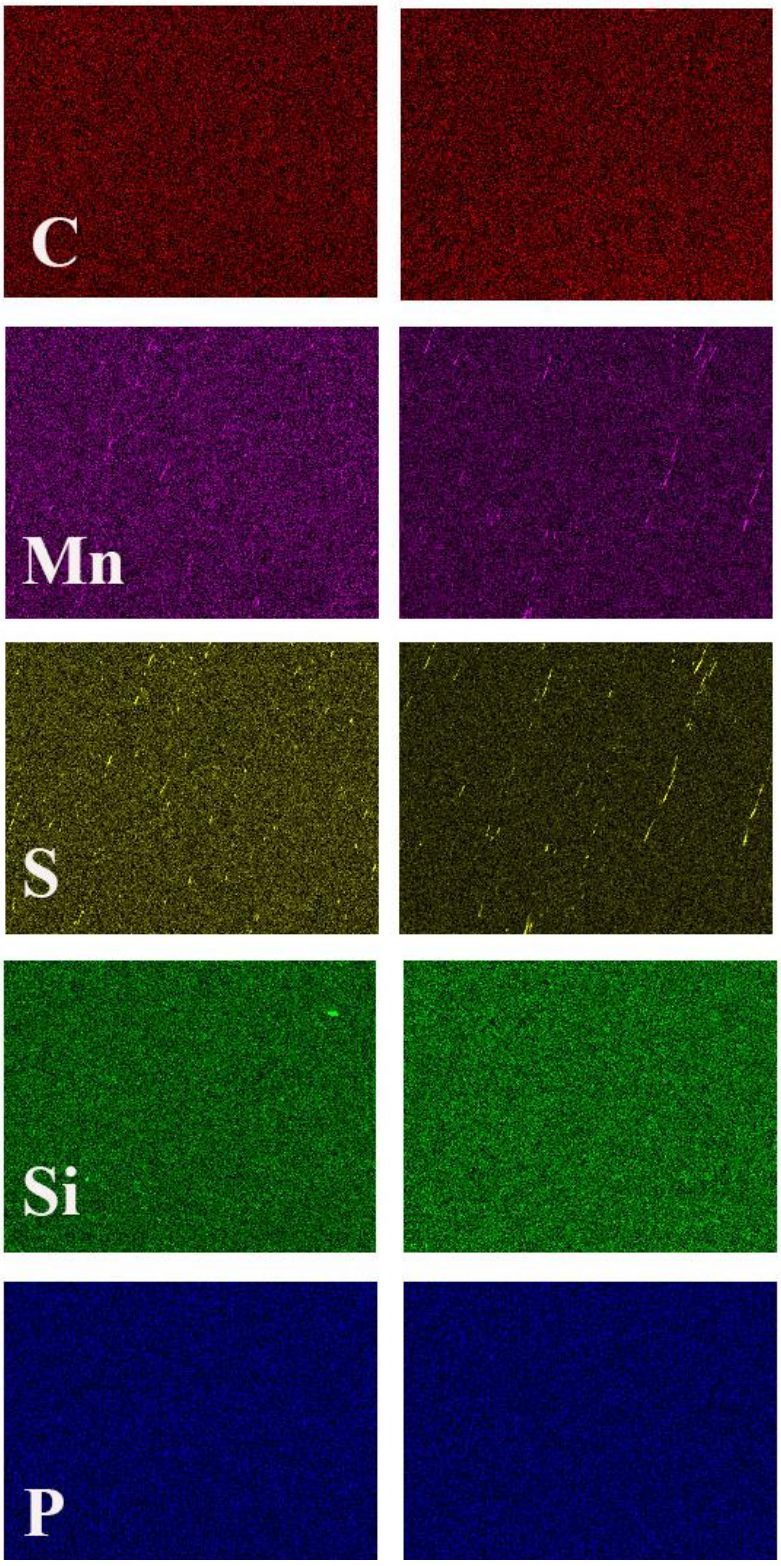

Figure 59. Elemental mapping from a region near the OD (left) and the core (right).

4.5.5 Hardness Testing

The hardness profile (OD to ID) from pipeline #5 and the average microhardness (HV) and equivalent HRB and tensile strength are presented in Figure 60 and Table 1, respectively. Hardness profile exhibited a lower hardness near the ID. No significant differences were observed between OD and core.

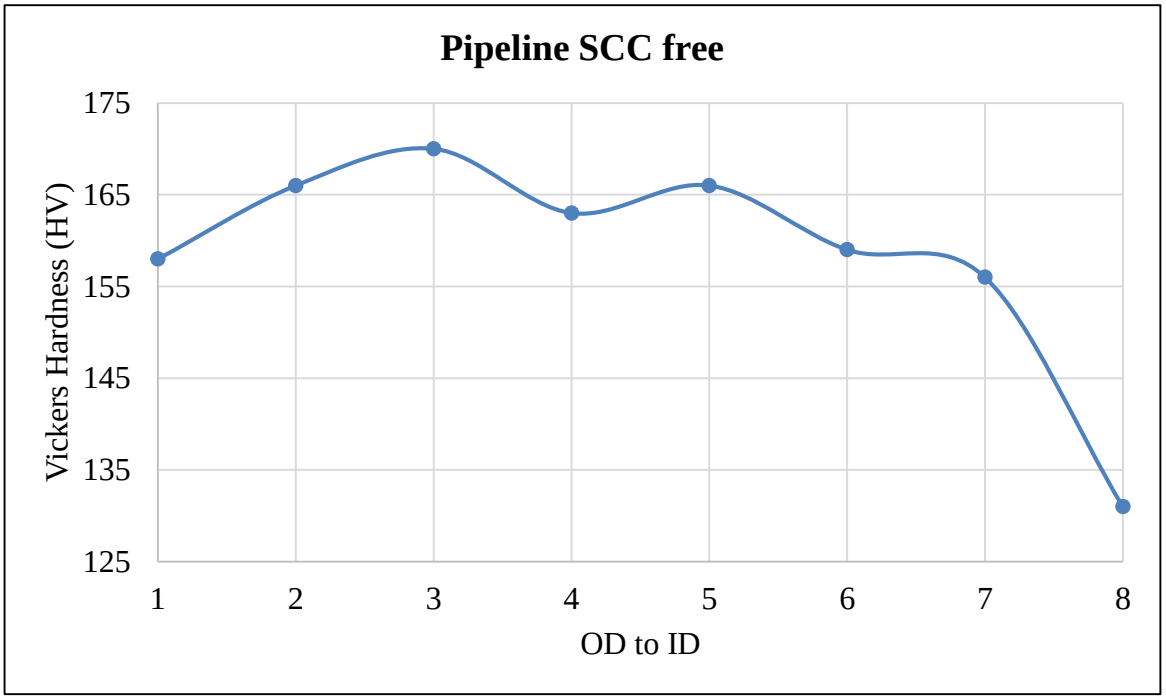

Figure 60. Pipeline #5 harness profile.

Table 17. Pipeline #5 Harness Testing Results

Region	Average Vickers (HV)	Converted Average HRB	Equivalent Tensile Strength (psi)
Base metal	159	81	509 (73824)

4.5.6 Microstructural Characterization

Crack morphology

Microstructural characteristics

Optical micrographs from pipeline #5 are presented in Figure 61 to Figure 64. The representative low magnification micrograph in Figure 61 revealed a somewhat uniform microstructure with no evident banding and noticeable pitting on the OD and the ID. Higher magnification optical images from the OD, ID, and core, are shown in Figure 62, Figure 63, and Figure 64, respectively.

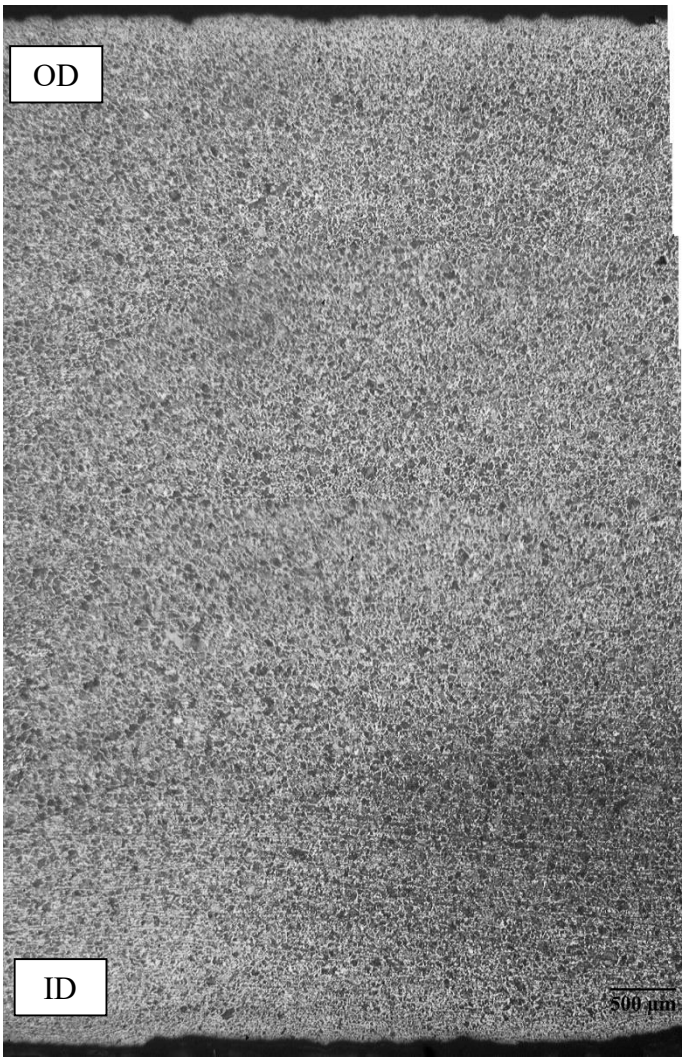

Figure 61. Low magnification light micrograph from pipeline #5 showing a fairly uniform microstructure and evident pitting on the OD and the ID. 2% Nital.

The region adjacent to the OD revealed pitting (Figure 62A), a decarburized layer (Figure 62B) and what appear to be very fine grains (Figure 62C). The average grain size close to the OD was estimated to be about 8 µm (ASTM G No. 10). The general microstructure in this region was characterized by polygonal and quasi-polygonal ferrite and pearlite (volume fraction about 36%). Furthermore, disconnected inclusions were also observed (Figure 62D).

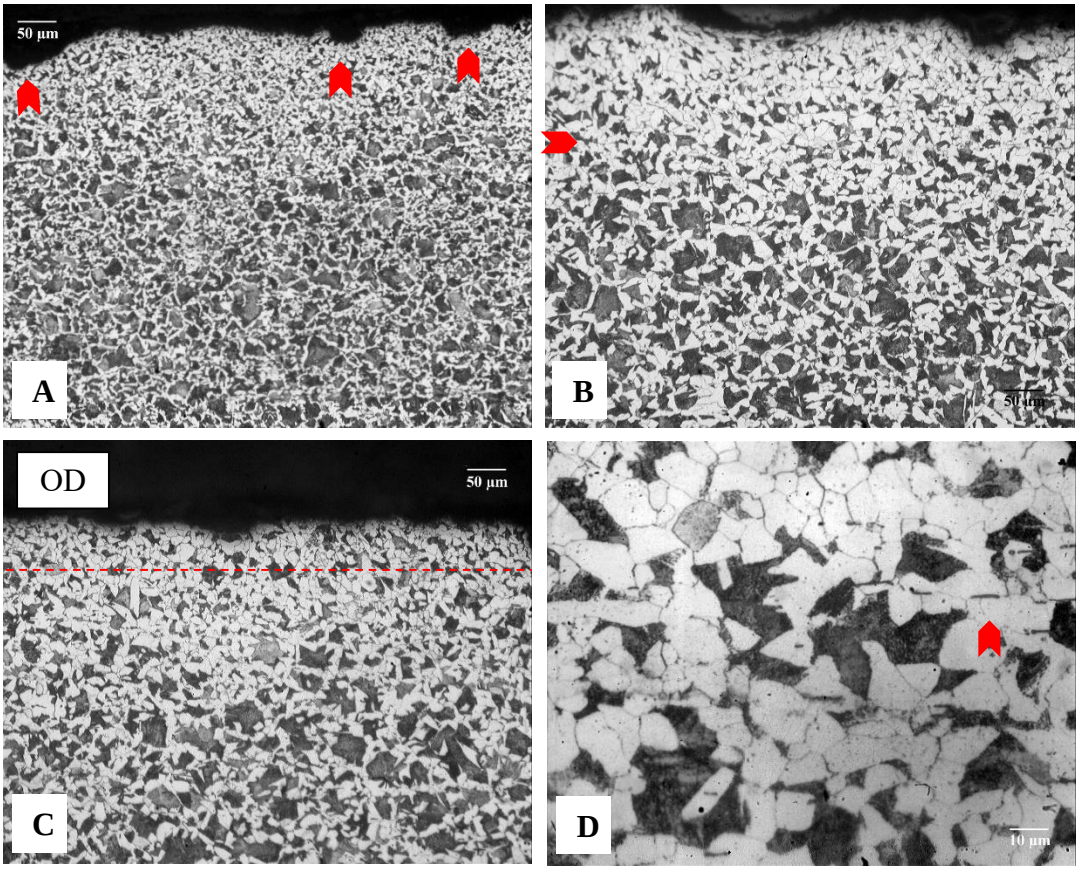

Figure 62. Light micrographs from the region near the OD of pipeline #5 exhibiting (A) pitting, (B) a decarburized layer (indicated by arrow), (C) very fine grains, and (D) polygonal ferrite with disconnected inclusions (arrow) and pearlite colonies (dark constituent). 2% Nital.

Despite the fact that no banding was observed in lower magnification images (Figure 61), higher magnification micrographs from the section close to the ID (Figure 63) exhibited a banded structure (Figure 63 A-C) characterized by alternating layer of ferrite and pearlite (dark constituent). The ID also exhibited what appears to be very small grains (Figure 63B) and evident pitting (Figure 63C). The general microstructure was polygonal and quasi-polygonal ferrite with pearlite colonies (Figure 63D).

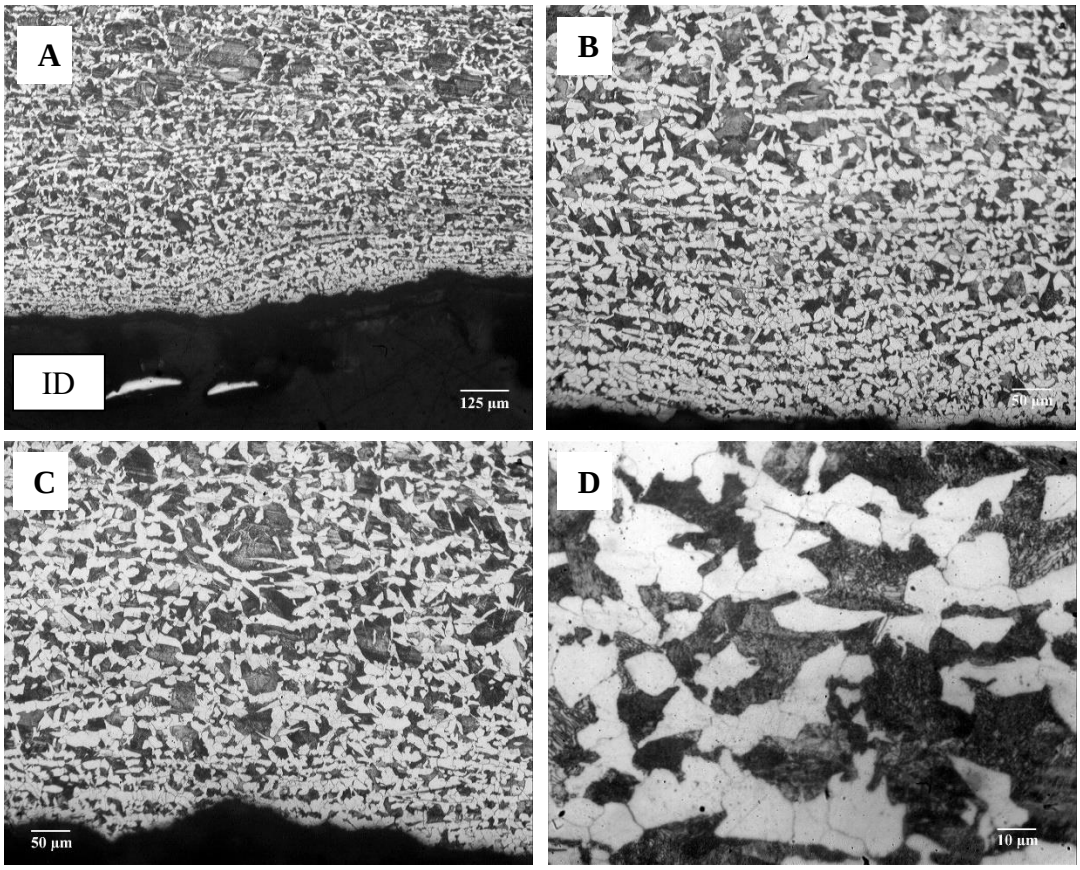

Figure 63. Light micrographs from the region near the ID of pipeline #5 showing (A-B) deformed banding, (B) grain refinement, (C) pitting and (D) a polygonal/quasi-polygonal ferrite morphology and pearlite. 2% Nital.

Lastly, the microstructure in the core region (Figure 64) was characterized by quasi-polygonal ferrite, larger pearlite colonies (volume fraction about 62%), and elongated inclusions with aspect ratios greater than 20. The average grain size calculated by the linear intercept method was 20 μm (ASTM G no. 8).

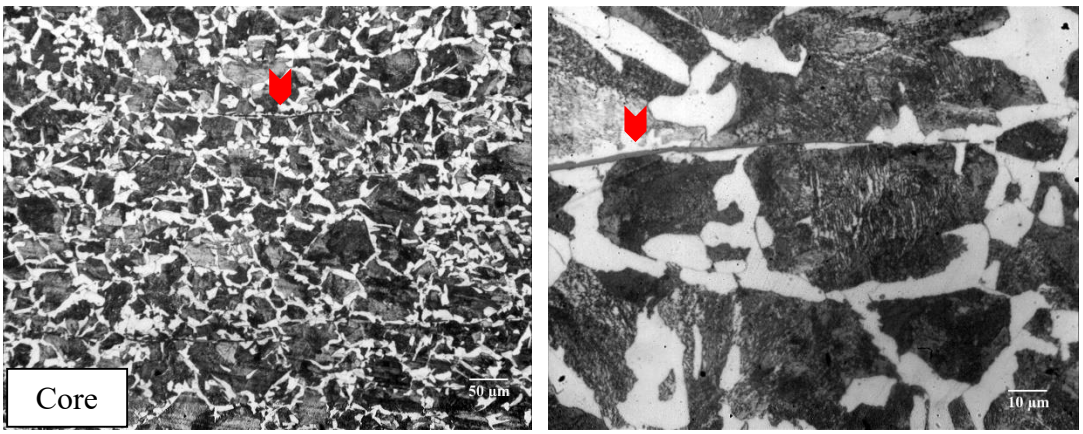

Figure 64. Light micrographs from the core region of pipeline #5 revealed a quasi-polygonal ferrite morphology with elongated inclusions and pearlite colonies. 2% Nital.

4.6 SUMMARY

During this investigation, five different pipelines were analyzed. Pipeline #5 (Figure 73) was removed from service after 45 years because “smart pigs” detected pitting, however after this long service period no SCC were developed. The remaining four service components analyzed (#2, #1, #3, and #4) were removed from operation due to stress corrosion cracking (Figure 74). In this manner, the aim of this investigation was to expand our knowledge on what constitutes a susceptible microstructure. Therefore, a systematic microstructural characterization was carried-out to uncover the main microstructural features as well as the conditional state of the region near the surface layer from SCC susceptible pipeline materials.

4.6.1 Background Information

A summary from the background information and operating conditions from each pipeline is presented in Table 18. All of the investigated pipelines were located in the southwest region and are classified as vintage pipes. The pipelines were produced around 1950-1960 by different manufactures. From the pipelines removed from service due to SCC, four failed after 40 years in service and one after 20 years (pipeline #4). On the other hand the SCC free pipeline remained in service for about 45 years before pitting was found.

Table 18. Investigated pipeline's attributes and operating conditions.

Pipeline Attributes and Operating Conditions					
Attributes	#2	#1	#3	#4	SCC free
Manufacturer	Newport Steel	Cal-Met	Republic Steel	A.O. Smith	Lone Star
Construction	1947 installed	1949	1951 installed	1947-1950	1966
Failure date	1993	1991	1995	1967	2011
Service (yrs.)	46	42	44	17-20	45
Crack depth	79.4% wt.	100% wt.	67% wt.	50% wt.	n/a
Pressure at failure	5MPa (744 psig)	n/a	8MPa (1160 psi)	n/a	n/a
Wall thickness	3.76mm (0.148″)	4.5mm (0.180″)	7mm (0.271″)	8.22mm(0.324″)	7.13mm (0.281″)
Outside diameter (cm)	152 (60″)	22 (8.625″)	61 (24″)	76 (30″)	41 (16″)
Type of weld seam	Pre 1970-ERW	SSAW	DSAW	DSAW	Long seam (ERW)
Coating	Coal-tar enamel	Coal tar enamel + CP	n/a	Coal tar enamel + CP	Coal tar enamel + CP
SMYS (MPa)	208(30000psi)	208(30000psi)	423(6135psi)	423(6135psi)	423(6135psi)
Classification	Vintage	Vintage	Vintage	Vintage	Vintage
Location	Lordsburg, NM	Willcox, AZ	Cocoino, AZ	Casa Grande, Az.	Waha, Tx.
Terrain/Soil	Dry, red sand	Apparent moisture	Dry, brown, sandy	No clay	n/a
Soil pH	High	9	High	7.4-8.8	n/a
UTS-Cracks	388 MPa	371 MPa	668 MPa	649 MPa	
UTS-No Cracks	388 MPa	423 MPa	526MPa	627 MPa	509 MPa

4.6.1 Chemistry

Chemical analysis (Table 19) revealed that grade A pipelines (pipeline # 1 and #2) were manufactured to a rimmed steel practice and were not made to Si and/or Mn deoxidation practice nor to a fine grain practice. Contrary to this, grade X52 pipelines were made to a semi-killed or killed steel practice product of partial deoxidation and in the case of pipeline #4 and #5 to an Al fine grain practice. Elemental mapping chemical analysis from different elements from a region close to the rim and core are presented in Figure 65 to Figure 71.

Table 19. Chemical Composition

Pipeline	C	Si	Mn	Cr	Mo	Ni	Al	Co	Cu	Nb
#2	0.02	0.004	0.31	0.01	0.004	0.03	0.01	0.01	0.06	<0.002
#1	0.05	<0.003	0.35	0.02	<0.002	0.02	0.01	0.01	0.09	<0.002
#3	0.14	0.03	0.80	0.005	0.003	0.05	0.003	0.02	0.22	<0.002
#4	0.19	0.02	1.3	0.002	0.002	0.004	0.03	0.01	0.02	<0.002
#5	0.27	0.006	1.5	0.002	0.002	0.003	0.02	0.0004	0.02	<0.002

Pipeline	Ti	V	W	Pb	Zr	Fe
#2	<0.001	<0.001	<0.02	<0.01	0.001	Rem.
#1	<0.001	0.016	0.023	<0.010	<0.001	Rem.
#3	<0.001	0.001	<0.02	<0.01	<0.001	Rem.
#4	0.012	0.002	0.03	0.01	0.002	Rem.
#5	0.003	<0.001	<0.02	<0.01	0.004	Rem.

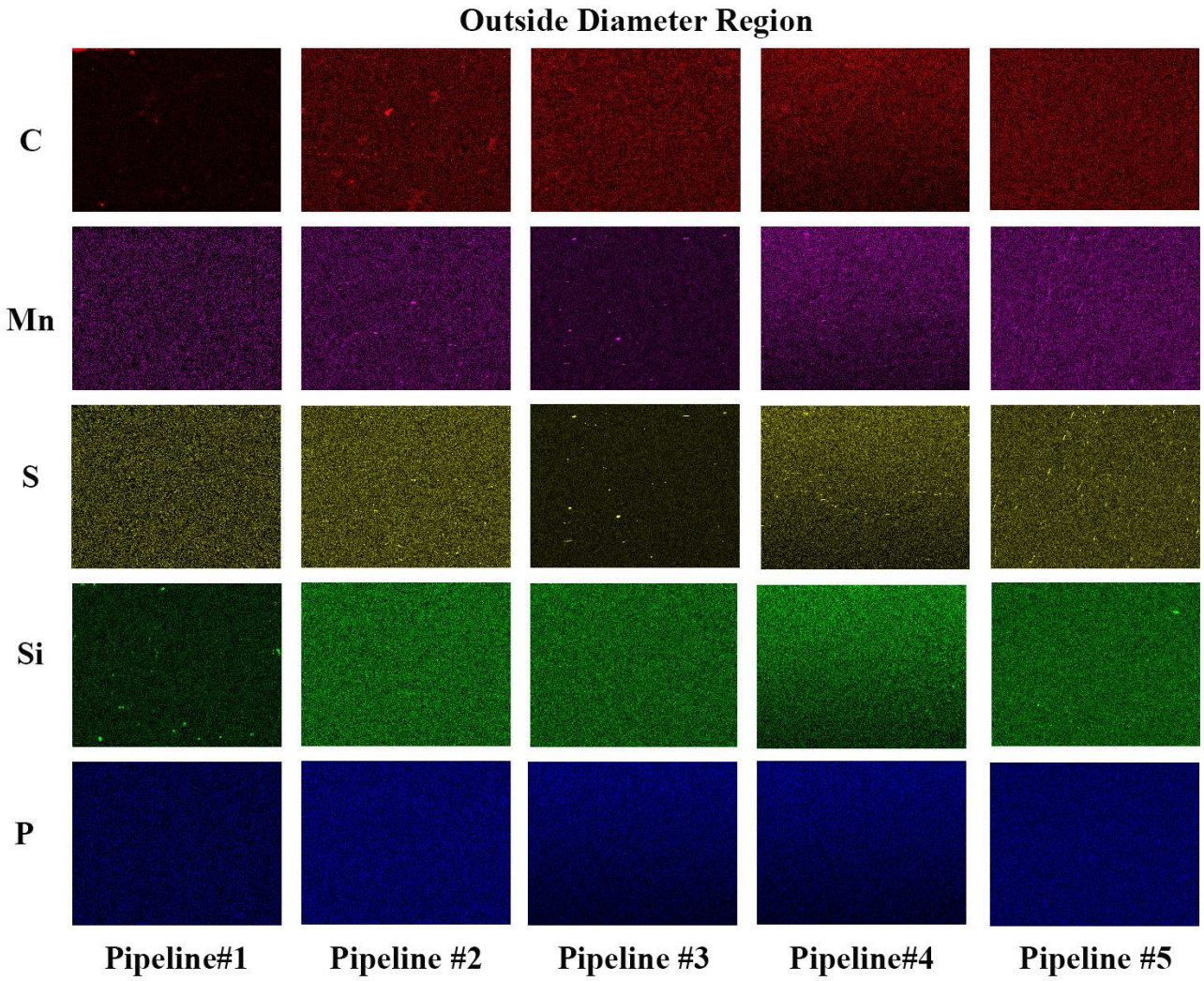

Figure 65. Elemental mapping near the OD region from all the investigated pipelines.

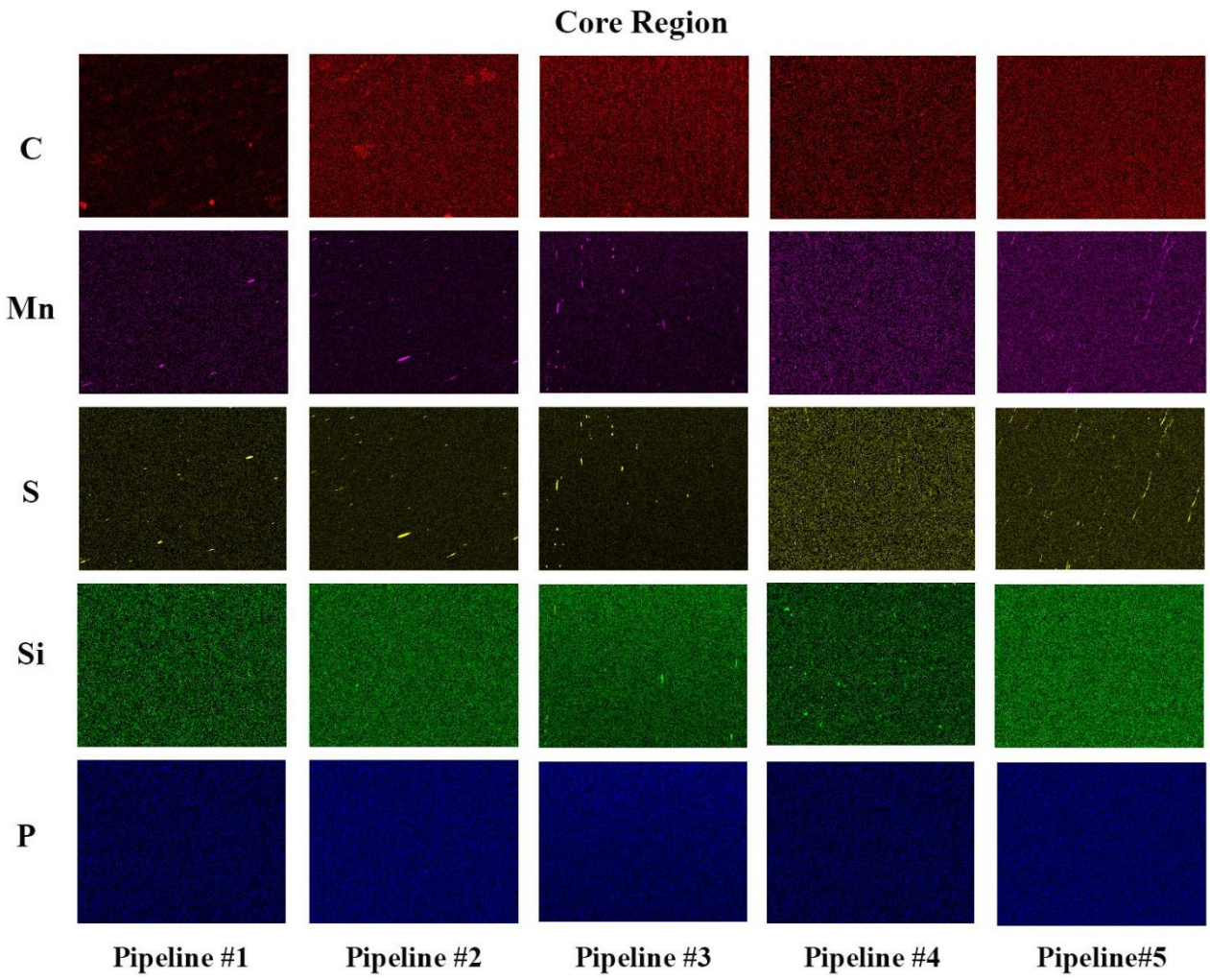

Figure 66. Elemental mapping from the core region from all the investigated pipelines.

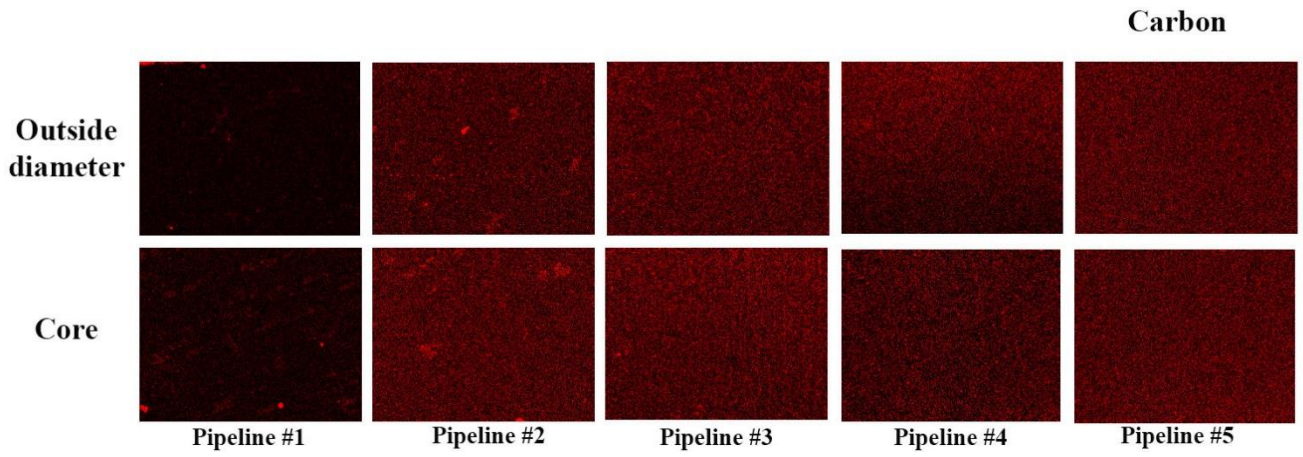

Figure 67. Elemental mapping of carbon near the OD and core region from all the investigated pipelines.

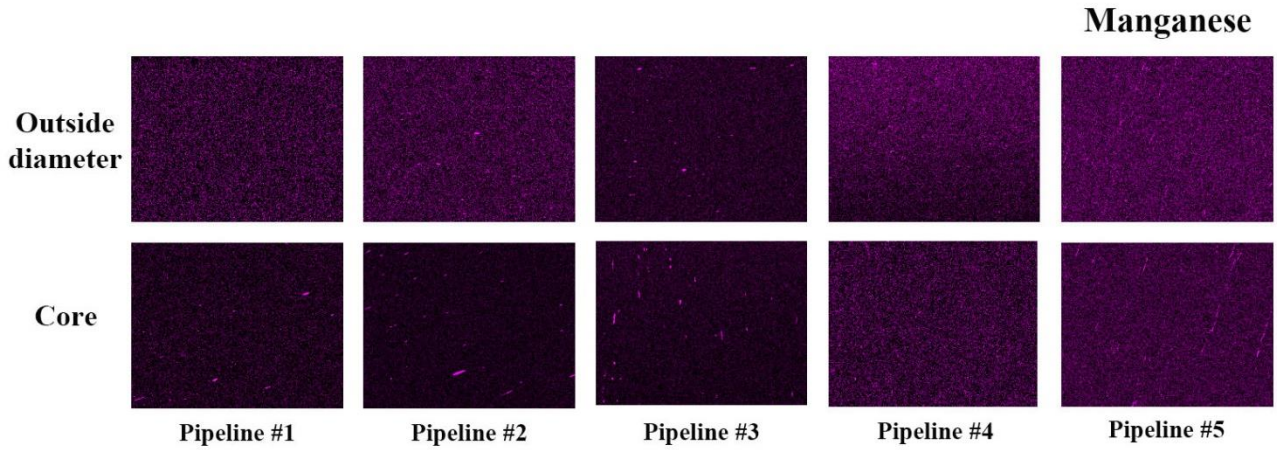

Figure 68. Elemental mapping of Manganese near the OD and core region from all the investigated pipelines.

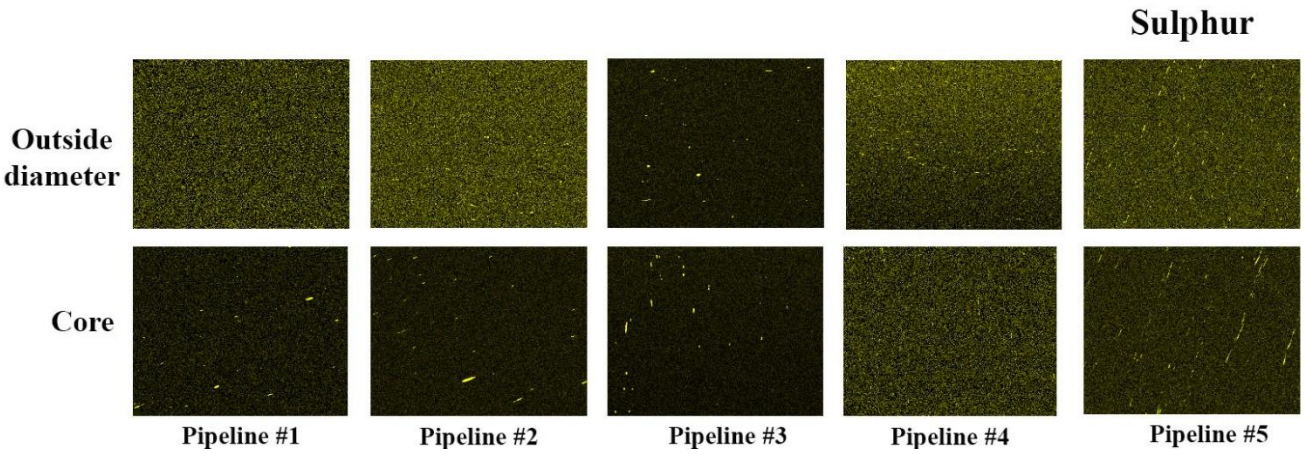

Figure 69. Elemental mapping of sulphur near the OD and core region from all the investigated pipelines.

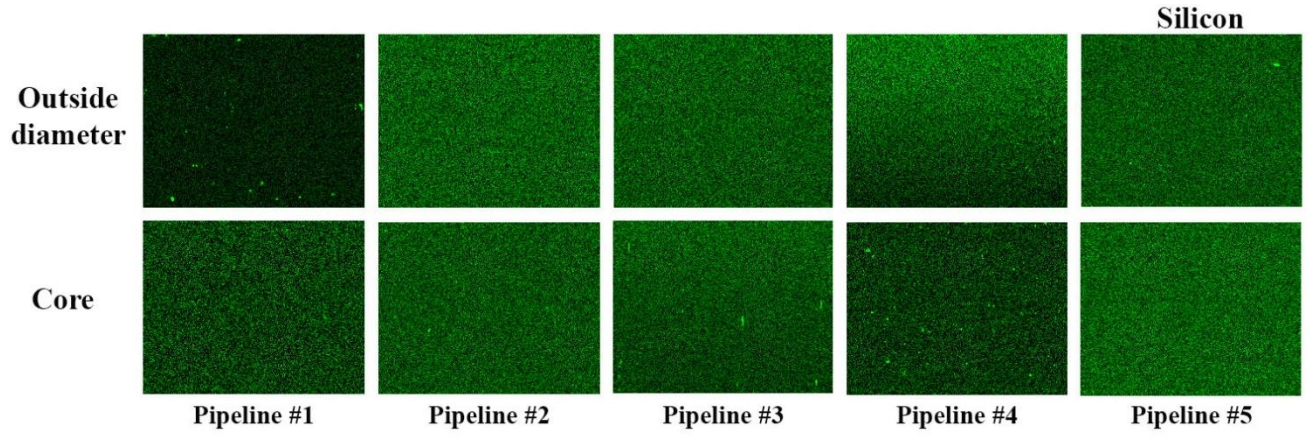

Figure 70. Elemental mapping of silicon near the OD and core region from all the investigated pipelines.

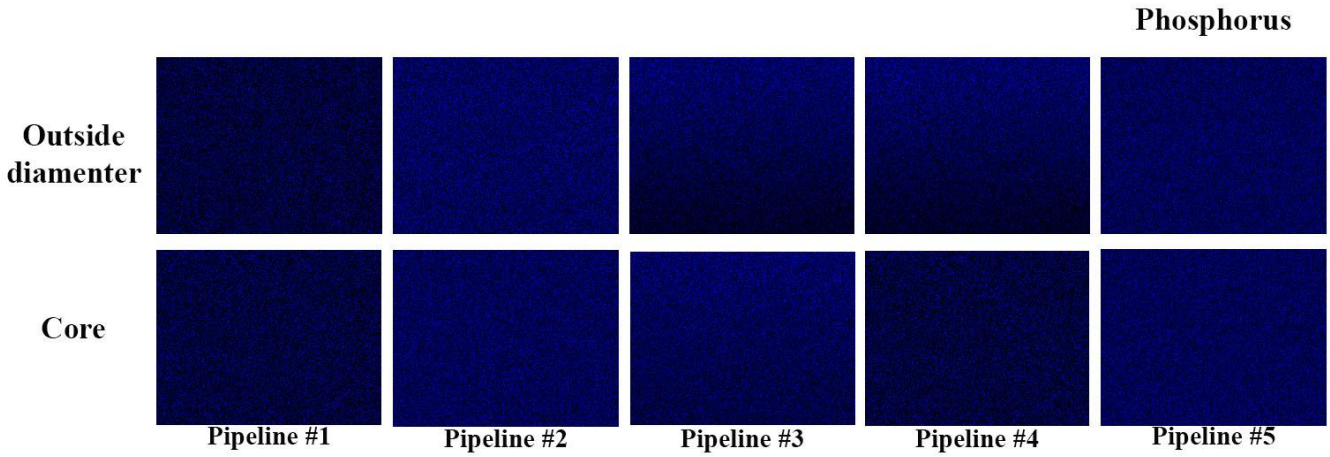

Figure 72. Elemental mapping of phosphorous near the OD and core region from all pipelines.

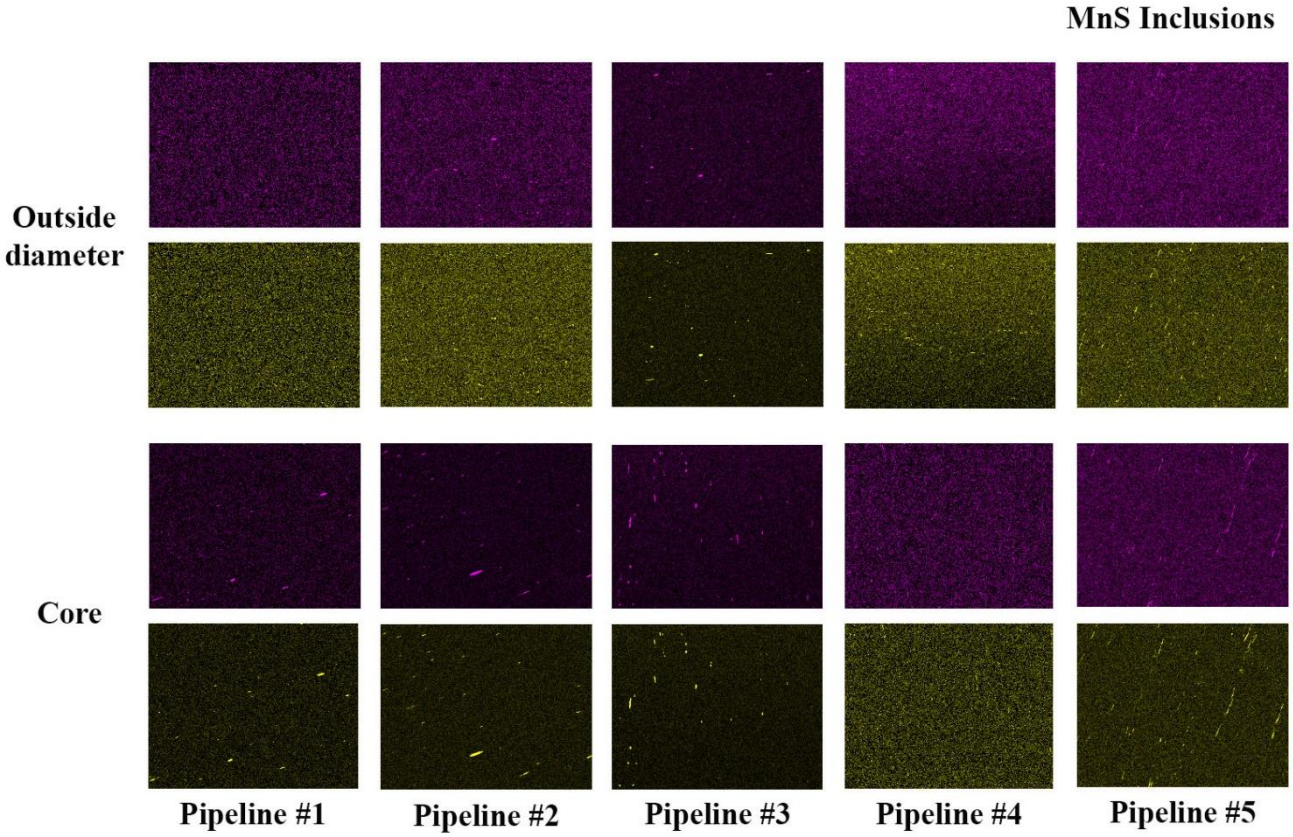

Figure 71. Elemental mapping of MnS inclusions near the OD and core region from all pipelines.

4.6.2 Microstructure

Light micrographs from each pipeline (rim and core) are shown in Figure 73 and Figure 74. During this investigation different microstructural features were observed, such as banding (pipelines #1 and #3), a decarburized layer on the OD region (pipelines #5, #4, and #3), and pitting (pipeline #5). Additionally, majority of the pipelines exhibited pro-eutectoid ferrite and in the case of higher carbon content X52 grade steel pipes more pearlite colonies. The ferrite morphology observed was primarily polygonal ferrite and some needle-shaped ferrite in addition to some grain boundary carbides for grade A pipelines but not for grade X-52 pipes.

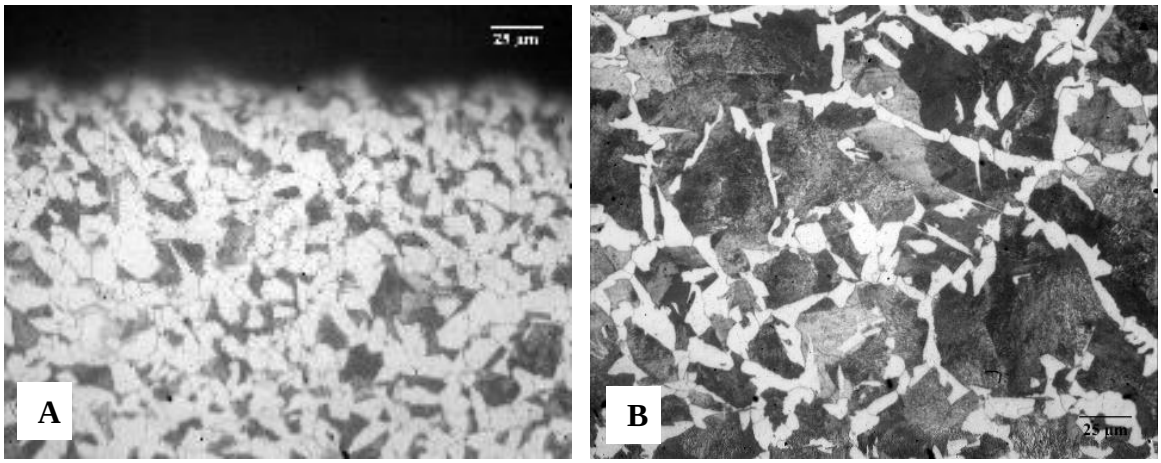

Figure 73. Light micrographs from SCC-free pipeline #5. (A) Outside diameter and (B) core microstructure. 2% Nital.

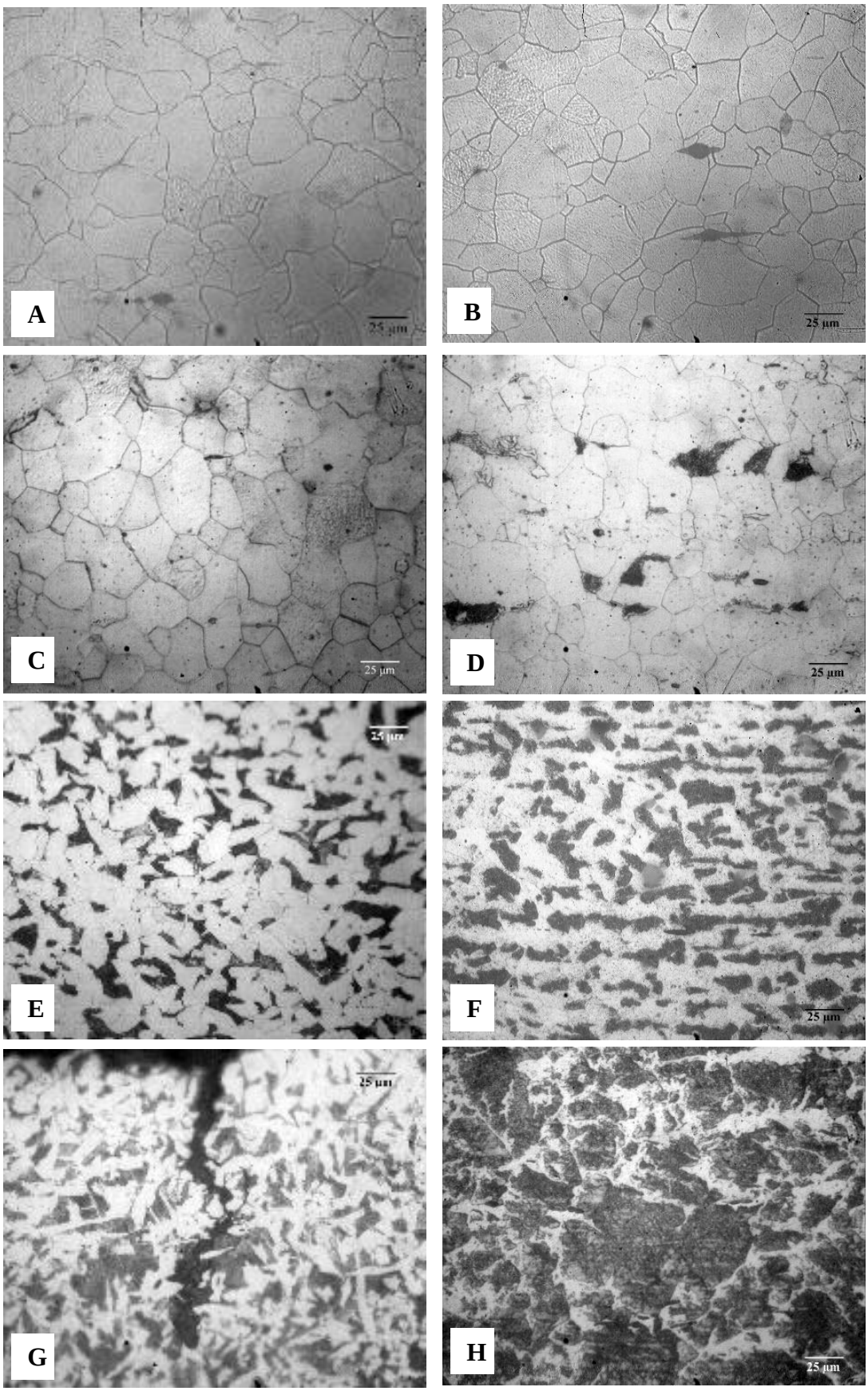

Figure 74. Light micrographs from service pipelines that exhibited SCC. (A) pipeline #2 OD and (B) core microstructure, (C) Pipeline #1 OD and (D) core, pipeline #3 (E) OD and (F) core, and pipeline #4 (G) OD and (H) core microstructure. 2% Nital.

Discussion

The emergence of natural gas as a global commodity underlies the importance of its processing, transmission, and distribution [1,3]. Particularly, as the demand of this energy efficient fossil fuel is expected to markedly increase in the near future [4-5] since natural gas can provide a sustainable energy source without an adverse impact to the environment [3]. Nevertheless, an increasing natural gas demand will require to increase the capacity of the existing systems by utilizing higher operating pressures and expanding the current transmission and distribution pipeline networks [3,6,33] which include miles of outdated, fragile, and vulnerable gas pipelines [20]. In fact, the North America pipeline infrastructure is currently one of the largest and oldest in the world [36]. Furthermore, buried pipelines are prone to in-service degradation as they are expose to aggressive service conditions which involve high and fluctuating pressure and harsh environments. The depletion of natural resources is another contributor factor to the challenges the industry faces to ensure the structural integrity of the gas infrastructure as in order to satisfy the future demand it will be necessary to go farther and deeper [3-4,7]. Among the different potential threats to gas pipeline integrity stress corrosion cracking (SCC) continues to be one of the most complex and least understood forms of corrosion and thus a major hazard to gas pipeline integrity.

SCC is a time-dependent [2], environmentally induced crack propagation mechanism [4,12] in which the interaction between a corrosive environment, applied stresses, and a susceptible microstructure lead to the initiation and propagation of cracks on the surface of the pipeline that can result in pipeline failure [13] in which the escaping gas can give rise to a sustained fire in couple of minutes [14]. A notably catastrophic pipeline incident occurred in Carlsbad NM, killing 12 persons. Moreover, despite the great advances in the SCC field to date no particular manufacturer, manufacturing technique, metallurgical features, or steel grade has been linked to SCC occurrence [4,16]. Therefore, the detection of SCC cracks on operational pipelines remains a challenge to the industry as it is difficult, expensive, and inconvenient [27-28]. Hence, the combine action between a complex SCC detection processes, an aging infrastructure, harsh service conditions, and the unpredictable and destructive nature of a gas blast [19] makes it particularly important to expand our knowledge on the mechanism behind SCC [18] to prevent future failures.

In order to gain a better understanding of the microstructural features and trends of highly SCC susceptible pipeline materials a detailed microstructural investigation was carried-out in five different gas transmission pipelines characterized by different chemical composition, dimensions, and service conditions. All of the pipelines were classified as vintage and were located in the southwest portion of the USA. From the investigated pipes, four were removed from service due to confirmed SCC and the fifth one due to pitting. The following sections discuss the metallurgical features observed during this investigation.

4.1 MATERIALS

The evolution of technologies and processes has led to the development of new pipeline steel grades that are characterized by higher strength and a bainitic microstructure as compared to lower strength steels which exhibit a mix pearlite-ferrite microstructure [32,78-79]. During this investigation all of the analyzed pipelines materials were manufactured by different companies from low strength steel grades such as grade A steel (#2 and #1 pipes) and grade X-52 steel (pipes #3, #4, and #5). Conventional lower strength steel pipelines were primarily used around 1950 or before [4,37] and compromise about 35% of the current gas transmission infrastructure [35]. Grade A steel has been determined to be very susceptible to SCC and therefore is no longer suitable as pipeline replacement [39]. On the other hand, grade X-52 was a particularly widely used steel [132], in fact the popularity of this steel could partly explain why a great number of the IGSCC failures have occurred in this pipeline material [41]. Nevertheless, SCC has been found not only in X52 steel but in a wide range of steels grades (from X25 to X65), microconstituents, manufactures, and dimensions [4]. Regardless of de advances in understanding SCC to date what constitutes a susceptible microstructure remains ambiguous.

Moreover, with the latest steel developments another key factor that has led to conflicting opinions is the role of strength, as presently there is not enough information about high strength steels and SCC susceptibility response [4]. On one hand, some authors believe that higher strength materials can lead to TGSCC due to their tendency to hydrogen embrittlement (HE) [133]. Contrary to this assumption researchers like Wang and coworkers found a weak correlation between SCC initiation and strength, concluding that the SCC initiation is independent of yield strength as it occurs below the yield stress [133-

134]. Consequently, with the current lack of information on the relation between the latest developments in steel technology and SCC, and a continuously aging infrastructure we must be able to delineate which are the microscopical factors influencing the SCC crack initiation in order to be able to guarantee the safety of the population.

4.1 CRACK MORPHOLOGY

Three out of the four SCC susceptible pipelines (pipes #1, #2, and #3) failed after 40 year in service with a maximum crack length over 50% of the wall thickness while remaining pipeline (pipe #4) failed after 20 years. This results are in agreement with the findings from the SCC model created by Jain et al. who concluded that the probability of cracks being as deep as the thickness of the pipeline significantly increases after 40 years [135]. The primary fracture in pipeline #2 which experienced a service rupture after 46 yrs. in service was oriented along the longitudinal axis. Wet magnetic particle inspection carried out near the main surface fracture revealed multiple secondary cracks with extensive branching, these cracks were oriented perpendicularly to the main fracture. As was the case with pipeline #2, pipeline #1 was manufactured from grade A steel. This pipeline was removed from service because multiple cracks with extensive crack coalescence were found in different sections of the pipeline. However, contrary to pipe #2, pipeline #1 exhibited cracks that followed a "non-classical" pattern traveling along the longitudinal axis of the pipe and then transversely. Pipelines #3 and #4 were manufactured from X-52 steel grade, both pipelines failed during hydrotesting. Pipeline #3 failed after 40 yrs. in service and pipeline #4 only after 20 years. The subsequent analysis carried-out after the failure determined SCC to be the cause. Likewise pipeline #2, the primary fracture in both X-52 pipes was oriented along the longitudinal axis, but in this case cracks exhibited little branching and were fairly densely spaced.

Gas transmission pipelines are subject to internal pressure variations and therefore to longitudinal and circumferential stresses with the latter being the highest stress component, consequently longitudinal cracks are more common than circumferential cracks [13]. This was confirmed by the crack orientation in the majority of the analyzed SCC susceptible vintage pipelines. The main contributor of stress in a pipeline is the operating pressure which is expressed in terms of a percentage of the SMYS [13], however pipelines rarely operate at their maximum allowable operating stress or the actual yield strength is usually higher

than the SMYS [13]. Therefore it is important to point out that SCC has been confirmed to occur below the SMYS, making this form of corrosion even more critical. This was the case of all the investigated pipelines which failed below they SMYS.

The soil environment for all of the provided pipeline materials was determined to have a high-pH by the investigation performed after the failure occurred. Despite the fact that IGSCC would be the expected SCC form, the metallographic inspection of transverse cross-sections containing SCC cracks revealed that while the crack propagation mode in all pipes followed a predominantly intergranular path, pipelines #2, #4, and #3 exhibited evidence of near-neutral SCC such as very wide cracks that became narrower as they grew deeper (Figure 19b), crack wall corrosion, and areas of transgranular attack where crack propagation apparently occurred through ferrite grains (#2 pipe) and pearlite (#4 and #3). In the case of pipeline #3 and #4 the width of the cracks can also be attributed to fact that they failed during hydrotesting. Some of the observed cracks such as those presented in Figure 19 grew incline as they grew deeper. The inclination of cracks as crack deepens has been associated to preferential dissolution at persistent slip band (PSB) [133].

A mixed propagation mode can be the result of a number of factors, such as the electrochemical differences between the various microconstituents (which can lead to anodic and cathodic sites that affect the metal dissolution rate [136]) or due to changes in the crack tip environment [137]. Changes in the crack tip environment can be the result of the migration of species to the region or the increase of H concentration due to the corrosion process [137]. During corrosion of the metal H is created which is then attracted to regions with a high triaxial tensile stress where the metals structure is dilated [138], the accumulation of H can then decrease the local fracture resistance of the material, assist in developing areas of intense plastic deformation [138], promote anodic dissolution, and thus cracking. Furthermore, H diffusion in BCC metals such as ferritic steels is very high as compared to FCC metals, therefore shorter time is require to embrittlement [138]. Nevertheless, this results confirmed the point that the type of SCC depends on the environment at the crack region—which can be altered by different factors—and not necessarily that of the soil environment [4].

4.2 CHEMICAL COMPOSITION

The chemical results from the investigated pipeline steels revealed that pipelines #3 and #4 have a higher carbon (in the range of 0.14-0.19), Si, and Mn content as compared to pipelines #2 and #1 in which carbon was in the 0.02%-0.05% range. These results demonstrate that grade A pipelines (pipelines #1 and #2) were made to a rimmed steel practice and not to a Mn and/or Si deoxidation practice nor a fine grain practice as indicated by the low percentage of elements such as Al, Nb, Cr, V, and Ti in pipelines [139]. Elements such as Al, Nb, V, and Ti form second phase particles which can pin the austenite grain boundaries and thus inhibit grain growth [136]. Contrary to this, grade X-52 pipelines were made to a semi-killed (#4 and #3) or killed steel practice (#4 and #5) [139]. Furthermore, pipelines #4 and #5 were manufactured to a fine grain practice as indicated by the Al content. The use of Al as a deoxidizer or grain refiner can have a profound effect not only on the surface quality but also on the structure of sulfides, in which complete but not excessive Al deoxidation can lead to intergranular sulfide chains which are detrimental to mechanical properties [140]. Furthermore, as the Mn and C content increases less Al is required to achieve a fine grain structure [140].

The steel manufacturing process—particularly the amount of deoxidation—appears to play a role in strain aging [2]. The susceptibility to strain aging according to deoxidizing practice in decreasing order is: rimmed steel, semi-killed, silicon-killed, aluminum-killed, killed, and microalloyed [2]. Albeit steel pipe is subject to natural aging this process can be accelerated by the service conditions [126]. Therefore, the effect of strain aging on the degradation of pipeline service life and SCC susceptibility remains unclear [2] and a major concern [4]. Strain aging is a time dependent diffusion process in which interstitial atoms such as carbon and nitrogen migrate to dislocations impeding their further movement and increasing the steel resistance to plastic deformation [2,4,125] and thus the yield and ultimate tensile strength but decreasing the ductility [4,125]. Over time, more precipitates are formed and their size increases until they become so large that they can no longer impede dislocation movement (over-aging) leading to the softening of the material [2]. In order to prevent the migration of N and C, carbide (Mo, V, Nb) and nitride (Al, Ti, B, V, Nb) forming elements are added to diminish the amount of “free” nitrogen and carbon [2].

However, in the absence of these elements only about 0.001% and 0.002% of C and N are required to cause strain aging [4].

Another significant chemical difference between SCC-free pipelines and the rest of the pipes is that the SCC free pipe (pipeline #5) exhibited a slightly higher carbon (0.27%) and Mn (1.5%) content as compared to the SCC susceptible pipelines. Flis et al reported that while steels with a carbon content in the 0.01-0.05% range are highly susceptible to SCC, those with a carbon above 0.25% and decarburized steels are highly resistant to SCC [141]. The role of carbon on SCC susceptibility is a function of its content and accumulation on the GBs which in turn depend on the heat treatment, environment, and other factors[141]. Contrary to the assumption that the total carbon content is the critical factor in regards to SCC susceptibility, Flis concluded that the segregation of carbon atoms in slowly cooled materials is a function of the carbon solubility in alpha-iron at room temperature—which is very low—and not necessarily on the total carbon content [141]. Therefore, heat treatments leading to the low accumulation of carbon either as atomic carbon or carbides are more detrimental to the SCC resistance than those leading to high accumulation (in a hot nitrite solution) [141]. A higher accumulation of carbon can contribute to the increased deposition of magnetite, this oxide film is believe to act as a protective layer preventing the electrolyte to come into contact with the grain boundary [92,137]. The reason why C can stimulate the formation of magnetite remains unclear, though it has been partly attributed to the belief that it can aid to the adherence of the oxide [141]. On the other hand, a low accumulation of carbon can lead to a depassivating action involving the reduction in the protective properties of the passive films [141].

A shared metallurgical feature observed in all the investigated pipelines was the presence of non-metallic inclusions, this was expected as non-metallic inclusions are commonly present in low grade steels [4] such as grade A and X52. Elemental mapping images from the region near the OD from all the pipelines revealed rounder MnS inclusions as compared to the elongated inclusions in the core region. However the SCC-free pipeline appear to have slightly larger inclusions near the OD as compared to the SCC susceptible pipelines. Rounder inclusions near the surface layer could be the result of the higher temperatures experienced by this area during rolling as compared to the core [142].The role of non-metallic inclusions on the susceptibility of pipeline steel to SCC has been investigated by multiple authors,

while some concluded that the shape of the inclusions is the deciding factor others believe that the critical variable is the size of the inclusion, concluding that longitudinal cracks will not form if the length of surface defects which in turn depend on the length of non-metallic inclusions is smaller than 200 to 250 microns [13]. Nevertheless, during this study all of the investigated pipelines in particular those with longitudinal cracks exhibited inclusions smaller than 250μm near the OD region. Moreover, it has been widely reported that inclusions near a free surface have a more deteriorating effect on fatigue limit and that clusters of sulfides can favor crack propagation and coalescence of small cracks [143]. Lastly Bulger et al. concluded that under corrosion the MnS inclusions become cathodic and the surrounding matrix—which has a high sulfur content—becomes anodic and therefore corrodes [137].

In addition to rounder MnS inclusion the OD region from pipelines#1, #2, #4, and #5 exhibited a higher Mn and S content then the core region, this effect was less noticeable in pipeline #3. The role of Mn still unclear, on one hand some authors believe that it can be detrimental to integranular cracking as it can promote the segregation of embrittling species to the GB [144]. Contrary to this assumption other authors reported that Mn can eliminate the segregation of S to the GB [145-146] which is considered a deleterious impurity [144-147]. The S content from all pipelines (except pipeline #3) appears to be higher near the OD region as compared to the core (this was more evident in pipeline #2). It has been well documented that the ductility and toughness can be considerable reduced by increasing the S content [143] moreover some authors have reported that pipeline steels with higher S content are more prone to crack initiation [145-146]. However, since only a qualitative S analysis was carried-out in order to gain a better understanding on the role of S a quantitative analysis is required.

Another important element in regards to SCC susceptibility is silicon, whose role has been reported to be strongly correlated to the environment; while silicon additions to ferritic steel in a NO_3 and OH environment had no effect to the SCC susceptibility, it had a detrimental effect on a CO_3/HCO_3 electrolyte [144]. Additionally, during temper embrittlement Si can increase the tendency for embrittlement by reducing the solubility of impurities in the bulk and thus promoting their segregation to the GB [147]. In this case, EDS mapping revealed a significant lower silicon content in the OD from

pipeline #1 as compared to the rest of the pipelines, other than this no significant differences were observed.

4.3 MECHANICAL PROPERTIES

The through thickness hardness profile from the grade A pipelines (#2 and #1) indicate that the minimum hardness exists in the mid-thickness with a magnitude approximately 10% lower than the hardness in the vicinity of the OD, this could be attributed to work hardening effect as the surface layer deforms before the bulk [75]. Conversely X52 pipelines (#3, #4, and #5) exhibited a more uniform through thickness microhardness profile. Moreover, while no significant differences between the microhardness profile between SCC and SCC-free regions were observed in pipeline #2; pipeline #1 exhibited a lower hardness in the SCC region located in the pipeline body and a slightly higher hardness in the SCC region near the weld seam (as compared to the BM). On the other hand, grade X-52 steel pipes (#3 and #4) exhibited a slightly higher hardness profile in crack containing regions than in non SCC zones, this was more evident in pipeline #3. Some authors have reported that the higher hardness in SCC zones in ferrite-pearlite steels are the result of a higher pearlite content, which is a harder phase as compared to ferrite [148] nonetheless, pearlite volume fraction analysis in SCC and SCC-free zones was not performed during this investigation.

4.4 MICROSTRUCTURAL FEATURES

4.4.1 Pitting, Scale, and More

In respect to other metallurgical features such as pitting only pipelines #4 and #5 exhibited evident pitting on the OD region. Interestingly while pipeline #4 exhibited an early SCC failure (after 20 years) pipeline #5 remained SCC free after 45 years in service. It is a well-known fact that pitting can lead to SCC, indeed pit cracks can initiate more easily than none pit cracks [137] and although most SCC cracks have been detected in the bottom of corrosion pits [12] not all pits develop cracks [149] and not all cracks initiate due to pits. During service conditions, pits can form if the potential exceeds the pitting potential, consequently once pits are formed the development of cracks will depend on a number of factors such as pit geometry—which in turn determines the stress and strain rate at the bottom of the pit—the

environment, and the chemical composition of the material [12]. However, the electrochemistry of the pit remains one of the most important variable in the formation of pit cracks [12]. Under certain circumstances the pit, the grain boundary, and the grains' chemistry will favor the formation of either intergranular or transgranular SCC in the bottom of the pit [12]. If the environment in the pit exhibits near-neutral characteristics, the grain will be anodic while the grain boundaries cathodic, leading to initiation of pitting in the grain interior rather than at the grain boundary, in this manner since the electrochemical driving force for crack growth within the grain is higher than that at the grain boundary cracks will propagate in a transgranular mode [150]. Additionally, a low pH environment inside the pit can facilitate dissolution and hydrogen discharge and therefore crack initiation and propagation [151].

In the absence of pitting, SCC cracks can initiate at surface discontinuities such as those formed from the localized corrosion at emerging slip planes [12] or due to scale [152]. During plastic deformation gliding slip planes on the top surface can lead to the formation and destruction of the protective film which in turn can lead to the formation of an electrolytic cell and therefore to tunnel shaped pitting which under the influence of stress can expand sideways leading to branched cracks [153]. On the other hand, scale which was observed in all the pipelines, has been linked to the development of TGSSC as the porous structure in the layer can lead to anodic and cathodic sites which can lead to localized dissolution under the deposit layer and therefore to a lower pH electrolyte under the pores and to TGSCC [152].

4.4.1 General Microconstituents

The relationship between microstructure and SCC is very complex and not fully understood, the main microstructural features of the highly SCC susceptible vintage pipeline materials observed during this study were primarily slow to intermediate cooling rate microconstituents. The microstructure of the grade A pipelines (#2 and #1) consisted of large amounts of polygonal ferrite, isolated cementite films at ferritic grain boundaries, and a small number of pearlite colonies. These constituents are the result of the combined action between a slow cooling rate and the low carbon content of the grade A steel. Similarly, the primary microstructural constituents observed on X52 grade pipelines (#4, #3, and #5) are consistent with a slow to intermediate cooling rate.

Throughout the slow cooling from the austenitizing temperature, polygonal ferrite nucleates and grows at a high temperature by rejecting carbon due to its low solubility [87], the rejected carbon can then partition to the untrasformed austenite or accumulate at the ferrite-austenite interface if the cooling rate is sufficiently slow, this prevents the carbon from being retain in solution and lead to the formation of grain boundary carbides [93] such as those observed in Figure 20. Subsequently, once the eutectoid temperature is reached the remaining carbon-rich austenite transforms to pearlite [93,142,154]. As the cooling rate increases the microstructure changes from polygonal ferrite and pearlite with lamellar and broken up lamellar (slow cooling rate); to a combination of coarse grains with high dislocation density, lath-shaped ferrite, and degenerated pearlite (intermediate cooling rate); and eventually at a high cooling rate to bainitic ferrite and cementite particles dispersed in the ferrite matrix [155].

Mixed microstructures are believe to be more susceptible to SCC due the differences between the micrococonstituents [32]. Lu et al determined that small cracks are more likely to initiate and propagate in pearlite colonies or along pearlite-ferrite as the strength differences between pearlite and ferrite can promote non-uniform plastic deformation, concluding that pearlite is a detrimental constituent to the SCC resistance [70]. Nevertheless, grade A pipelines which have a very low pearlite content also exhibit a high SCC susceptibility with cracks propagation along ferrite:ferrite grain boundaries. Furthermore, the presence of different microstructural constituents could enhance the metal dissolution by promoting anodic and cathodic sites, nevertheless their role is strongly correlated to the environment [136]. A clear example is the case of cementite, which under certain circumstances is believe to promote the dissolution of ferrite however, under very specific conditions such as a pH around 5.5-6 and a temperature of 60 ºC, cementite can promote the formation of a protective iron carbonate layer [136].

4.4.2 Banding

Banding is a metallurgical feature—characterized by alternating ferrite and pearlite bands—attributed to the combined action between microsegregation of alloying elements, cooling rate, and austenite grain size [87, 156]. This feature was observed in pipes #1,#3, #4, and #5. The formation of banding has been linked to a slow cooling rate as a fast cooling rate can hide the underlying pattern of segregation leading to more uniform structures such as bainitic or martensitic [157]. One of the elements

associated to the formation of banding is manganese, therefore a reduction in the manganese content can help reduce or eliminate this feature which can have a detrimental impact in the materials toughness and final ductility [87,158]. Moreover, reduction of the Mn content can also reduce the tendency to form elongated inclusions, as the plasticity of MnS inclusions during hot rolling is proportional to the Mn content [159]. This can partly explain the fact that pipelines #1 and #2 exhibited MnS with a smaller aspect ratio as compared to pipelines #3, #4 and #5 that have a higher Mn content. Albeit MnS inclusions are typical in low grade steels its role on SCC susceptibility remains ambiguous and contradictory. Some authors believe that large and elongated inclusions as well as a Mn content >1% increases the HIC susceptibility [159] and thus to some extent to TGSCC since any factors that alter the hydrogen permeation and adsorption [4,75] can alter the response to TGSCC. Moreover, deformable manganese sulfides can also lead to changes in stress concentrations in the transverse and longitudinal directions and thus affect the properties in each direction differently [143].

Contrary to assumption that elongated inclusions are detrimental to the SCC susceptibility, in their investigation CANMET compared the inclusion size from samples with significant and non-significant cracking, concluding that the un-cracked samples exhibited longer inclusions than the crack ones [4,13]. This observation is more consistent with the results obtained during this investigation since all of the vintage pipelines removed from service due to SCC exhibited smaller inclusions near the surface layer as compared to the SCC-free pipeline which was characterized by slightly more elongated near surface layer inclusions.

4.4.3 Decarburized Layer

Carbon differences between the surface and core layers with carbon content decreasing from the surface to the center can arise during material processing. A decarburized surface layer is the result of the interaction of the carbon content in this region and the furnace atmosphere which leads to the removal of surface carbon as a gaseous phase and to a carbon gradient between the rim and the core. This in turn leads to poor wear resistance and fatigue life [160]. Moreover, some authors have reported that locally soft microstructures such as a decarburized layer decreases the resistance to SCC [32]. While pure iron exhibits a very high resistance to SCC [141] there is evidence that SCC is possible below 0.001% carbon [92].

During this investigation X-52 pipelines, SCC susceptible and SCC-free pipes exhibited a decarburized surface layer, this effect was not that evident in grade A pipelines due to its low carbon content. Nevertheless, in order to gain a better understanding of the role of a decarburized layer on SCC crack initiation it is necessary to determine the amount of decarburization and the relationship with the environment.

4.4.3 Grain Size

The average grain size for grade A steel pipes was about 20µm (ASTM G No.8) and exhibited a bimodal configuration with some of the smallest grains being about 5 times smaller than the average. Whereas, the average grain size for pipeline #3 was about 12µm (ASTM G No.9.5) and that for pipeline #4 about 9 µm (ASTM G No.10.5). Additionally, all X-52 pipes exhibited smaller pearlite colonies in the OD region as compared to the core. The SCC free pipelines (#5) exhibited a slightly smaller grain size near the OD region with an average grain size about 8µm (ASTM G No.10) as compared to the X52 SCC susceptible pipelines. However, the grain size difference between pipeline #4 (high SCC susceptibility) and pipeline #5 (no SCC) was minimum leading to the conclusion that the effect of grain size on the corrosion resistance of an alloy appears to be strongly correlated to the environment-material combination and to other metallurgical features, and not necessarily on grain size only. Moreover, the region near the rim on pipeline#5 was characterized by an equiaxed ferrite morphology while pipeline #4 exhibited more needle-shaped ferrite [98] which could be an indication of overheating in rolling.

In regards to the relationship between grain size-environment some authors have concluded that a fine grain structure is detrimental in electrolytes that promote active behavior while it can be beneficial in those that promote passivity, due to the fact that finer grains exhibit a more rapid repassivation rate and more stable films as compared to coarser grain structures [99]. Moreover, Bulger et al. concluded that a smaller grain size is more detrimental to near-neutral SCC [137]. The mixture of very small and large grains is an indication of grain growth, this effect was more noticeable in ID of pipeline #1. Grain growth is strongly influenced by the finish temperature during rolling and can be the result of a low finishing temperature [142]. When a low finishing temperature is used, the final rolling pass will be performed in a material containing ferrite and austenite, which can lead to the formation of very large grains, especially

near the surface layer such in the case of pipeline #1 (Figure 31). On the other hand grain coarsening effects could also be an indication of overheating; overheating takes place when the metal is heated to such a high temperature that its properties are compromised and cannot be restored by further heat treatment [142].

4.4.4 Sub-Surface Layer Microconstituents

The sub-surface layer from pipelines #2 and #1 exhibited a predominance of PF ferrite with some lath-like ferrite grains, whereas pipelines #3 and #4 were characterized by a more mixed microstructure featuring PF or QF ferrite, some needle-shaped ferrite in addition to colonies of lamellar and degenerated pearlite, and the casual presence of a discontinuous carbide layer in the ferritic grain boundary [154]. Mixed microstructures have been reported to have a higher susceptibility to SCC [32] due to the chemical and structural inhomogeneity between the various microstructural constituents which can strongly affect the corrosion resistance of steels [145] and lead to passivation variances that affect the electrochemical behavior of the material and thus result in TGSCC or IGSCC [81].

The formation of the different ferrite morphologies observed are the result of mechanisms involving shear and diffusion, and due to the constraints imposed by the grain boundary and the dislocation tangles [81,161] such in the case of lath-shaped ferrite surrounded by PF. This mixture of polygonal and lath-shaped ferrite could also be an indication of overheating during plate rolling. From the different ferrite forms available acicular ferrite has been reported to provide higher resistance to crack propagation [43,70,90-91], nevertheless, PF was the predominant ferrite morphology observed in the investigated pipelines. PF is characterized by straight, smooth, and continuous boundaries [86-87] and it has been reported to favor the incidence of IGSCC [81]. Some authors have demonstrated that after hydrogen charging the GBs of polygonal ferrite develop microcracks but not those of acicular ferrite [81]. Therefore when the microstructure consists of polygonal and acicular ferrite, PF is more vulnerable to H attack and cracking [162].

In addition to ferrite, X-52 grade steels pipes exhibited higher volume fraction of pearlite as compared to the very low carbon steel pipes #1 and #2 which was expected due to the higher carbon content in the X-52 pipelines. The formation of pearlite and degenerated pearlite occurs due to a diffusion

process where the lack of sufficient carbon to diffuse can lead to the discontinuous or broken-up lamellae [155]. The lamellae characteristics and orientation in the pearlite colony are believe to play an important role in the materials mechanical properties. On one hand, the lamellar morphology of pearlite has been reported to have inappropriate mechanical properties for highly demanding components [163]. Meanwhile degenerated pearlite has been linked to an improvement in the materials toughness [155] as a result of the finer cementite which can endure larger strains and a more uniform strain distribution during deformation leading to increased ductility [164]. Furthermore, a globular morphology of cementite can also provide high toughness and machinability [163].

The tendency for the development of degenerated pearlite—usually observed in low carbon steels transformed at high temperatures—is related to manganese content, deoxidation practice, and transformation temperatures [142]. Manganese content >0.5%, especially in the 0.4-0.7% range—considered the Mn critical range—leads to spheroidal cementite instead of long thin cementite films, this can partially explain why pipeline #3 with an 0.80% Mn content exhibits more degenerated pearlite colonies as compared to pipeline #4 which had about 1.3% Mn. On the other hand silicone-deoxidized steel tend to develop highly lamellar structures while aluminum deoxidized steels result in degenerated pearlite [142]. The dog-bone cementite termination shown in Figure 43 is a form of degeneracy and a typical feature of aluminum deoxidized steels [142]; nevertheless, the low aluminum content in #3 indicates that this is not an aluminum deoxidized steel.

4.4.5 Dislocation Character

The predominant microconstituent in the sub-surface zone of highly SCC susceptible pipelines was PF. This ferrite morphology is normally characterized by a low dislocation density because it occurs at high transformation temperatures which promote the ease of dislocation rearrangement and annihilation [154]. Nevertheless, the area near the OD from all the SCC susceptible pipelines exhibited PF with evidence of high dislocation density and dislocation cells which could be the result of processing (cooling rate) or service conditions (plastic deformation). During pipeline manufacturing and operation, pipelines are subject to different conditions that can cause localized microplastic deformation below the yield stress of the steel [75]. Plastic deformation leads to an increase in the number of dislocation which in turn allow

for further deformation with their movement through the crystal lattice [165]. Strengthening on the other hand takes place when the dislocation movement is reduced [165]. The movement of dislocations takes place in particular slip systems (plane and direction) which depend in the crystal structure; while FCC structure has the greatest number of available slip systems (12) and therefore greater capacity for deformation, the BCC structure is strongly sensitive to temperature, meaning that a reduction in temperature can lead to a ductile to brittle transition in some of the available slip systems causing them to fail before reaching its full plastic deformation capability [165]. Furthermore, this could also lead to low temperature brittleness because the operable slip system in BCC varies with composition, strain rate, and temperature so any changes to this any of these variables will in turn affect the transition from brittle to ductile behavior [166-167].

The goal of any system is to lower its energy, so a way of achieving this is for a total dislocation to splits into partials, when this occurs the difference in energy between a perfect lattice and the stacking fault between the partial dislocations is known as the stacking fault energy (SFE) this energy plays a role during deformation [168]. Materials in which the distance between the partials is small have a high SFE while those with a large separation have a low SFE [168]. In low SFE materials where cross-slip is rather difficult planar arrangements of dislocations are formed even at high strains [107] contrary to this the easy of cross-slip in materials with a high SFE allow primarily dislocations to interact with secondary dislocations leading to the formation of dislocation loops, tangles, and eventually dislocation cells [107-108]. Dislocation cell structures not only allow for further deformation as they lower the energy stored in the material [169] but can also break down to form persistent slip bands (PSB) during cyclic loading cell structures [167]. Materials in which cross-slip is readily exhibit PSB with a sharper surface appearance as compared to those in which cross-slip is difficult, these sharp PSB can act as crack initiation sites and/or disrupt the protective film [167]. Nevertheless, the increased fatigue resistance with the decreased in cross-slip is only effective under a given stress and grain size [167].

BCC materials are normally characterized by a very high stacking fault energy in which the slip direction is the <111> and the planes are {110}, {211}, and {321} being the former the most common one [170]. During deformation 3 of the {110} planes intersect a <111> direction allowing for screw

dislocation to move in any of these planes, this in turn lead to wavy dislocation lines such as those observed in Figure 53A [166,170]. The easy of cross-slip can also lead to a polygonised structured if deformation is carried-out at elevated temperature. Poligonization is one of the first steps of the recovery process. Since dislocations and dislocation structures are an essential element in the deformation process some authors have suggested that their behavior can qualitatively predict or affect the susceptibility to SCC [108]. In fact some authors have reported that dislocation behavior can qualitatively predict the SCC susceptibility of FCC materials and that the SFE might be the deciding factor [112]. Douglas et al observed that stainless steels with a low SFE exhibit a high susceptibility to TGSCC while those with a high SFE showed less susceptibility [112] concluding that cross-slip reduces the tendency for localized attack [112] which occurs in the slip plane because of the composition differences between the stacking fault and the matrix [112]. During this investigation pipelines with high IGSCC susceptibility exhibited dislocation cells near the surface layer which is an indication of cross-slip and thus of a high SFE material, leading to believe that SFE could influence the material's response to IGSCC. Nevertheless, it's important to point out that in BCC metals the role of dislocation and SCC could be more complex due to their strong temperature sensitivity. As previously discussed disassociation of dislocation takes place in order to lower the energy of the system, despite than in BCC structures split is limited due to its high SFE a possible unit dislocation can arise from the reaction a/2[111] = a/2[111] = a/2[001], this unit dislocation can form at the intersection of normal slip band and is normally immobile [170]. Therefore, this dissociation leads to a reduction in the strain energy but also to a new a[001] dislocation which is edge in character and lies in the (001) plane [166]. The new a[001] dislocation can act as a crack initiator since it acts like a wedge inserted between the (001) plane [165-166,170]. If the dislocation was screw in character the dislocation could glide [166].

The higher dislocation densities near the surface layer as compared to the core has been reported to be the result of a combination of factors such as differences in cooling rate between rim and core [83], machining effects [102], and because the surface layer deforms before the bulk [75]. Although the role of dislocation on the susceptibility to SCC remains unclear some author have reported that since dislocations can act as hydrogen trapping sites [83] a higher dislocation density implies a higher number of available hydrogen trapping sites, higher hydrogen adsorption coverage on the surface [75] and therefore higher

number of potential crack nucleation sites [96]. Moreover, mobile dislocation can not only trap hydrogen but they can transport it to possible cracking sites reducing the SCC resistance [89]. This effect can be eliminated by the presence of small carbonitrides which can impede dislocation motion and thus block the hydrogen from potential sites [89,109]. However, if particles are too large (particles > 1 microns) they cannot pin the dislocations and the material becomes susceptible to hydrogen embrittlement [110]. Hydrogen can also reduce the atomic cohesion by expanding the lattice and therefore increasing the corrosion susceptibility [74] or migrate to the crack tip and promote anodic dissolution [97] and thus promote crack propagation [75]. Migration of hydrogen to crack tip is aided by the increased in the hydrostatic stress field around the crack tip caused by the increased in yield strength and decrease in ductility as result of large amount of cold work [75].

Other theories about the role of dislocations suggest that the strain energy stored in dislocations from the deformation process can promote the dissolution of specific sites as the corrosion of a stressed metals can release energy [111]; that dislocations can cause the crack tip to be film-free [113]; and that the coalescence of dislocations can aid to formation of corrosion tunnels [52]. On the other hand, Smith et al concluded that in aluminum alloys dislocations and dislocations pile-ups are not necessary for SCC [114].

4.4.5 Sub-Surface Region other Features

TEM observations also demonstrate the presence of a significant number of triple point junctions and what appears to be the precipitation of small particles within the grains and along some of the grain boundaries. Grain boundaries are an important microstructural feature that play a key role during IGSCC [171] but the question remains why. Yu and coworkers reported that under certain electrochemical circumstances preferential dissolution of triple junctions and GB can take place because of their unique electrochemical properties [172] furthermore, GB and triple junctions are believed to aid to the increased adsorption of species from solution that in turn can contribute to preferential dissolution of the GB [171].

Grain boundaries are also known to be prefer sites for precipitation because lower interfacial free energy is required as compared to that needed for matrix precipitation [173]. However, a sufficiently high diffusion rate is needed in order for atoms to migrate from the matrix to GB, which is more easily achieved

at higher temperatures. On the other hand, when the temperature is low precipitation tends to be more general and in some cases a narrow precipitation free region is created adjacent to the GB [173]. GB precipitates as well as the precipitate free zone adjacent to the GB are believed to influence the materials SCC susceptibility, so there are several theories on how GB carbides can lead to the different SCC types. In the case of IGSCC, Tauber et al. concluded that GB carbides can remain unpassivated and promote the anodic dissolution of the GB and thus intergranular cracking [121]. Otherwise, TGSCC can occur because the GB precipitates can act as cathodic points facilitating the dissolution of adjacent ferrite [59] or they can act as hydrogen traps. Nevertheless, not all of the observed grain boundaries exhibited evidence of precipitation, in fact some appeared to be relatively clean, this findings are consistent with other authors findings who concluded that because of the discontinue nature of GB precipitation, this cannot be completely responsible for SCC [57,93,144]. Therefore, the segregation of impurity atoms to GB has gained attention as a factor that can influence the susceptibility to IGSCC.

According to Faulker et al the strength of the grain boundaries is strongly influenced by impurity atoms which tend to migrate to grain boundaries because they can lower their energy there and/or because they are dragged by vacancies which are attracted to GB being that GB are vacancies sinks. In this manner accumulation of impurity atoms very close (few nanometers) to the grain boundary takes place, which in turn affects the grain boundary strength and therefore the susceptibility to cracking [174]. Similarly, Mishin et al. found that during annealing atoms diffused faster along the grain boundary than into grain interior, however atoms eventually leave the GB and travel into the region adjacent to the boundary creating a volume diffusion region next to the GB [175]. Moreover, some elements appear to exhibit a faster diffusion to GB than others [176], for example in their investigation Sun et al determine that SCC of aluminum alloys might be linked to Mg segregated along the GB a not necessarily to Zn as no significant amounts of segregated Zn was observed, the reason was attributed to the presence of large GB precipitates containing Zn [177]. Furthermore, it could be possible that the chemical interaction between the different impurities that can segregate to the GB could increase of decrease the embrittlement of the material depending on the degree of co-segregation in the GBs. For example, there is evidence that hydrogen

interacts with solute impurities in prior austenitic GBs in steels, and that Sn, Sb, P, and Si have an attraction to Ni, or that C and S are attracted to Mn.

The role of substitutional components on the SCC susceptibility was confirmed by Flis et al who observed that a decarburized steel—considered immune to SCC—exhibited evidence of cracking in hot nitrite solution suggesting the possibility that other elements besides carbon were involved [141]. Albeit other elements appear be involve in the response of materials to SCC carbon remains one of the most controversial. Despite the fact that solute segregation to GB can strongly influences the main physical properties of the GB and therefore the materials macroscopic behavior [171] such as its resistance to SCC, solute segregation to GB is a complex phenomenon that depends on different factors such as: the disorientation angle, the tilt, and rotation components of the GB, and the presence of large precipitates which can deplete certain elements hindering their further segregation to GB, and the environment [171].

In addition to some GB precipitation the presence of small precipitates decorating the dislocation lines was also revealed by TEM. These precipitates can pin down the dislocations and reduce their motion which coupled with the presence of dislocation structures can convey additional strength to the final microstructure [178] but it can also reduce the materials ductility. In addition to the small particles observed in the grain interior, pipeline #2 and #3 exhibited coarse cuboidal shaped precipitates on the OD region. These type of precipitates do not contribute to the overall strength of the material because of their size they cannot impede dislocation motion [154], what is more Bulger et concluded that large (0.1-1 μm) cuboidal titanium nitride in a X70 pipe steel can act as cathodic regions and can initiate brittle fracture [80,137]. Nevertheless, due to the low volume fraction of this type of precipitates they cannot be responsible for SCC.

Lastly, a grain boundary crack located near a large particle at a triple junction was observed on pipeline #1, its well-known fact that high local stress conditions are one of the main responsible for the development of cracks, among some of the main contributors to high local stress are high dislocation densities formed near surfaces during fatigue and other sub-critical cracking conditions; stress concentrators near the interfaces between embedded particles and the surrounding matrix; and grain boundary triple points. Contrary to the assumption that triple point boundaries can act as stress

concentrators some authors have determined that cracks can be arrested through the intersection with grain boundary precipitates or at triple points [108].

Conclusion

A systematic microstructural characterization of different gas transmission pipeline materials removed from service due to the detection of SCC was carried-out to gain a better understanding of the microscopical conditions typifying the sub-surface zone and the general metallurgical features of actual service components with high SCC susceptibility. In this manner, the aim of this investigation is to add to the knowledge of what defines a susceptible microstructure. During this study, the analyzed pipelines were characterized by different chemical composition, manufacturing practice, manufacturers, and service conditions. Albeit, the results obtained during this study appears to support the idea that what defines a susceptible microstructure is most likely the result of the synergistic effect between environment, alloying elements, grain boundary character (tilt, disorientation angle, rotation components), and microconstituents. Some factors appear to have a higher influence of the SCC response:

- Pipeline materials that exhibited a higher resistance to SCC were characterized by a higher carbon (>0.25%) and Mn (1.5%) content as compared to SCC susceptible pipelines in which carbon was in the 0.02-0.19% range, and the Mn content in the 0.31-1.3% range. Leading to the conclusion that C and Mn play a critical role during SCC.
- The pipeline manufactured to a Mn semi-killed or killed steel deoxidation method.
- Mixed microstructures are not necessarily more susceptible to SCC.
- The subsurface region of highly IGSCC susceptible pipelines was characterized by slow to intermediate cooling rate microconstituents such as large polygonal ferrite with high dislocation density and dislocation cells, indication of a high stacking fault energy.
- Highly SCC susceptible pipeline materials exhibited evidence of a non-controlled process such a bimodal grain size with evidence of grain growth (indication of overheating).
- The surface layer of materials with ferrite-pearlite microstructure appear to exhibit better properties when the pearlite colony is characterized by a de-generated structure as compared to a more lamellar pearlite colony. Nevertheless further investigation still required to support this observation.

- SCC-free pipeline exhibited more elongated inclusions in the OD region as compared to the SCC susceptible materials in which surface layer inclusions had a smaller appearance. This could indicate that SCC susceptible pipelines were subject to higher temperatures during processing.

This investigation opened the doors to expanding our knowledge of the near surface layer microstructural features where crack nucleation must take place. However in order to fully understand and take advantage of this information further research still required.

Future works

This investigation evaluated the microstructural features (sub-surface and general) of four different vintage with high SCC susceptibility and compared the general metallurgical characteristics to those observed in a SCC-free pipeline. Nevertheless, in order to fully understand what constitutes an SCC susceptible microstructure and therefore be able to develop more resistant materials further research is needed. Therefore in order to complement this investigation it is necessary to carry-out:

- TEM microstructural characterization from the OD region of the SCC-free sample #5.
- Thru-thickness TEM microstructural investigation from different locations on the SCC and SCC-free pipelines, including crack containing regions.
- Quantitative analysis of critical elements in the sub-surface and core region.
- Atom probe analysis on the subsurface region to gain a better understanding of the structural and chemical features of the GBS in the region where crack nucleation must take place.
- Residual stress analysis near surface layer.
- Correlation between the microstructural features and the environment.

Summary

Gas transmission pipelines are subjected to harsh service conditions and environments which can lead to the degradation of the material and thus to failure. One of the main threats to pipeline integrity is stress corrosion cracking (SCC) which continues to be one of the most complex forms of corrosion due to its multivariate nature. One of the required factors for this form of external corrosion to develop is a susceptible microstructure. However, to date the metallurgical features associated to vulnerable materials remain ambiguous due to the wide range of steel grades and microstructures which have experienced this type of failure. Therefore, in an effort to contribute to the understanding of the microstructural features of highly susceptible SCC pipeline materials a systematic microstructural characterization of components removed from service due to SCC was carried-out by optical microscopy, TEM, and X-ray SEM mapping. The objective was to analyzed not only the general microstructure but the microstructural features in the sub-surface zone where crack nucleation must take place, in this manner the goal of this investigation was to identify systematic microstructural trends that can help establish the optimal parameters to design the future generation of pipeline materials.

The results obtained during this research appear to indicate that SCC is a system in which a susceptible microstructure is more likely the result of the combined action between environment, alloying elements, grain boundary character (tilt, disorientation angle, rotation components), and microconstituents. Nevertheless, some of the factors that appear to play an important role in the SCC susceptibility, particularly for IGSCC appear to be the carbon and manganese content, deoxidation practice and thus strain aging effects, and a sub-surface region characterized by slow to intermediate cooling rate microconstituents such as large polygonal ferrite with high dislocation density and dislocation cells which indicate a high SFE material. In this manner this investigation presented a new approach to SCC materials characterization and thus opened the door to understanding the microscropical processes taking place near the surface layer of highly susceptible materials. Nevertheless, further research still required to fully understand the relationship between microstructure and SCC. In this manner

References

[1] Bott, I., De Souza, L. F. G., Teixeira, J. C. G., 2005, "High-Strength Steel Development for Pipelines: A Brazilian Perspective," Metallurgical and Materials Transactions A, 36App. 443-454.

[2] Clark, E.B., and Leis, B.N., 2005, "Integrity Characteristics of Vintage Pipelines Report," INGAA Foundation Inc, F-2002-50435, Columbus, OH.

[3] Mokhatab, S., and Poe, W.A., 2012, "Handbook of Natural Gas," Gulf Professional Publishing, USA, pp. 765.

[4] Cheng, Y.F., 2013, "Stress Corrosion Cracking of Pipelines," Wiley, New Jersey, pp. 255.

[5] Sturm, F.J., 1997, "Trading Natural Gas," PennWell Publishing Company, Oklahoma, pp. 199.

[6] Shanmugam, S., Ramisetti, N. K., Misra, R. D. K., 2008, "Microstructure and High Strength-Toughness Combination of a New 700MPa Nb-Microalloyed Pipeline Steel," Materials Science and Engineering A, 478pp. 26-37.

[7] Shin, S. Y., Hwang, B., Lee, S., 2007, "Correlation of Microstructure and Charpy Impact Properties in API X70 and X80 Line-Pipe Steels," Materials Science and Engineering: A, 458(1–2) pp. 281-289.

[8] National transportation safety board, 2003, "Natural Gas Pipeline Rupture and Fire near Carlsbad, New Mexico, August 19, 2000." National transportation safety board, NTSB/PAR-03/01 OB2003-916501, Washington D.C.

[9] Kemp, J., 2013, "Small Texas Town Forced to Evacuate After Gas Pipeline Explodes," 2013 (November, 14). http://www.nydailynews.com/news/national/small-texas-town-forced-evacuate-gas-pipeline-explodes-article-1.1516779.

[10] Sanchez, R., 2014., "New York Explosion Exposes nation’s Aging and Dangerous Gas Mains," 2013(March, 17) . http://www.cnn.com/2014/03/15/us/aging-gas-infrastructure/.

[11] McKirdy, W., and Erdman, S. L., 2014, "Dozens Dead as Taiwan Gas Explosions Treat Up Streets." CNN World, http://www.cnn.com/2014/07/31/world/asia/taiwan-explosions/.

[12] Jones, R.H., 1992, "Stress-Corrosion Cracking Materials Performance and Evaluation," ASM International, USA, pp. 448.

[13] National Energy Board, 1996, "Public Inquire concerning Stress Corrosion Cracking on Canadian Oil and Gas Pipelines," National Energy Board, MH-2-95, Canada.

[14] Stephens, M.J., 2000, "A Model for Sizing High Consequence Areas Associated with Natural Gas Pipelines," Gas Research Institute, GRI-00/0189.

[15] Kabirian, A., and Hemmati, M. R., 2007, "A Strategic Planning Model for Natural Gas Transmission Networks," Energy Policy, 35(11) pp. 5656-5670.

[16] Leis, B. N., and Eiber, R. J., 1997, "Stress-Corrosion Cracking on Gas Transmission Pipelines: History, Causes, and Mitigation," First International Business Conference on Onshore Pipelines. Ontario, Canada.

[17] Ru, X., and Staehle, R. W., 2013, "Historical Experience Providing Bases for Predicting Corrosion and Stress Corrosion in Emerging Supercritical Water Nuclear Technology: Part 3—Review." Corrosion, 69(5) pp. 423-447.

[18] Van Boven, G., Chen, W., and Rogge, R., 2007, "The Role of Residual Stress in Neutral pH Stress Corrosion Cracking of Pipeline Steels. Part I: Pitting and Cracking Occurrence," Acta Materialia, 55pp. 29-42.

[19] Metcalfe, J., 2014, "How Gas Leaks Disasters Happen," Http://news.Msn.com/us/how-Gas-Leak-Disasters-Happen, 2014(03/18) .

[20] Crary, D., 2014, "Explosion Reminds of NYC's Aging Infrastructure," Http://abcnews.Go.com/US/wireStory/explosion-Reminder-Nycs-Aging-Infrastructure-22902709, 2014(03/18) .

[21] Kirkham, C., and Knafo, S., 2014, "Deadly New York Explosion Highlights Urgent Need to Fix Citys Crumbling Gas Lines," Http://www.Huffingtonpost.com/2014/03/13/nyc-explosion_n_4958318.Html, 2014(03/18).

[22] National Research Council, 2011, "Research Opportunities in Corrosion Science and Engineering," The National Academy Press, Washington, D.C., pp. 176.

[23] Liang, P., Li, X., Du, C., 2009, "Stress Corrosion Cracking of X80 Pipeline Steel in Simulated Alkaline Soil Solution," Materials & Design, 30(5) pp. 1712-1717.

[24] Gamboa, E., Linton, V., and Law, M., 2008, "Fatigue of Stress Corrosion Cracks in X65 Pipeline Steels," International Journal of Fatigue, 30(5) pp. 850-860.

[25] Fazzini, G. P., and Otegui, L. J., 2007, "Experimental Determination of Stress Corrosion Crack Rates and Service Lives in a Buried ERW Pipeline," International Journal of Pressure Vessels and Piping, 84pp. 739-748.

[26] Kentish, J. P., 1985, "Gas Pipeline Failure. The Australian Experience," British Corrosion Journal, 20(3) pp. 139-146.

[27] Contreras, A., Hernández, S. L., Orozco-Cruz, R., 2012, "Mechanical and Environmental Effects on Stress Corrosion Cracking of Low Carbon Pipeline Steel in a Soil Solution," Materials & Design, 35(0) pp. 281-289.

[28] Canadian Energy Pipeline Association, 2007, "Stress Corrosion Cracking: Recommended Practices, 2nd edition," CEPA, Canada.

[29] Baker, M., 2004, "Stress Corrosion Cracking Study," Michael Baker Jr., Inc, OPS TT08, .

[30] Hernandez-Rodrıguez, L. A. M., Martınez-Delgado, D., and Gonzalez, R., 2007, "Corrosive Wear Failure Analysis in a Natural Gas Pipeline," Wear, 263pp. 567-571.

[31] Holditch, S. A., and Chianelli, R. R., 2008, "Factors that Will Influence Oil and Gas Supply and Demand in the 21st Century," MRS Bulletin, 33pp. 317-323.

[32] Asahi, H., Kushida, T., Kimura, M., 1999, "Role of Microstructure on Stress Corrosion Cracking of Pipeline Steels in Carbonate-Bicarbonate Solution," Corrosion, 55(7) pp. 644-652.

[33] Simonoff, J. S., Restrepo, C. E., and Zimmerman, R., 2010, "Risk Management of Cost Consequences in Natural Gas Transmission and Distribution Infrastructures," Journal of Loss Prevention in the Process Industries, 23(2) pp. 269-279.

[34] U.S. Energy Information Administration, "Natural Gas," Http://www.Eia.gov/pub/oil_gas/natural_gas/analysis_publications/ngpipeline/index.Html, 2013(02/05).

[35] US Department of Transportation, 2009, "The State of the National Pipeline Infrastructure," US Department of Transportation, USA.

[36] Parkins, R. N., 1982, "Stress Corrosion Cracking of Coated High Pressure Gas Transmission Pipelines Subjected to Cathodic Protection," UK National Corrosion Conference, Institution of Corrosion Science & Technology, London, pp. 177.

[37] Zhou, M., Du, L., Zhao, Y., 2012, "Microstructure Characteristics and Mechanical Properties of X-80 Pipeline Steel," Journal of Wuham University of Technology-Mater Sci Ed, 27(2) .

[38] Sankara, P., 2013, "Corrosion control in the oil and gas industry," Gulf Professional Publishing, pp. 1021.

[39] Schumura, E., Paster, M., and Bruber, J., 2005, "Existing Natural Gas Pipeline Materials and Associated Operational Characteristics," DOE Hydrogen Program, FY 2005, USA.

[40] Beavers, A.J., and Thompson, G.N., "ASM Handbook, Volume 13C, Corrosion: Environments and Industries, "ASM International, USA, , Chap. External Corrosion of Oil and Natural Gas Pipelines.

[41] Parkins, N. R., and Fessler, R. R., 1978, "Stress Corrosion Cracking of High-Pressure Gas Transmission Pipelines," International Journal of Materials in Engineering Applications, 1(2) pp. 80-96.

[42] Parkins, R.N., 1994, "Overview of Intergranular Stress Corrosion Cracking," Committee of American Gas Association, NG-18, England.

[43] Chu, R., Chen, W., Wang, S. H., 2004, "Microstructure Dependence of Stress Corrosion Cracking Initiation in X-65 Pipeline Steel Exposed to a Near-Neutral pH Solid Environment," Corrosion, 60(3) pp. 275-283.

[44] Liu, Z. Y., Li, X. G., Du, C. W., 2009, "Effect of Inclusions on Initiation of Stress Corrosion Cracks in X70 Pipeline Steel in an Acidic Soil Environment," Corrosion Science, 51(4) pp. 895-900.

[45] Lu, T. B., Song, F., Gao, M., 2011, "Crack Growth Prediction for Underground High Pressure Gas Lines Exposed to Concentrated carbonate–bicarbonate Solution with High pH," Engineering Fracture Mechanics, 78(1452) pp. 1465.

[46] Fessler, R. R., 1969, "Stress-Corrosion Cracking," A.G.A Fourth Symposium on Line Pipe Research Dallas, Texas November 18-19.

[47] Brown, B. F., 1972, "A Preface to the Problem of Stress Corrosion Cracking," Stress Corrosion Cracking of Metals-A State of the Art, ASTM STP 518, L. H. Craig, ed. American Society for Testing and Materials, pp. 3-15.

[48] Review, R.W., "Stress Corrosion Cracking on Canadian Pipelines," CANMET Materials Technology Laboratory, Ottawa Ontario, Canada.

[49] Gan, F., Sun, Z. W., Sabde, G., 1994, "Cathodic Protection to Mitigate External Corrosion of Underground Steel Pipe Beneath Disbonded Coating," Corrosion, 50(10) .

[50] Poulson, B., 1975, "The Fractography of Stress Corrosion Cracking in Carbon Steels," Corrosion Science, 15(6–12) pp. 469-477.

[51] Parkins, R. N., 2000, "A review of Stress Corrosion Cracking of High Pressure Gas Pipelines," Corrosion 2000, Corrosion, NACE International, Orlando, Florida .

[52] Naumenko, V. V., Filippov, A. G., Shlyamnev, P. A., 2011, "Corrosion Cracking of Alloy Steel," Steel in Translation, 41(12) pp. 1033-1039.

[53] Elboujdaini, M., and Revie, R. W., 2009, "Metallurgical Factors in Stress Corrosion Cracking (SCC) and Hydrogen-Induced Cracking (HIC)," J Solid State Electrochem, 13pp. 5-1099.

[54] Asher, S. L., Leis, B., Colwell, J., 2007, "Investigating the Mechanism for TGSCC on Buried Pipelines in Near-Neutral pH Environment," Corrosion, 63(10) pp. 933-939.

[55] Liu, Z. Y., Li, X. G., Du, C. W., 2010, "Effect of Dissolved Oxygen on Stress Corrosion Cracking of X70 Pipeline Steel in Near-Neutral pH Solution," Corrosion, 66(1) pp. 015006-1-015006-6.

[56] Shipilov, S. A., and Le May, I., 2006, "Structural Integrity of Aging Buried Pipelines having Cathodic Protection," Engineering Failure Analysis, 13(7) pp. 1159-1176.

[57] Wang, J., and Atrens, A., 2003, "Microstructure and Grain Boundary Microanalysis of X70 Pipeline Steel," Journal of Material Science, 38pp. 323-330.

[58] Mitsu, H., Tkahashi, R., Asano, H., 2008, "Susceptibility to Stress Corrosion Cracking for Low Carbon Steel Welds in Carbonate-Bicarbonate Solution." Corrosion, 64(12) pp. 939-948.

[59] Li, J., Eboujdain, M., Fang, B., 2006, "Microscopy Study of Intergranular Stress Corrosion Cracking of X-52 Line Pipe Steel," Corrosion, 62(4) pp. 317-321.

[60] Newman, R. C., 2009, "2.09-Stress Corrosion Cracking," Elsevier, 2pp. 864-901.

[61] Niu, L., and Cheng, Y. F., 2007, "Corrosion Behavior of X-70 Pipe Steel in Near-Neutral pH Solution," Applied Surface Science, 253(21) pp. 8626-8631.

[62] Pikey, A. K., Lambert, S. B., and Plumtress, A., 1995, "Stress Corrosion Cracking of X60 Line Pipe Steel in a Carbonate Bicarbonate Solution," Corrosion, 51(2) pp. 91-96.

[63] Scully, J. C., 1983, "Depassivation and passivation in localized corrosion," Passivity of metals and semiconductors proceeding of the 5th international symposium on passivity, M. Frommet, ed. Elsevier, Bombannes, France, pp. 253.

[64] Galvale, J. R., 1999, "1999 W.R. Whitney Award Lecture: Past, Present, and Future of Stress Corrosion Cracking," Corrosion, 55(8) pp. 723-731.

[65] Might, J., and Duquette, D. J., 1996, "Stress Corrosion Cracking of High-Purity Carbon Steel in Carbonate Solutions," Corrosion, 52(6) pp. 428-434.

[66] Parkins, R. N., 1995, "Mechanistic Aspects of Intergranular Stress Corrosion Cracking of Ferritic Steels," Corrosion, 52(5) pp. 363-374.

[67] Parkins, R. N., and Se, B., 1952, "The Stress Corrosion Cracking of Mild Steels in Nitrate Solutions," Journal of the Iron and Steel Institute, 172(9) pp. 149-162.

[68] Eslami, A., Fang, B., Kania, R., 2010, "Stress Corrosion Cracking Initiation under the Disbonded Coating of Pipeline Steel in Near-Neutral pH Environment," Corrosion Science, 52(11) pp. 3750-3756.

[69] Fang, B., Han, E. H., Wang, J., 2004, "Mechanical and Environmental Influences on SCC of an X-70 Pipeline Steel in Dilure Near-Neutral pH Solutions," Corrosion, 65(5) pp. 419-431.

[70] Lu, B. T., and Luo, J. L., 2006, "Crack Initiation and Early Propagation and X70 Steel in Simulated Near-Neutral pH Groundwater," Corrosion, 62(8) pp. 723-731.

[71] Parkins, R. N., 1982, "Stress Corrosion Cracking of Coated High Pressure Gas Transmission Pipelines Subjected to Cathodic Protection," UK National Corrosion Conference Institution of Corrosion Science & Technology, London, pp. 177.

[72] Asher, S. L., and Singh, P. M., 2009, "Role of Stress in Transgranular Stress Corrosion Cracking of Transmission Pipelines in Near-Nuetral pH Environments," Corrosion, 65(2) pp. 7987.

[73] Hamid, M., and Davis, J., 1988, "Evaluating the Susceptibility of Steels to Hydrogen Embrittlement using Statistical Analysis," Journal of Mat. Sci, 23pp. 3688-3691.

[74] Gu, B., Luo, J., and Mao, X., 1995, "Hydrogen Facilitated Anodic Dissolution Type Stress Corrosion Cracking of Pipeline Steels in Near-Neutral pH Solution," Corrosion, 55(1) pp. 442 105-106.

[75] Li, X. C., Eadie, R. L., and Luo, J. L., 2008, "Influence of Plasticity on Corrosion and Stress Corrosion Cracking Behavior in Near Neutral pH Environment," Corrosion Engineering, Science, and Technology, 43(4) pp. 297-303.

[76] Danielson, M. J., 2001, "Effect of Microstructure and Microchemistry on the SCC behavior of Archival and Modern Pipeline Steels in High pH Environments," Corrosion 2001, NACE, Houston Tx, pp. 01211.

[77] Danielson, M. J., Jones, R. H., and Krist, K., 2000, "Effect of Microstructure and Microchemistry on the SCC behavior of Pipeline Steels in a High pH Environment," Corrosion 2000, NACE, Houston Tx., pp. 00359.

[78] Mousavi Anijdan, S. H., Rezaeian, A., and Yue, S., 2012, "The Effect of Chemical Composition and Austenite Conditioning on the Transformation Behavior of Microalloyed Steels," Materials Characterization, 63(0) pp. 27-38.

[79] Torres-Islas, A., Gonzalez-Rodriguez, J. G., Uruchurtu, J., 2008, "Stress Corrosion Cracking Study of Microalloyed Pipeline Steels in Dilute NaHCO3 Solutions," Corrosion Science, 50(10) pp. 2831-2839.

[80] Sharma, U., and Douglas, G. I., 2000, "Microstructures of Microalloyed Line Pipe Steels," Proceedings of the International Pipeline Conference ASME 2000, Canada, 1, pp. 193-210.

[81] Zhu, M., Du, C., Li, X., 2014, "Effect of Strength and Microstructure on the Stress Corrosion Cracking Behavior and Mechanisms of X-80 Pipeline Steel in High pH Carbonate-Bicarbonate Solution," Journal of Materials Engineering and Performance, .

[82] Carpintero-Moreno, E. J., Gonzalez-Rodriguez, J. G., Uruchurtu-Chavarin, J., 2013, "Effect of Heat Treatment on Stress Corrosion Cracking Susceptibility of Dual-Phase Steel," Corrosion, 69(9) pp. 843-850.

[83] Haq, A. J., Muzaka, K., Dunne, D. P., 2013, "Effect of Microstructure and Composition on Hydrogen Permeation in X70 Pipeline Steels," International Journal of Hydrogen Energy, 38(5) pp. 2544-2556.

[84] Wang, C., Wu, X., Liu, J., 2006, "Transmission Electron Microscopy of martensite/austenite Islands in Pipeline Steel x70," Materials Science and Engineering A, 4pp. 267-271.

[85] Wang, W., Shan, Y., and Yang, K., 2009, "Study of High Strength Pipeline Steels with Different Microstructures," Materials Science and Engineering A, 502pp. 38-44

[86] El-Danaf, E., Baig, M., Almajid, A., 2013, "Mechanical, Microstructure and Texture Characterization of API X65 Steel," Materials & Design, 47(0) pp. 529-538.

[87] Krauss, G., 2005, "Steels: Processing, Struture, and Performance,"ASM International, Ohio, pp. 101-118, Chap. 7.

[88] Wang, Y. K., Pan, J. H., Yang, K., "High Performance Micro-Alloys Pipe Steel in China,"

[89] Kon, S. U., Lee, J. M., Yang, B. Y., 2007, "Effect of Molybdenum and Chromium Additions on the Susceptibility to Sulfide Stress Cracking of Hihg-Strength Low Alloy Steels," Corrosion, 63(3) pp. 220-230.

[90] Fang, B. T., Atrens, A., Wang, J. Q., 2003, "Review of Stress Corrosion Cracking of Pipeline Steels in "Low" and "High" pH Solutions," Journal of Material Science, 38pp. 127-132

[91] Bulger, J. T., Lu, B. T., and Luo, J. L., 2006, "Microstructural Effect on Near-Neutral pH Resistance of Pipeline Steels," J. Mater. Sci, 41pp. 5001-5005.

[92] Flis, J., and Scully, J. C., 1968, "Transmission Electro Microscopical Study of Corrosion and Stress-Corrosion of Mild Steel in Nitrate Solution," Corrosion Science, 9pp. 235-244.

[93] Wang, L. W., Du, C. W., Liu, Z. Y., 2013, "Influence of Carbon on Stress Corrosion Cracking of High Strength Pipeline Steel," Corrosion Science, 76(0) pp. 486-493.

[94] Nakayama, T., 2007, "Stress Corrosion Cracking of Carbon Steels and Low Alloy Steels," Welding International, 21(2) pp. 89-44.

[95] Mohtadi-Bonab, M. A., Szpunar, J. A., and Razavi-Tousi, S. S., 2013, "A Comparative Study of Hydrogen Induced Cracking Behavior in API 5L X60 and X70 Pipeline Steels," Engineering Failure Analysis, 33(0) pp. 163-175.

[96] Park, G. T., Koh, S. U., Jung, H. G., 2008, "Effect of Microstructure on the Hydrogen Trapping Efficiency and Hydrogen Induced Cracking of Linepipe Steel," Corrosion Science, 50(7) pp. 1865-1871.

[97] Meng, G. Z., Zhang, C., and Cheng, Y. F., 2008, "Effects of Corrosion Product Deposit on the Subsequent Cathodic and Anodic Reactions of X-70 Steel in Near-Neutral pH Solution," Corrosion Science, 50(11) pp. 3116-3122.

[98] Ralston, K. D., and Birbilis, N., 2010, "Effect of Processing on Grain Size and Corrosion of AA2024-T3," Corrosion, 66(7) pp. 075005-1

[99] Ralston, K. D., and Birbilis, N., 2013, "Effect of Grain Size on Corrosion: A Review," Corrosion, 66(7) pp. 075005-075005-13.

[100] Green, J. A. J., and Parkins, R. N., 1968, "Electrochemical Properties of Ferrite and Cementite in Relation to Stress Corrosion of Mild Steels in Nitrate Solutions," Corrosion, 24pp. 66-69

[101] Ahmed, T. M., Lambert, S. B., Sutherby, R., 1997, "Cyclic Crack Growth Rates of X60 Pipeline Steel in Near Neutral Dilute Solution," Corrosion, 53(7) pp. 581-590.

[102] Ru, X., and Staehle, R. N., 2010, "Historical Experience Providing Bases for Predicting Corrosion and Stress Corrosion in Emerging Supercritical Water Nuclear Technologies- Part2: Review," Corrosion, 69(4) pp. 319-334.

[103] Zhao, M. C., Yang, K., and Shan, Y., 2002, "The Effects of Thermomechanical Control Process on Microstructures and Mechanical Properties of a Commercial Pipeline Steel," Materials Science and Engineering A, 335pp. 14-20.

[104] Hardie, D., Charles, E. A., and Lopez, A. H., 2006, "Hydrogen Embrittlement of High Strength Pipeline Steels," Corrosion Science, 48pp. 4378-4385.

[105] Capelle, J., Dmytrakh, I., Azari, Z., 2013, "Evaluation of Electrochemical Hydrogen Absorption in Welded Pipe with Steel API X52," International Journal of Hydrogen Energy, 38(33) pp. 14356-14363

[106] Xu, L. Y., and Cheng, Y. F., 2012, "An Experimental Investigation of Corrosion of X100 Pipeline Steel Under Uniaxial Elastic Stress in a Near-Neutral pH Solution," Corrosion Science, 59(0) pp. 103-109.

[107] Meyers, M.A., and Chawla, K.K., "Mechanical Behavior of Materials", Cambridge University Press, 2009. 851pp.

[108] Holt, A. H., 1967. “Deformation Substructure and Susceptibility to Intergranular Stress Corrosion Cracking in an Aluminum Alloy”. Corrosion, 23(6) pp. 173-180

[109] Hirth, J. P., 1980, "Effects of Hydrogen on the Properties of Iron and Steel," Metallurgical and Materials Transactions A, 11App. 861-890.

[110] Pound, B. G., 2000, "The Effect of Aging on Hydrogen Trapping in Precipitation-Hardened Alloys," Corrosion Science, 42(11) pp. 1941-1956.

[111] Scully, J. C., 1980, "The Interaction of Strain-Rate and Repassivation Rate in Stress Corrosion Crack Propagation," Corrosion Science, 20(8–9) pp. 997-1016.

[112] Douglass, D. L., Thomas, G., and Roser, W. R., 1964, "Ordering, Stacking Fault and Stress Corrosion Cracking in Austenitic Alloys," Corrosion, 20(1) pp. 15T-28T.

[113] Parkins, R. N., 1969, "Stress Corrosion Cracking of Low Carbon Steels," Fundamentals Aspects of Stress Corrosion Cracking. National Association of Corrosion Engineers, Houston, Texas, pp. 361-373.

[114] Smith, T. J., and Staehle, R. W., 1967, "Role of Slip Steps Emergence in the Early Stages of SCC in Face Center Iron-Nickel-Chromium Alloy," Corrosion, 23(5) pp. 117-129.

[115] Jin, T. Y., Liu, Z. Y., and Cheng, Y. F., 2010, "Effect of Non-Metallic Inclusions on Hydrogen-Induced Cracking of API5L X100 Steel," International Journal of Hydrogen Energy, 35(15) pp. 8014-8021.

[116] Jarman, R., and Thomas, J. G. N., 1985, "The Influence of Non Metallic Inclusion on the Corrosion Fatigue of Mild Steels," Corrosion Science, 25(3) pp. 171-184.

[117] Wang, J. Q., and Atrens, A., 2003, "SCC Initiation for X65 Pipeline Steel in the “high” pH carbonate/bicarbonate Solution," Corrosion Science, 45(10) pp. 2199-2217.

[118] Grabke, H. J., 1988, "Surface and Grain Boundary Segregation on and in Iron and Steels," ISIJ International, 29(7) pp. 529-583.

[119] Krautschick, H. J., Grabke, H. J., and Diekmann, W., 1988, "The Effect of Phosphorus on the Mechanism of Intergranular Stress Corrosion Cracking of Mild Steels in Nitrate Solutions," Corrosion Science, 28(3) pp. 251-258.

[120] Flis, J., and Ziomek-Moroz, M., 2008, "Effect of Carbon on Stress Corrosion Cracking and Anodic Oxidation of Iron in NaOH Solutions," Corrosion Science, 50(6) pp. 1726-1733.

[121] Tauber, G., and Grabke, H. J., 1979, "Electrochemical and Auger-Spectroscopic Studies on the Intergranular Corrosion of Iron in Nitrate Solutions," Corrosion Science, 19(11) pp. 793-798.

[122] Flis, J., 1970, "Effect of Carbon on the Corrosion of Fe in NH2NO3 Solution within a Wide Potential Range," Corrosion Science, 10pp. 745-759.

[123] Atrens, A., Wang, J. Q., Stiller, K., 2006, "Atom Probe Field Ion Microscope Measurements of Carbon Segregation at an a:A Grain Boundary and Service Failures by Intergranular Stress Corrosion Cracking," Corrosion Science, 48pp. 79-92.

[124] Flis, J., and Scully, J. C., 1968, "The Role of Interstitial and Substitutional Impurities in Stress Corrosion Cracking of Low Carbon Steel in Nitrate Solutions," Corrosion, 24pp. 326-334.

[125] Key to Metals AG, Feb, 2013, "Strain Ageing of Steels," Http://www.Keytometals.com/page.Aspx?ID=CheckArticle&site=kts&NM=392, Feb, 2014.

[126] Vargas-Arista, B., Angeles-Chavez, C., Albiter, A., 2009, "Metallurgical Investigation of the Aging Process on Tensile Fracture Welded Joints in Pipeline Steel," Materials Characterization, 60(12) pp. 1561-1568.

[127] Kotrechko, S. O., Krasowsky, A. Y., Meshkov, Y. Y., 2004, "Effect of Long-Term Service on the Tensile Properties and Capability of Pipeline Steel 17GS to Resist Cleavage Fracture," International Journal of Pressure Vessels and Piping, 81(4) pp. 337-344.

[128] Homma, K., Miki, C., and Yang, H., 1998, "Fracture Toughness of Cold Worked and Simulated Heat Affected Structural Steel," Engineering Fracture Mechanics, 59(1) pp. 17-28.

[129] GAO, 2013, "Gas Pipeline Safety," GAO, GAO-13-577, USA.

[130] Was, G. S., Ampornrat, P., Gupta, G., 2007, "Corrosion and Stress Corrosion Cracking in Supercritical Water," Journal of Nuclear Materials, 371(1–3) pp. 176-201.

[131] Gomez, M., Valles, P., and Medina, S. F., 2011, "Evolution of Microstructure and Precipitation State during Thermomechanical Processing of a X80 Microalloyed Steel," Materials Science and Engineering: A, 528(13–14) pp. 4761-4773.

[132] Javidi, M., and Horeh, S. M., 2014, "Investigating the Mechanism of Stress Corrosion Cracking in Near-Neutral and High pH Environments for API 5 LX52 Steel," Corrosion Science, 80pp. 213-220.

[133] Chen, W., King, F., and Vokes, E., 2002, "Characteristics of Near-Neutral-pH Stress Corrosion Cracks in an X-65 Pipeline," Corrosion, 58(3).

[134] Wang, Z. F., and Atrens, A., 1996, "Initiation of Stress Corrosion Cracking for Pipeline Steels in a Carbonate-Bicarbonate Solution," Metallurgical and Materials Transactions A, 27App. 2686-2691.

[135] Jain, S., Beavers, J. A., Ayello, F., 2013, "Probabilistic model for stress corrosion cracking of underground piepelines using bayesian networks," NACE International, Corrosion, NACE International, Houston, Tx, paper 2616, pp. 1-15.

[136] Farelas, F., Brown, B., and Nesic, S., 2013, "Iron Carbide and its Influence on the Formation of Protective Iron Carbonate in CO2 Corrosion of Mild Steel," NACE International, Houston Texas, 2291.

[137] Bulger, J. T., Fall 2000, "The Effect of Microstructure on Near Neutral SCC," Thesis.

[138] National Physical Laboratory, 1982, "Stress corrosion cracking," National Physical Laboratory, Teddingtond, Meddlesex.

[139] Leslie, W.C., 1981, "The Physical Metallurgy of Steels," Mc Graw Hill, United States, pp. 396.

[140] AMG Vanadium, Inc. http://amg-v.com/aluminumpage.html Copyright © 2011.

[141] Flis, J., 1973. “Action of Carbon in Stress Corrosion Cracking of Mild Steel in Nitrate Solutions”. Corrosion, 29(1) pp.36-44.

[142] Samuels, L.E., 1980, "Optical Microscopy of Carbon steels," American Society for Metals, Ohio, USA, pp. 594.

[143] Cyril, N.S., Fatemi, A., 2009, “Experimental Evaluation and Modeling of Sulfur Content and Anisotropy of Sulfide Inclusions on Fatigue Behavior of Steels”, International Journal of Fatigue 31pp 526-537.

[144] Briant, C. L., and Banerji, S. K., 1978, "Intergranular Failure in Steel: The Role of Grain Boundary Composition," International Metals Reviews, (4) pp. 164-199.

[145] King, F., 2010, "Development of Guidelines for Identification of SCC sites and Estimation of Re-inspection Intervals for SCC Direct Assessment," Integrity Corrosion Consulting, USA.

[146] Olefjord, I., 1978, "Temper Embrittlement," International Metals Reviews, (4) pp. 149-163.

[147] Shibaeva, T. V., Laurinavichyute, V. K., Tsirlina, G. A., 2014, "The Effect of Microstructure and Non-Metallic Inclusions on Corrosion Behavior of Low Carbon Steel in Chloride Containing Solutions," Corrosion Science, 80(0) pp. 299-308.

[148] Lu, B. T., and Luo, J. L., 2006, "Relationship between Yield Strength and Near-Neutral pH Stress Corrosion Cracking Resistance of Pipeline Steel--an Effect of Microstructure," Corrosion, 62(2) pp. 129-140.

[149] Zhu, L., Yan, Y., Li, J., 2014, "Stress Corrosion Cracking Under Low Stress: Continuous of Discontinuous Cracks," Corrosion Science, 80pp. 350-358.

[150] Liu, Z. Y., Li, X. G., and Cheng, Y. F., 2010, "In-Situ Characterization of the Electrochemistry of Grain and Grain Boundary of an X70 Steel in a Near-Neutral pH Solution," Electrochemistry Communications, 12(7) pp. 936-938.

[151] Parkins, R. N., Blanchard, W. K., and Delanty, B. S., 1994, "Transgranular Stress Corrosion Cracking of High Pressure Pipelines in Contact with Solutions of Near-Neutral pH," Corrosion, 50(5) pp. 395-408.

[152] Chen, W., Kania, R., Worthingham, R., 2009, "Transgranular Crack Growth in the Pipeline Steels Exposed to Near-Neutral pH Soil Aqueous Solutions: The Role of Hydrogen," Acta Materialia, 57(20) pp. 6200-6214.

[153] Woodtli, J., Kiwselbach, R., 2000, “Damage due to Hydrogen Embrittlement and Stress Corrosion Cracking”, Engineering Failure Analysis 7pp427-450.

[154] Collins, L. E., Gooden, M. J., and Boyd, J. D., 1983, "Microstructures of Linepipe Steels," Canadian Metallurgy Quarterly, 22(2) pp. 169-179.

[155] Shanmugam, S., Ramisetti, N. K., Misra, R. D. K., 2007, "Effect of Cooling Rate on the Microstructure and Mechanical Properties of Nb-Miccroalloyed Steels," Materials Science and Engineering: A, 460-461pp. 335-343.

[156] Offerman, S.E., Van Dijf, N.H., Rekveldat, M.Th., Sietsma, J., Van der Swaag, S., 2002, “Ferrite/Pearlite Band Formation in Hot Rolled Medium Carbon Steel”, Materials Science and Technology 18pp 297-303.

[157] Lung, T., Mathy, H., Gracia de Andres, G.,, 2007, “Suppression of Banded Structure and Refinement of the Microstructure of High Strength Cold-Rolled Steels by Optimization of the Hot Rolling Cooling Path” European Communities, Report EUR 22830.

[158] Caballero, F.G., Garcia-Juneda, A., Capdevila, C., Garcia de Andres, C., 2006, “Evolution of Microstructural Banding during the Manufacturing Process of Dual Phase Steels”, Materials Transactions 47(9) pp. 2269-2276.

[159] Hejazi, D., Haq, A. J., Yazdipour, N., 2012, "Effect of Mn Content and Microstructure on the Susceptibility of X70 Pipeline Steel to Hydrogen Cracking." Materials Science and Engineering: A, 551pp. 40-49.

[160] Vander Voort, G.F. 2015. “Understanding and Measuring Decarbutization”. Advance Materials and Processes, pp. 20.

[161] Ghosh, S. K., Haldar, A., and Chattopadhyay, P. P., 2009, "The Influence of Copper Addition on Microstructure and Mechanical Properties of Thermomechanically Processed Microalloyed Steels." J. Mater. Sci, 44pp. 580-590.

[162] Dong, C. F., Li, X. G., Liu, Z. Y., 2009, "Hydrogen-Induced Cracking and Healing Behavior of X70 Steel," Journal of Alloys and Compounds, 484(1–2) pp. 966-972.

[163] Storojeva, L.; Ponge, D.; Kaspar, R. and Raabe, D., 2004. “Development of Microstructure and Texture of Medium Carbon Steel during Heavy Warm Deformation”. Acta Materialia, 52(8) pp. 2209-2220.

[164] Shanmugam, S., Misra, R. D. K., Mannering, T., 2006, "Impact Toughness and Microstructure Relationship in Niobium and Vanadium Microalloyed Steels Processes with Varied Cooling Rates to Similar Yield Strengths," Materials Science and Engineering: A, 437pp. 436-445.

[165] Cottrell, A.H., 1953, “Dislocations and Plastic Flow in Crystals”, Clarendon Press, Oxford, 1953.

[166] Hull, D., Bacon, D.J. “Introduction to Dislocations”, Elsevier, Oxford, 1965.

[167] McEvily, A.J.; Johnston, K.T.; 1985. “The role of Cross-Slip in Brittle Fracture and Fatigue”. International Conference on Fracture, Sendai Japan.

[168] Smallman, R.E., Ngan, A.H.W., “Physical Metallurgy and Advance Materials”. Btterworth-Heinemann, 2011.

[169] Galindo-Nava, E.I.; Rivera-Diaz del Castillo, P.E.J., 2012. “A Thermodynamic Theory for Dislocation Cell Formation and Misorientation in Metals”. Acta Materiali, 60 pp. 4370-4378.

[170] Smallman, R.W., Bishop, R.J. “Modern Physical Metallurgy and Materials Engineering”, Butterworth-Heinemann Elsevier Science, Oxford 2002.

[171] Sha, G., Yao, L., Liao, X., 2011, "Segregation of Solute Elements at Grain Boundaries in an Ultrafine Grained Al–Zn–Mg–Cu Alloy," Ultramicroscopy, 111(6) pp. 500-505.

[172] Yu, B., Woo, P., and Erb, U., 2007, "Corrosion Behaviour of Nanocrystalline Copper Foil in Sodium Hydroxide Solution," Scripta Materialia, 56(5) pp. 353-356.

[173] Mclean, D., 1957, "Grain boundaries in metals," Oxford Claredon Press, 1957. 346pp.

[174] Faulker, R. G., 1996, "Segregation to Boundaries and Interfaces in Solids," International Materials Reviews, 41(5) pp. 198-208.

[175] Mishin, Y., Herzing, C., Bernardini, J., 1997, "Grain Boundary Diffusion, Fundamentals to Recent Developments," International Metallurgial Reviews, 42pp. 155-178.

[176] Farelas, F., Galicia, M., Brown, B., 2010, "Evolution of Dissolution Process at the Interface of Carbon Steel Corroding in CO2 Environment Studied by EIS," Corrosion Science, 52pp. 509-517.

[177] Sun, X. Y., Zhang, B., Lin, H. Q., 2014, "Atom Probe Tomographic Study of Elemental Segregation at Grain Boundaries for a Peak-Aged Al–Zn–Mg Alloy," Corrosion Science, 79(0) pp. 1-4

[178] Vargas-Arista, B., Hallen, M. J., and Albiter, A., 2007, "Effect of Artificial Aging on the Microstructure of Weldment on API 5L X-52 Steel Pipe," Materials Characterization, 58pp. 721-729.

Curriculum Vitae

Monica Torres earned her Bachelor of Science Degree in Industrial Engineering from Tecnologico de Monterrey, Campus Juarez, while working for Delphi Automotive Systems. During this time, she had the opportunity to work with many talented individuals from the materials laboratory, which awoke her interest in materials science. In 2007, she enrolled in the Graduate School at The University of Texas at El Paso to pursue a Master of Science in Metallurgical and Material Engineering. After a year into the program, she started working with Dr. Luis Trueba on friction stir welding. This lead to new opportunities and challenges; in 2009, she worked with Jacobs Engineering and NASA as part of her research project. After graduation, Monica Torres enrolled in The Graduate School at The University of Texas at El Paso to pursue a PhD in Materials Science and started working with Dr. S.W. Stafford on stress corrosion cracking on gas transmission pipelines.

Contact Information: matorres9@miners.utep.edu

This dissertation was typed by Monica Torres